Marin

Internship

Lagrangian model with bubble dynamics for cavitating nuclei

Author:
Simon Beelen

Supervisor:
ir. Martijn van Rijsbergen

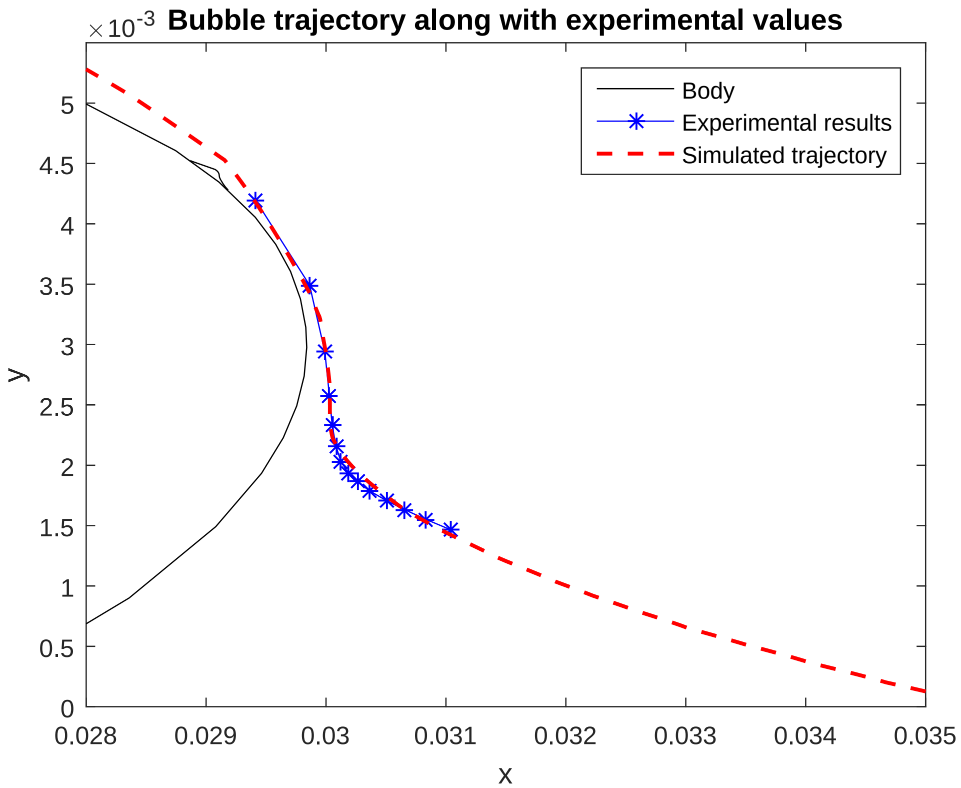

June 13, 2017

Internship

The influence of the trajectories of gas nuclei on cavitation inception

June 13, 2017

ir. Martijn van Rijsbergen

Simon Beelen

Marin
Internship Master Mechanical Engineering

Number of pages of content: 59

MARIN/UT/ME-June 13, 2017

Contents

Summary

In this report a model for cavitating nuclei in a flow field and the possible extensions of this model are examined.
In the paper by Johnson and Hsieh [1] such a model is introduced. In this paper a simple equation of motion along with a quasi steady equation for the bubble growth is solved in a potential flow field. This model leads to a prediction of cavitation inception based on the critical pressure coefficient. Cavitation inception is therefore also assumed to occur when the bubble starts to grow asymptotically. One could say that the model presented by Johnson and Hsies is the absolute basis. The equation of motion only has three terms, which is the minimum, the bubble growth is described by a quasy-steady equation and the flow field is a potential flow field.

Step by step the complexity of (parts of) the model is increased. Starting with a bubble dynamics equation, the Rayleigh-Plesset equation is used at first. Eventually the Rayleigh-Plesset equation is replaced by the general Keller-Herring equation, which is a more advanced bubble dynamics equation and includes damping due to the emitted sound wave. The equation of motion is extended by using more forces, of which the buoyancy force is the most influential. The volume-changing force (the force due to the changing volume of the wake of the bubble) turned out to be very dominant during collapses of the bubble. The model has the mass of the nucleus incorporated so that the model is suitable for solid particles.

The history force has been included as the Basset force. This is done in an iterative way. The history force smears out the trajectory of the bubble, and is especially reactionary towards the volume-changing force as it is a very unsteady force. The Basset force turned out not to be a good choice for the history force, since it overestimates this force significantly, especially over longer time spans.

Finally a new flow field has been taken, in this flow field the simple equation of motion has been solved along with the general Keller-Herring equation. The result is a trajectory in this flow field. The trajectory has been compared with the results found by [8], it was found that locally taking the streamline as a trajectory was a good approximation. The trajectory has also been compared with the trajectory found in experiments which gave encouraging results regarding the trajectories. The bubble diameter was less comparable.

Introduction

This report concludes the work for the internship at MARIN.

Sheet cavitation is in many cases induced by free-stream nuclei. These nuclei can be gaseous or solid and range in diameter between approximately 10 and 500 micrometer. A scale effect that could occur is bubble screening, the deflection of a bubble from the leading edge of a foil due to buoyancy forces. High-speed observations of the nuclei-induced inception process made at MARIN, show that both gas and solid nuclei can deflect significantly from calculated streamlines. This data set may be used to validate a Lagrangian model which uses an equation of motion to determine the trajectory of a point mass in a known velocity and pressure field. Once validated, this model can be used to calculate the trajectories of nuclei for a large range of nuclei diameters, velocities and leading edge geometries.

Understanding the underlying cavitation inception mechanisms is crucial to make suitable models for implementation in simulations. Cavitation inception will be defined in this report as the unstable growth of a gas bubble in a flow. The bubble dynamics will be the driving force for cavitation inception. Its input, namely the local pressure, depends on the trajectory of the bubble. In this way the trajectory and the bubble dynamics are coupled, and will therefore be solved together.

The basis of this work was already founded by Johnson and Hsieh [1]. The results in this paper have been reproduced as a first exercise.

Later on more advanced equations for both the motion and dynamics of the bubble will be introduced. Especially a look will be taken at the History/Basset force, since this force might be relevant in unsteady conditions, which can originate from the bubble dynamics equation.

Finally an attempt has been made to start simulations in a given flow field. The results found by these simulations are compared with experiments.

The report contains appendices, which can be a helpful addition if the reader has particular interest. Otherwise, the report is complete without the appendices.

1. Reproducing the results of Johnson and Hsieh

The paper by Johnson and Hsieh [1] has been used as a starting point to get a better understanding of cavitation inception. The paper has been divided in three main parts, namely: Static stability of spherical gas bubbles, Bubble trajectory and Application to a two-dimensional half body in an infinite fluid. This structure will be kept, since it refers to the bubble dynamics, the trajectory and the flow, which will stay relevant.

Review of the equations

In this section a review will be given on the equations derived by Johnson and Hsieh [1].

Static stability of spherical gas bubbles

Johnson and Hsieh used an equation which is based on the static stability of spherical gas bubbles surrounded by liquid. This equation is given in Eq. 1.1.

$$\frac{p - p_v}{p_0 - p_v} = \left(\frac{R_0'}{R'}\right)^3 \left[1 + \frac{8}{\sigma_v W}\left(1 - \frac{R'^2}{R_0'^2}\right)\right] \tag{1.1}$$

The definition of the variables in Eq. 1.1 can be found in Appendix A. The derivation of the gas stability can be found in Appendix A. Johnson and Hsieh used Eq. 1.1 as the basis of three equations. The first being the dimensionless form of Eq. 1.1, the second being the solutions to the third degree polynomial function (which is Eq. 1.1) in terms of the bubble growth, and lastly a critical pressure coefficient is found by finding a critical point in the bubble growth. The derivations of these equations can also be found in Appendix A.

The equations derived concerning the static stability of spherical gas bubbles thus include the growth of the bubble. The bubble growth depends on the Weber number, the cavitation number and the pressure coefficient. A smaller cavitation number means that the bubble will grow more easily. A smaller pressure coefficient also means more growth. A larger Weber number means more growth.

It is important to note that there are some minor mistakes in [1], namely in the third equations (3a-3c), in equation 3a a term of $\frac{1}{2}Q$ is missing, in equation 3b and 3c the division signs are missing.

Bubble trajectory

The equation of motion is constructed via a force balance. The forces which will be included in the equation of motion are the pressure force, the drag force and the added mass force. The force due to the acceleration of the bubble is neglected, since the mass of the bubble is much smaller than the added mass of the bubble. The force balance is given in Eq. 1.2.

$$\underbrace{\frac{1}{2}\frac{4}{3}\pi R'^3 \rho \frac{d\boldsymbol{w}_b}{dt}}_{\text{Added mass force}} = \underbrace{\frac{1}{2}\rho(\boldsymbol{w}-\boldsymbol{w}_b)|\boldsymbol{w}-\boldsymbol{w}_b| C_D \pi R'^2}_{\text{Drag force}} - \underbrace{\frac{3}{2}\frac{4}{3}\pi R'^3 \boldsymbol{\nabla} p}_{\text{Pressure force}} \tag{1.2}$$

The derivation is given in Appendix B. After establishing the force balance, the equation of motion is made dimensionless and written term wise. This has also been done in Appendix B.

Application to a two-dimensional half body in an infinite fluid

The flow field which will be used is a potential flow field. The benefit of a potential flow field is that with the superposition of very basic elements an analytically defined flow field can be found. The elements used in this case are uniform flow and a source at the origin. The source strength is chosen such that the stagnation point is in $(x, y) = (-\frac{1}{\pi}, 0)$. The resulting body shape is given in Eq. 1.3.

$$x = -y \cot \pi y \tag{1.3}$$

The full derivation, including the outcome with respect to the velocities and the pressure coefficient can be found in Appendix C.

The resulting dimensionless equations of motion are given in Eqs 1.4-1.5.

$$\frac{d\dot{x}}{d\tau} = \frac{18}{R^2 R_f}\frac{R_B C_D}{24}\left[\left(1 + \frac{1}{\pi}\frac{x}{x^2+y^2}\right) - \dot{x}\right] - \frac{3}{\pi}\left[\frac{x^2 - y^2 + \frac{x}{\pi}}{(x^2+y^2)^2}\right] \tag{1.4}$$

$$\frac{d\dot{y}}{d\tau} = \frac{18}{R^2 R_f} \frac{R_b C_D}{24} \left[\left(\frac{1}{\pi} \frac{y}{x^2 + y^2} \right) - \dot{y} \right] - \frac{3}{\pi} \left[\frac{y \left(2x + \frac{1}{\pi} \right)}{(x^2 + y^2)^2} \right] \tag{1.5}$$

So the equation of motion depends on the acceleration, the velocity and the position, and is therefore a second-order Ordinary Differential Equation(ODE).

Solving the system of ODE's

The resulting equations of motion are second-order coupled non-linear ODE's. These kind of systems can be solved efficiently via numerical integration. Most of these numerical integration schemes are designed to solve systems of first-order ODE's efficiently, therefore the set of second-order ODE's will be reduced to a system of first-order ODE's. The actual reduction is straightforward, and can be found in Appendix D.
The numerical integration scheme which will (mostly) be used is the Runge-Kutta scheme. This scheme will be incorporated via the ode functions in MATLAB, since these have adjusted time stepping, which speeds up the process significantly.

Even though no initial conditions on the velocities are mentioned by Johnson and Hsieh the initial conditions that seemed to be used are given in Eq. 1.6.

$$z_0 = \begin{bmatrix} u_{b0} = 0 \\ x_0 = x_0 \\ v_{b0} = 0 \\ y_0 = y_0 \end{bmatrix} \tag{1.6}$$

Only with zero initial bubble speed it makes sense to alter the initial horizontal location of the bubble (second Figure in [1]). A probably better option would be that the bubble follows the fluid.

Results

In this part the results will be discussed and compared with the results of [1].

Variation of the initial vertical position

The effect of the vertical initial location on the bubble path is examined first. The trajectory of a bubble with $y_0 = 0.01$ is shown in Figure 1.1.

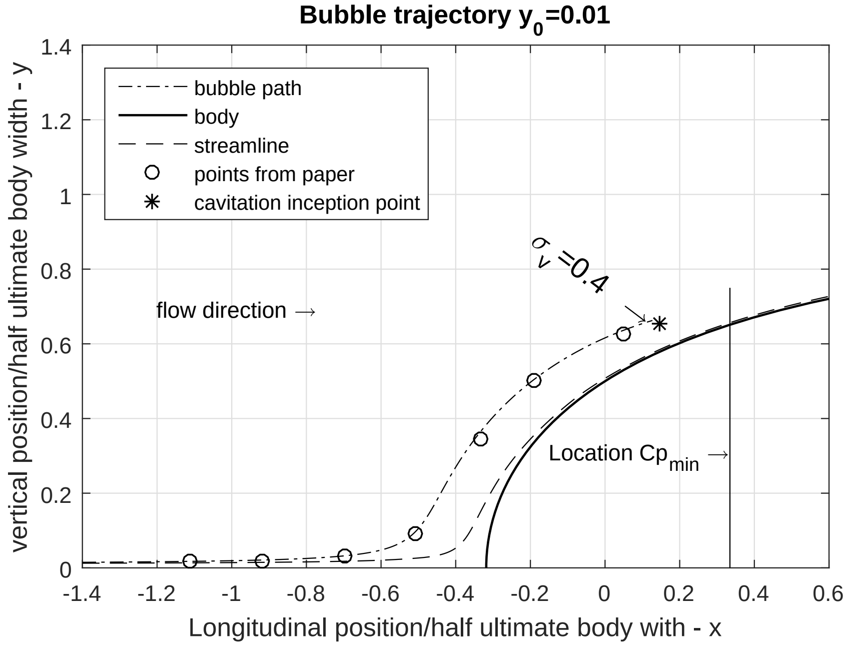

Figure 1.1: The bubble trajectory when $y_0 = 0.01$

The resulting trajectory is comparable, however the trajectory is overall slightly higher in the vertical position. The same trend can be seen when the initial conditions of $y_0 = [0.02\ 0.05\ 0.1\ 0.2]$ are used, see Figure 1.2.

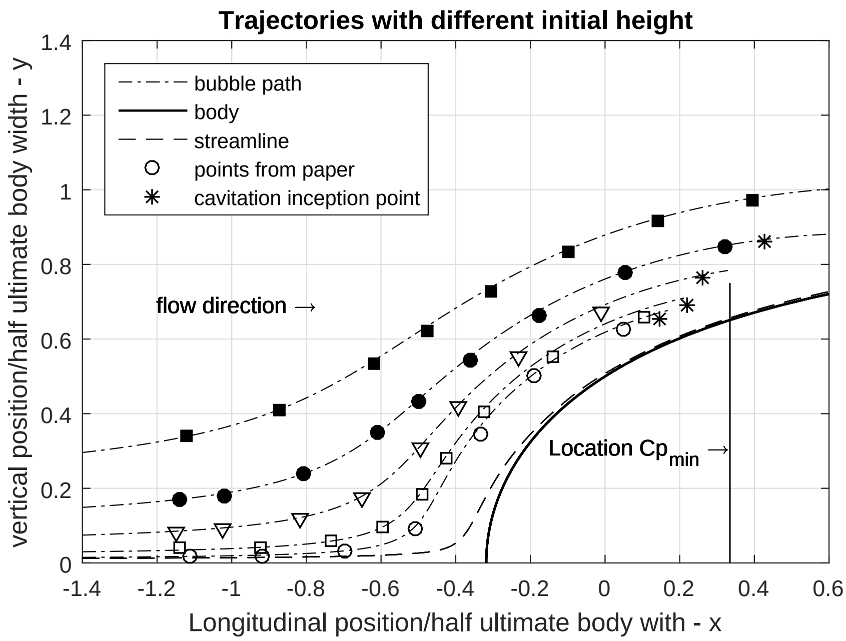

Figure 1.2: Trajectories with different initial height $y_0 = [0.02\ 0.05\ 0.1\ 0.2]$

Variation of initial radius

The trajectories of varying initial radii are being compared to the trajectories with the same initial radii in [1]. The initial radii are $R_0 = [0.24\ 0.12\ 0.08\ 0.04\ 0.02]$, the result can be seen in Figure 1.3.

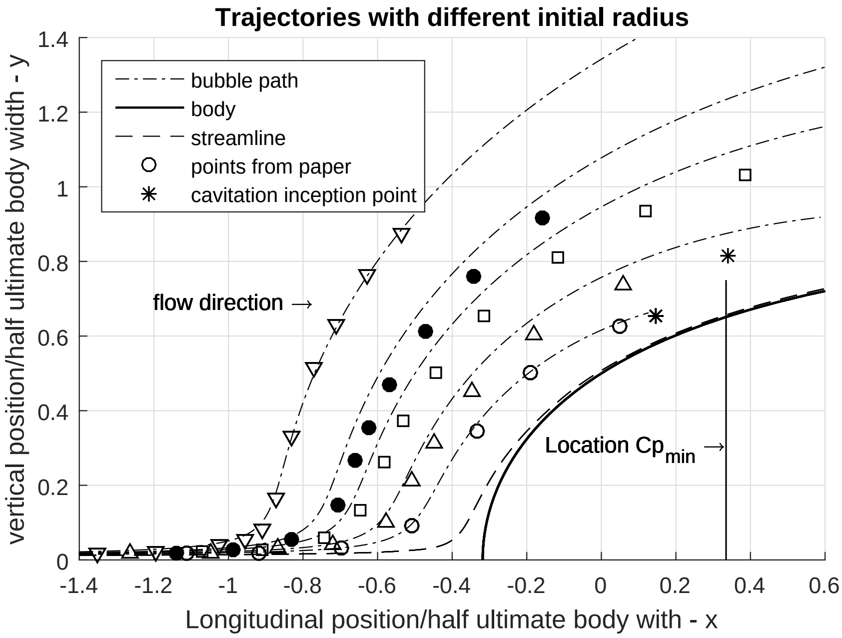

Figure 1.3: Bubble trajectory with different initial radii

It can be seen that the calculated trajectories deviates significantly in some cases ($R_0 =$ [0.12 0.08 0.04]). The trajectories with $R_0 =$ [0.24 0.02] are reasonably comparable.

Varying the cavitation number

Johnson and Hsieh changed the cavitation number from $\sigma_v = 0.4$ to $\sigma_v = 0.58$. In the next section on stability, this will be investigated in more detail. For now, it suffices to say that both by the calculation of Johnson and Hsieh and in this calculation the cavitation number does not seem to change the bubble trajectory significantly.

Stability

The stability of the nuclei can be checked by means of the growth of the bubble. If this goes asymptotically the growth has passed the critical point. Cavitation inception occurs past this point. The sixth Figure in [1] shows the stability of a bubble with different cavitation numbers. The stability has been analyzed, leading to Figure 1.4.

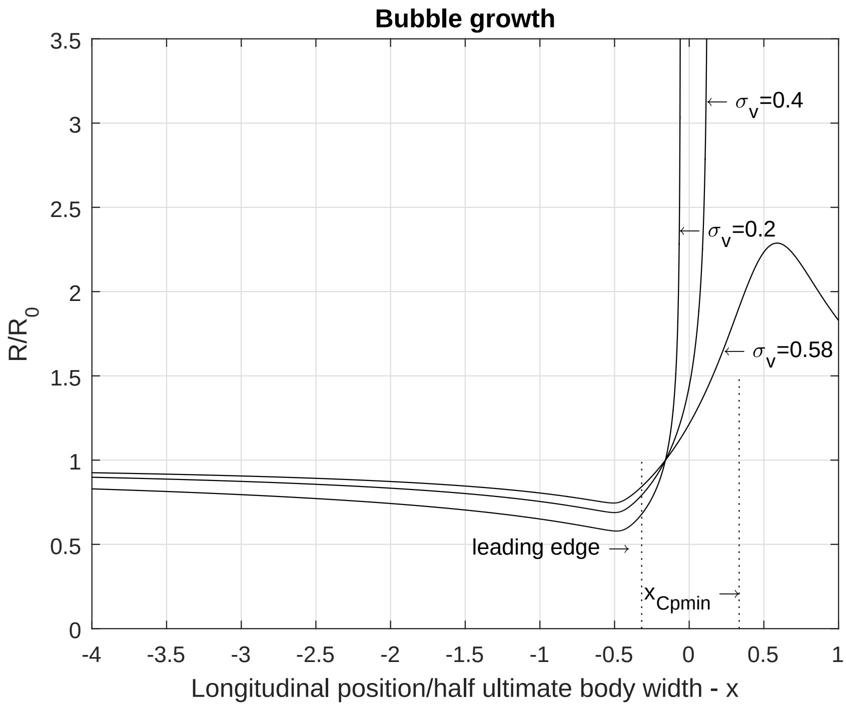

Figure 1.4: Variation of the size of a gas nucleus along its trajectory

It can be seen that the stability is not fully comparable. When the bubble growth of $\sigma_v = 0.58$ is taken as a reference, the bubble growth is slightly lower than the growth calculated by Johnson and Hsieh. The according trajectories can be seen in Figure 1.5.

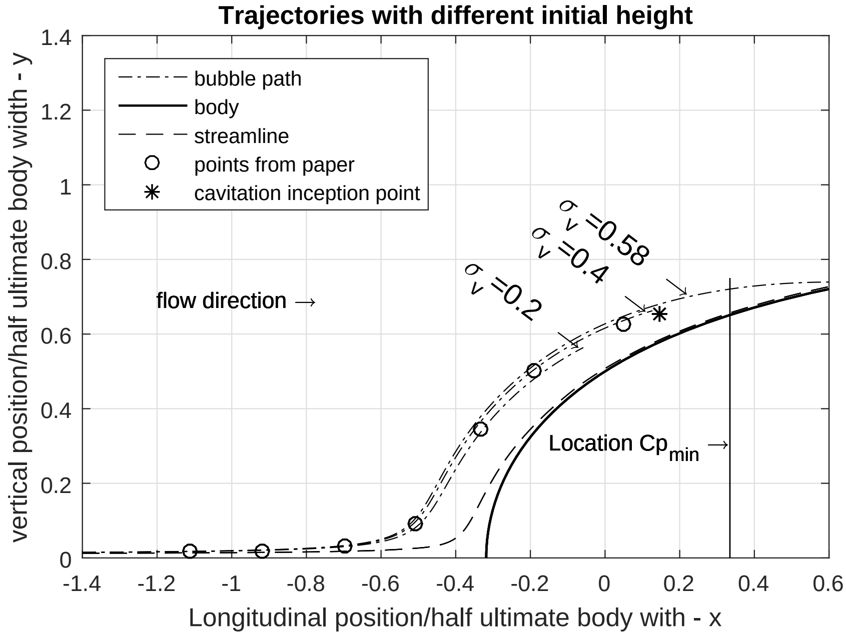

Figure 1.5: Bubble trajectories with different cavitation number

Critical size of bubble

The seventh figure in [1] is also compared. If one looks in [1] at $h = 0.6\,in$ and $R_0' = 0.02\,in$ ($R_0 \approx 0.033$) one can find that the critical cavitation number is around $\sigma_v \approx 0.46$, a slightly lower critical cavitation number of $\sigma_v \approx 0.43$ is found and can be seen in Figure 1.6.

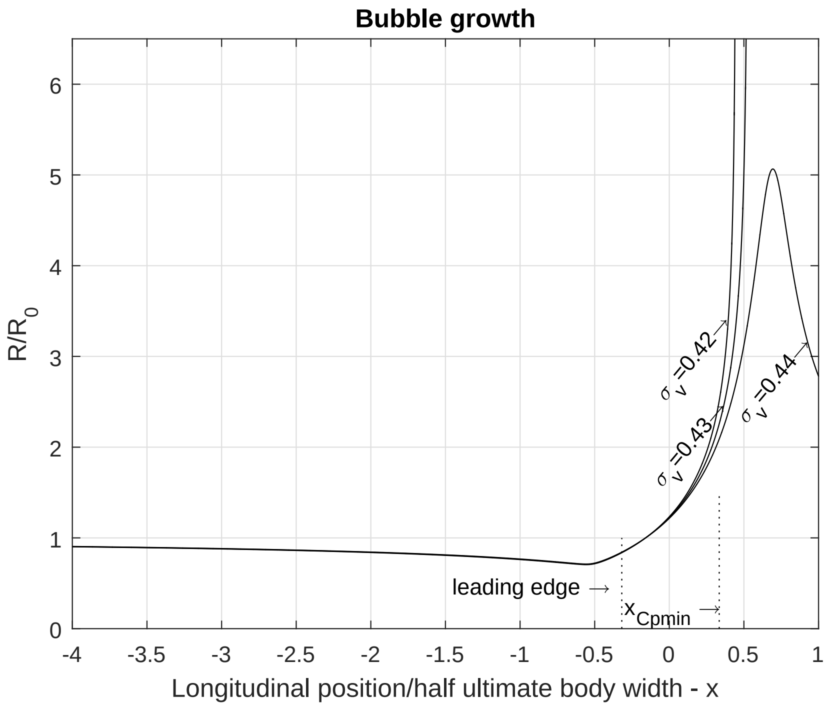

Figure 1.6: Variation of the size of a gas nucleus along its trajectory

The argument can also be turned around and it can be seen that the initial critical size of bubble is $R_0' = 0.02\,in$ if $h = 0.6\,in$ and $\sigma_v \approx 0.43$.

Discussion

The results found in the prior section are not the same as in [1]. A suggestion on the cause of this discrepancy might be the temporal step involved in solving the coupled differential equation. This time step is namely in this report variable, meaning that when more change in time is expected (derivative based) the temporal step automatically decreases. The time step or solving procedure of [1] is not known. The Runge-Kutta method is named, but in a later stadium and without a time step. Another option is that the transfer of dimensions causes some minor altered conditions. For example going from inch to meters requires some accuracy. It can not be ruled out that the these accuracies play a role.

The overall slightly higher trajectory will automatically lead to encountering less low pressures, which means less growth. This could be seen in Figure 1.4.

The general trends which can be seen in the results are that a higher initial height means a higher trajectory. A larger initial bubble radii means a higher trajectory. A higher trajectory means less growth. And finally a larger cavitation number means more stability.

The parameter describing the body size (h) as specified by Johnson and Hsieh is not clear. The flow Reynolds number is specified as $R_f = \frac{2hU}{\nu}$, by which h is most likely to represent the half body width. But shortly below the definition of the Reynolds number h is called the body size. Later on h is defined as the semi-thickness of the two-dimensional half body. In this report the semi-thickness is used as a definition for h, since this corresponds to both the Reynolds number and the non-dimensional flow field. The semi-thickness is therefore interpreted as the half body width when the body width is considered infinitely far downstream.

Interesting to note is that the same trajectory can be reproduced by combining the main parameters of the flow (body size, h, initial bubble radius, R_0' and free stream velocity, U). For example the same trajectory can be reproduced with a higher free stream velocity (25 times higher, $381\,m/s$). This free stream velocity is however approximately a quarter of the speed of sound in water and therefore not realistic. The observation however is interesting. Another example of this phenomena is increasing the initial bubble size by a factor of $1\frac{2}{3}$ and increasing the body size by a factor of 2, this combination also leads to the same trajectory. The figures are not included since the result is the same as in Figure 1.1.

Conclusions

The objective of this chapter was to reproduce the results found in the literature, more specifically those found in [1]. This has been done quite successfully, but needs further investigation. The trajectories were overall slightly higher which led to different growth figures for the bubbles. The difference in results are minor, and might be explained by the different solving procedure or the transfer of units.

The model itself however has been reproduced, and the trends in the results are the same. Because the trends reflect physical effects, the model is adequate in providing theoretical understanding.

2. Expanding the basic model

In the prior chapter the paper by Johnson and Hsieh has been reviewed. In this chapter their basic model will be expanded, by both a more advanced equation of motion and a more advanced equation for the bubble dynamics.

Review of equations

In this section a brief overview will be given of the new derived equations.

Bubble growth

Rayleigh-Plesset equation

To describe the bubble growth multiple methods are possible, the most convenient one being the Rayleigh-Plesset equation. The Rayleigh-Plesset equation is given in Eq. 2.1.

$$\rho_f \left[R' \frac{d^2 R'}{dt^2} + \frac{3}{2} \left(\frac{dR'}{dt} \right)^2 \right] = p_v - p + p_g(t) - 2\frac{\gamma}{R'} - \frac{4\mu_f}{R'} \frac{dR'}{dt} \tag{2.1}$$

The derivation of Eq. 2.1 is based on the mass conservation equation and the Navier-Stokes equations. In the derivation a spherical bubble is assumed. The derivation can be seen in Appendix E. In Appendix E the derivation of the dimensionless form of the Rayleigh-Plesset equation is given as well, the outcome can be seen in Eq. 2.2.

$$\frac{d^2 R}{d\tau^2} = \frac{1}{R} \left[-\frac{3}{2} \left(\frac{dR}{d\tau} \right)^2 + \frac{1}{2} \left(-C_p - \sigma_v \right) + \left(\frac{1}{2}\sigma_v + \frac{4}{W} \right) \left(\frac{R_0}{R} \right)^{3\frac{c_p}{c_v}} - \frac{4h}{W R_0' R} - \frac{8}{R_f R} \frac{dR}{d\tau} \right] \tag{2.2}$$

The general Keller-Herring equation

The Rayleigh-Plesset equation does not include damping. And it assumes that the wall velocity of the bubble is not close to that of the speed of sound. The damping of the bubble's dynamic behavior is partly due to the energy loss in the radiation of a sound wave (at high enough wall velocities) and partly due to the rise in temperature of the gas in the bubble due to the fast volumetric change. The first effect is included in the general Keller-Herring equation, which is derived in Appendix E. The outcome can be seen in Eq. 2.3.

$$\begin{aligned}\left(1-(\lambda+1)\frac{\frac{dR'}{dt}}{c}\right)\rho_f R'\frac{d^2R'}{dt^2}+\frac{3}{2}\frac{dR'}{dt}^2\rho_f\left(1-(\lambda+\frac{1}{3})\frac{\frac{dR'}{dt}}{c}\right)=\\ \left(1+(1-\lambda)\frac{\frac{dR'}{dt}}{c}\right)[p_v-p+p_g(t)]+\frac{R'}{c}\frac{dp_g(t)}{dt}-4\mu\frac{\frac{dR'}{dt}}{R'}-\frac{2\gamma}{R'}\end{aligned} \tag{2.3}$$

If the factor λ is set to 0 the Keller-Miksis equation is found, and if λ is set to 1 the equation used by Herring and Trilling is found.
Eq. 2.3 can be completed using the van der Waals equation of state given in Eq. 2.4.

$$p_g\left(R'^3-R'^3_{hc}\right)^\kappa=C \tag{2.4}$$

In Eq. 2.4 C is a constant and R'_{hc} is the van der Waals hard core radius which is $R'_{hc}=\frac{R'_0}{8.54}$ ([4]) for air. Using Eq. 2.4 to non-dimensionalize Eq. 2.3 gives Eq. 2.5.

$$\begin{aligned}&\left(1-(\lambda+1)\dot{R}\frac{U}{c}\right)R\ddot{R}+\frac{3}{2}\dot{R}^2\left(1-\left(\lambda+\frac{1}{3}\right)\dot{R}\frac{U}{c}\right)=\\ &\frac{1}{2}\left(1+(1-\lambda)\dot{R}\frac{U}{c}\right)\left[-\sigma_v-C_p+\left(\sigma_v+\frac{8}{W}\right)\left(\frac{R_0^3-R_{hc}^3}{R^3-R_{hc}^3}\right)^\kappa\right]\\ &+R\frac{U}{c}\left(\frac{1}{2}\sigma_v+\frac{4}{W}\right)\left[\frac{3\kappa R^2\left(\frac{R_0^3-R_{hc}^3}{R^3-R_{hc}^3}\right)^\kappa}{R_{hc}^3-R^3}\right]-\frac{8}{R_f}\frac{\dot{R}}{R}-\frac{4}{W}\frac{R_0}{R}\end{aligned} \tag{2.5}$$

So an alternative for the Rayleigh-Plesset equation is found. It is still a second-order ODE.

Equation of motion

The equation of motion is constructed using the force balance of the bubble. A very elaborate derivation of an equation of motion of a solid sphere in creeping flow is given by Maxey and Riley [5]. Starting from their equation of motion the equation of motion which will be used is derived in Appendix F, the outcome being Eq. 2.6.

$$\underbrace{\frac{4}{3}\pi R'^3(\frac{1}{2}\rho_f+\rho_b)\frac{d\boldsymbol{w}_b}{dt}}_{\text{Accelerating force}}=\underbrace{\frac{1}{2}\rho(\boldsymbol{w}-\boldsymbol{w}_b)|\boldsymbol{w}-\boldsymbol{w}_b|C_D\pi R'^2}_{\text{Drag force}}-\underbrace{\frac{3}{2}\frac{4}{3}\pi R'^3\boldsymbol{\nabla}p}_{\text{Pressure force}}+\underbrace{\frac{4}{3}\pi R'^3\boldsymbol{g'}(\rho_b-\rho_f)}_{\text{Buoyancy force}}$$
$$+\underbrace{2\pi\rho_f R'^2(\boldsymbol{w}-\boldsymbol{w}_b)\frac{dR'}{dt}}_{\text{Changing volume force}} \tag{2.6}$$

Eq. 2.6 is the result of assuming steady potential flow with a one-way coupling of the bubble dynamics equation and neglecting fluid acceleration. The dimensionless form of this equation is given in Eq. 2.7.

$$\frac{d\boldsymbol{w}_b}{d\tau}=\frac{9\alpha}{R^2R_f}\frac{C_DR_b}{24}(\boldsymbol{w}-\boldsymbol{w}_b)-\frac{3}{4}\alpha\boldsymbol{\nabla}C_p+\boldsymbol{g}\beta+\frac{3}{2}\frac{\alpha}{R}(\boldsymbol{w}-\boldsymbol{w}_b)\frac{dR}{d\tau} \tag{2.7}$$

Where $\alpha=\frac{\rho_f}{\rho_b+\frac{1}{2}\rho_f}$ and $\beta=\frac{\rho_b-\rho_f}{\rho_b+\frac{1}{2}\rho_f}$, and $\boldsymbol{w}$ is now dimensionless.

The equation found in this report is the same as in the paper by Farrell [6]. The only difference is the history force, which will be included later on, and the inclusion of the mass of the bubble.

Application to a two-Dimensional half body in an infinite fluid

This part will not change compared to [1].

Solving the system of ODE's

The system of ODE's will again be a second-order system of coupled non-linear Ordinary Differential Equations. The method for solving will again be using the ode function in MATLAB. The order of the system needs to be reduced, which is done in Appendix G. In Appendix G the initial conditions are given as well and are straightforward.

Results

The results will be discussed in terms of the trajectory and in terms of the bubble growth. The trajectories will be discussed first.

Trajectories

The trajectories will be shown with more forces included successively.

First the original equation (neglecting the mass of the bubble, gravity and the volume changing force) in combination with the Rayleigh-Plesset equation is shown in Figure 2.1.

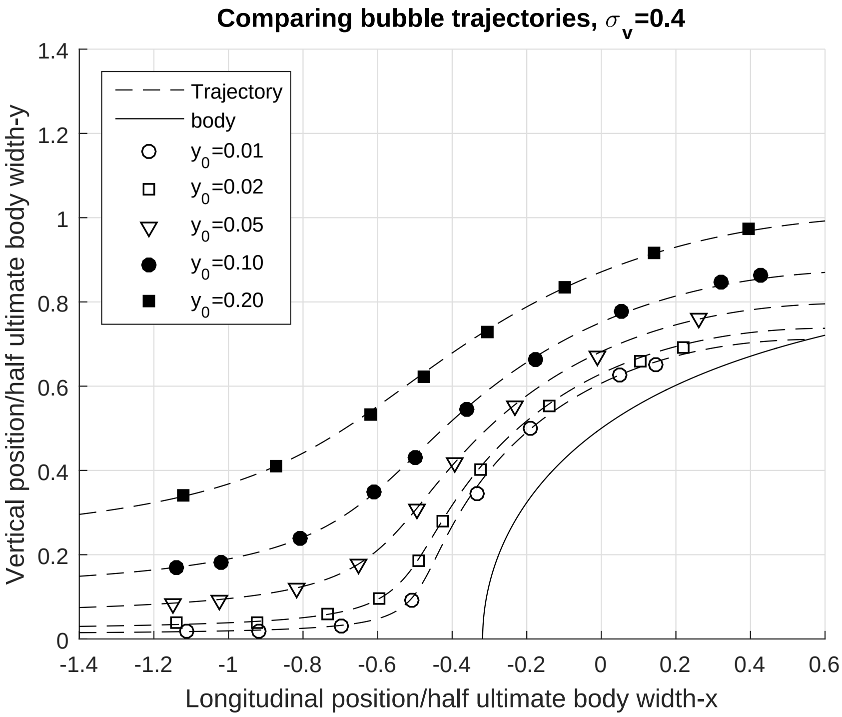

Figure 2.1: Bubble trajectories with the Rayleigh-Plesset equation, compared with the results from [1].

It can be seen in Figure 2.1 that the trajectories slightly deviate in the region where the bubble is growing.

Including the mass of the bubble and the volume-changing force gives Figure 2.2.

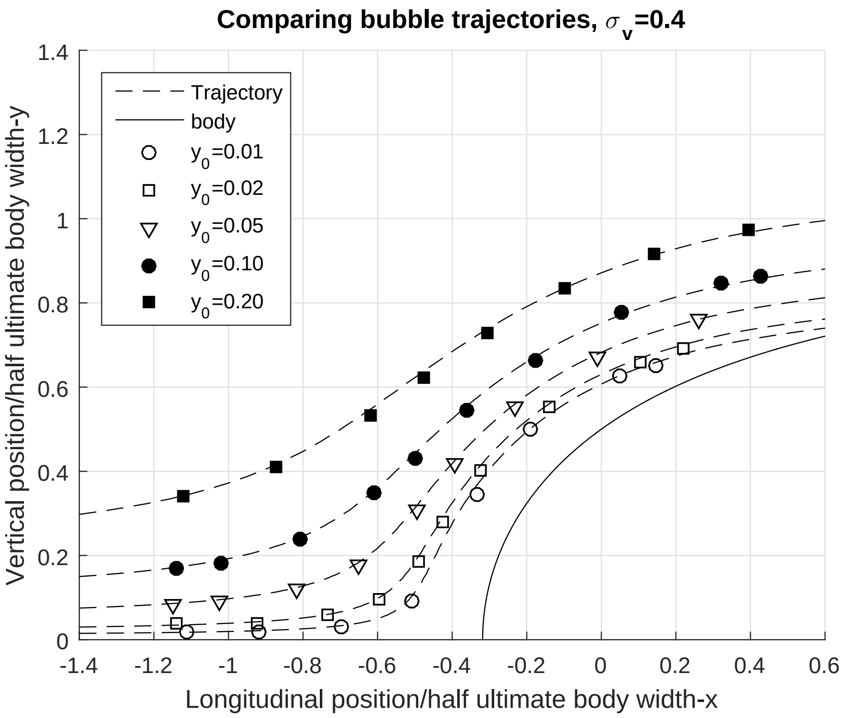

Figure 2.2: Bubble trajectories with the Rayleigh-Plesset equation and the volume changing force and mass of the bubble, compared with the results from [1].

The differences between Figure 2.1 and Figure 2.2 are small. This is because, as will be shown later, the $\frac{dR}{dt}$-term is not very large. At the end of the trajectory, there where the bubble hits the body, the effect of the collapsing bubble can be seen, see Figure 2.3.

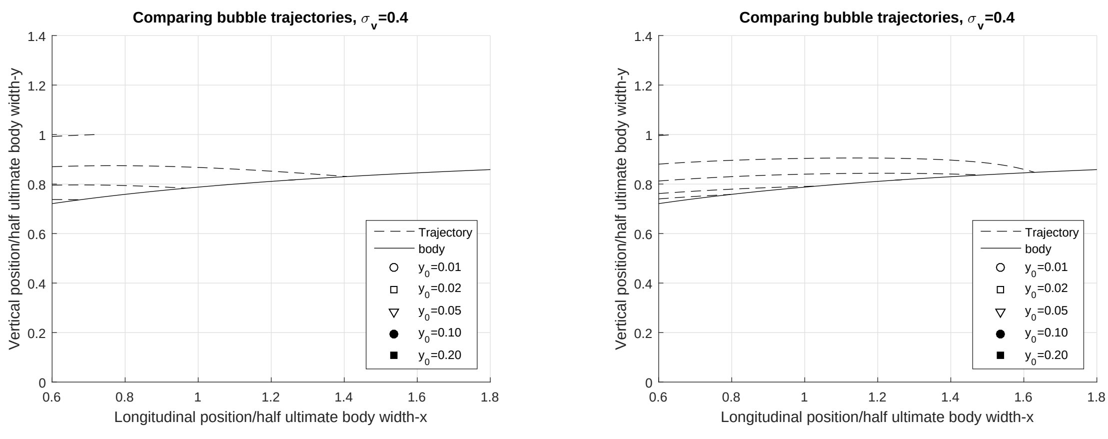

(a) Without volume-changing force and mass of the bubble

(b) With volume-changing force and mass of the bubble

Figure 2.3: Comparison of the trajectories with different forces

In Figure 2.3 it can be seen that when the pressure increases, and thus the bubble shrinks (fast), the bubble is drawn towards the body. When the trajectory exceeds 1 in the vertical height the calculations are stopped. The trajectories are still introduced at roughly the same height at $x = 0.6$, but start to deviate when the bubble collapses. The bubble collapse can be seen in Figure 2.13(a) and will be discussed later on. The effect of the mass of the bubble indeed seems to be negligible, but gives the opportunity to switch to solid particles easily.

Including gravity means introducing the bouyancy force. This force significantly influences the results. This can be seen in Figure 2.4.

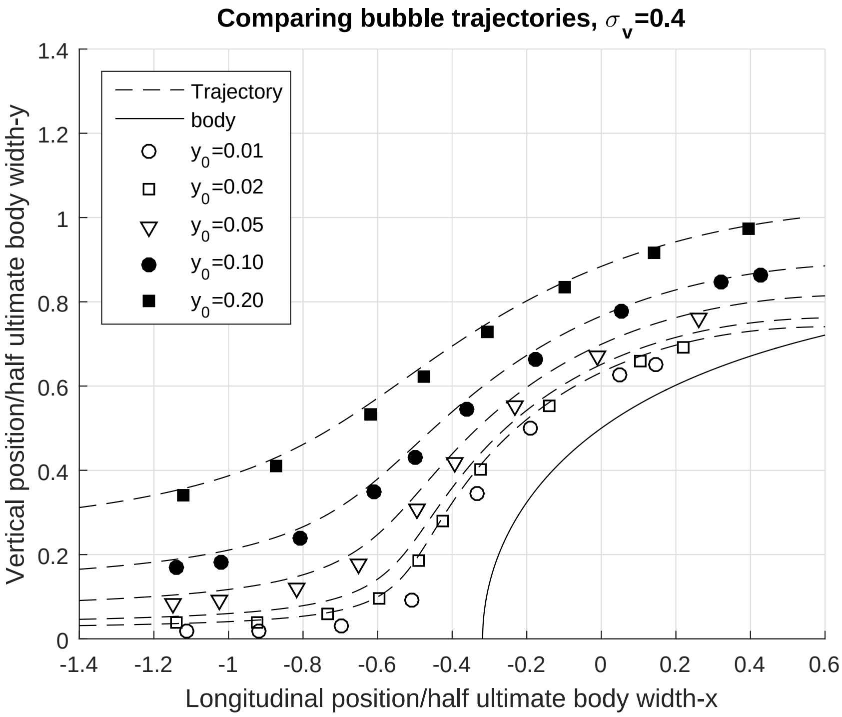

Figure 2.4: The bubble trajectories with the full equation of motion and the Rayleigh-Plesset equation

The bubbles are released at the same starting position ($x = -10$), but because the bubble is lighter than water the bubble rises, and therefore the vertical position at which the bubble reaches the body is higher. Since the bubbles are further away from the body the bubbles encounter less low pressures, meaning less violent collapses, by which the $\frac{dR}{dt}$-term is less influential. This can lead to a more straight trajectory near the body, which can be seen in Figure 2.5.

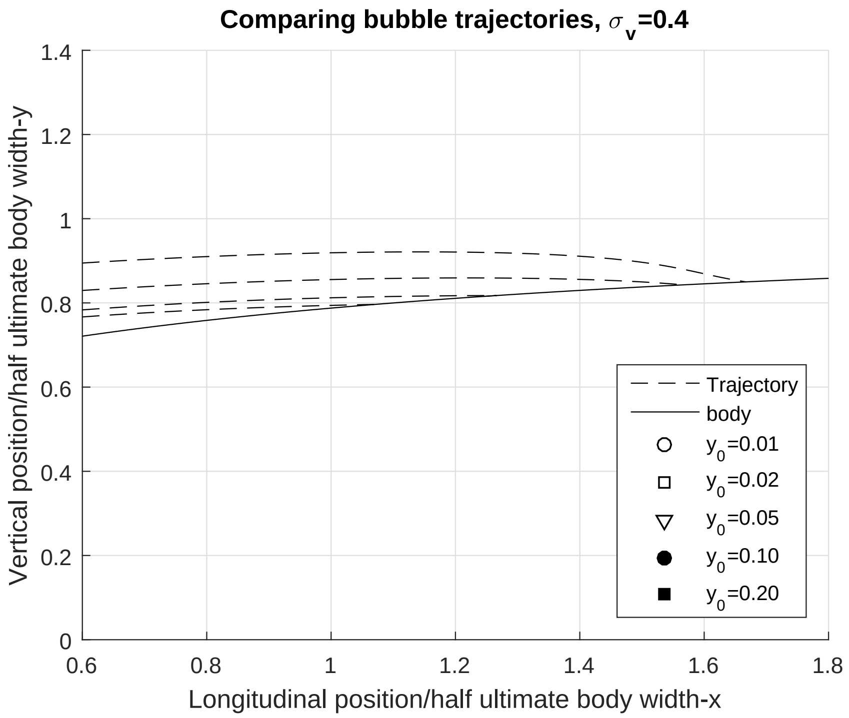

Figure 2.5: The end of the trajectories

So including buoyancy makes the bubbles hit the body further down stream.

The general Keller-Herring equation will also be used for the bubble growth with $\lambda = 0$. The result can be seen in Figure 2.6

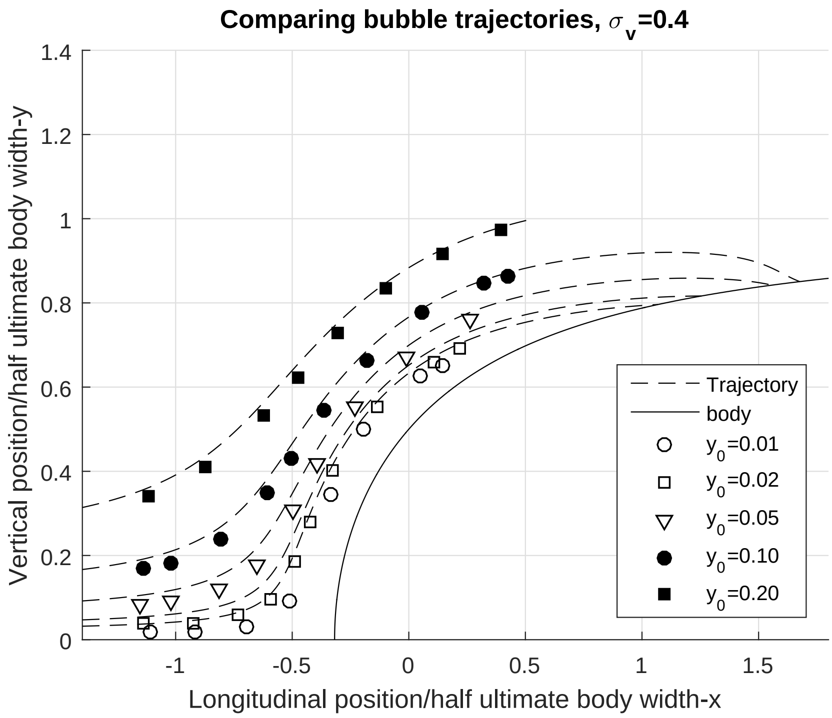

Figure 2.6: Bubble trajectories with full equation of motion and the general Keller-Herring equation with the van der Waals equation of state and $\lambda = 0$

The trajectories are practically the same as those when the Rayleigh-Plesset equation is used. The calculation with the general Keller-Herring equation is faster in terms of computational time due to the damping term.

Stability

The stability of the bubble will be observed with an initial condition of $y_0 = 0.01$ and with a cavitation number of $\sigma_v = [0.2\ 0.4]$. The bubble is either in the first growing state or in the first collapsing state when it hits the body. For that reason the calculation will be continued in the body to show the behavior of both equations.

The pressure input for both equations can be seen in Figure 2.7.

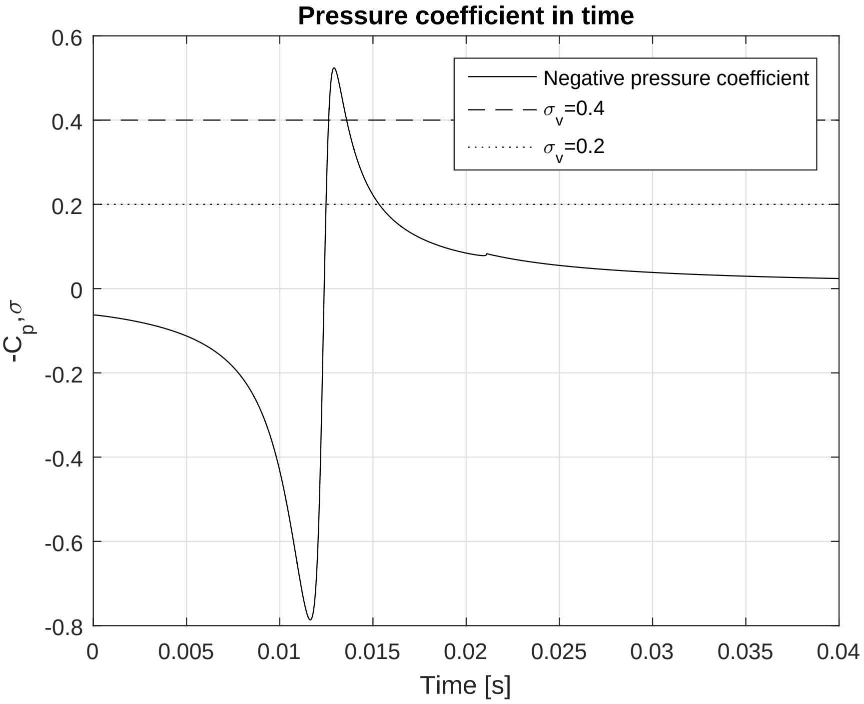

Figure 2.7: Pressure input to show the reaction of both equations

First the behavior of the Rayleigh-Plesset equation can be seen in Figure 2.8.

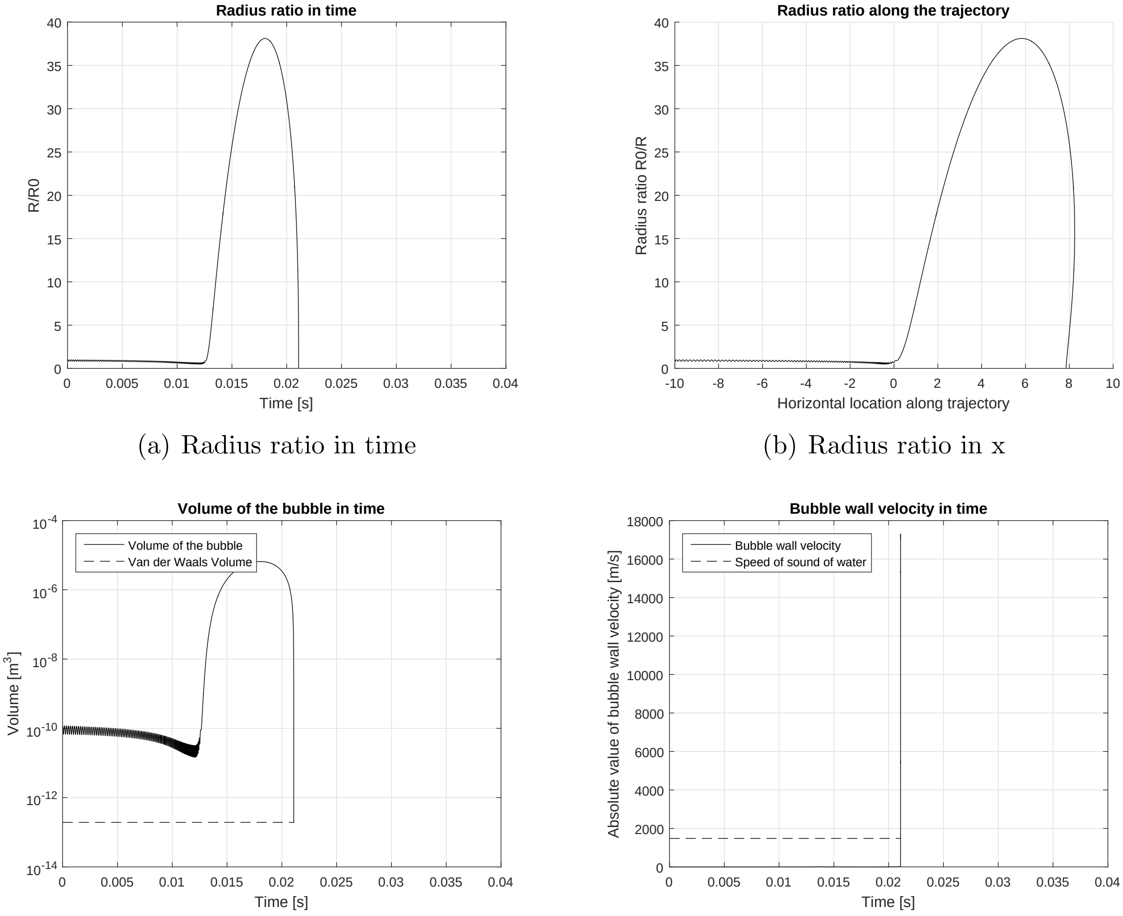

(a) Radius ratio in time

(b) Radius ratio in x

(c) Volume of the bubble in time

(d) Velocity of the wall in time

Figure 2.8: Behavior of the Rayleigh-Plesset equation in the flow field, not stopped by the body, $y_0 = 0.01$ and $\sigma_v = 0.2$.

The integration is stopped since the collapse is too violent. The bubble wall velocity can be seen to be well above the speed of sound, the bubble volume is only just above the van der Waals volume and the bubble is moving backwards in the flow at the time of the collapse. Furthermore it can be seen that the initial condition is not the equilibrium initial condition since the bubble radius oscillates.

If the cavitation number is increased, Figure 2.9 is found. In Figure 2.9 it can be seen that the Rayleigh-Plesset equation does not damp the solution. The rebound of the bubble is only lower because of the increased pressure. Due to the increased pressure the collapses becomes more violent as can be seen by the increasing wall velocity.

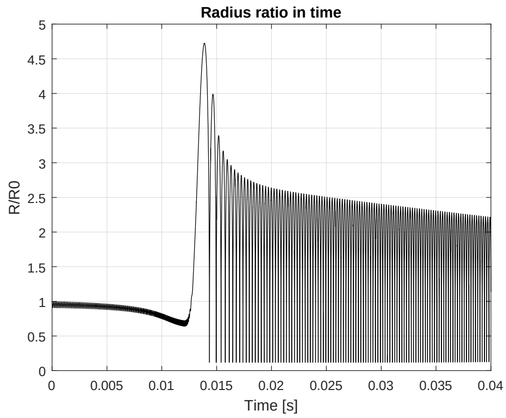

(a) Radius ratio in time

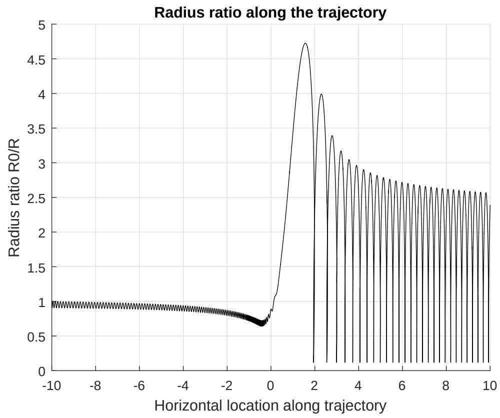

(b) Radius ratio in x

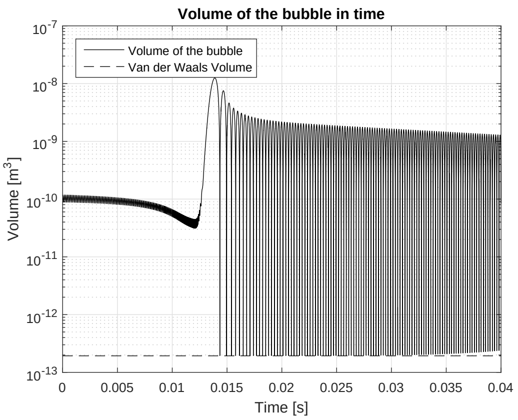

(c) Volume of the bubble in time

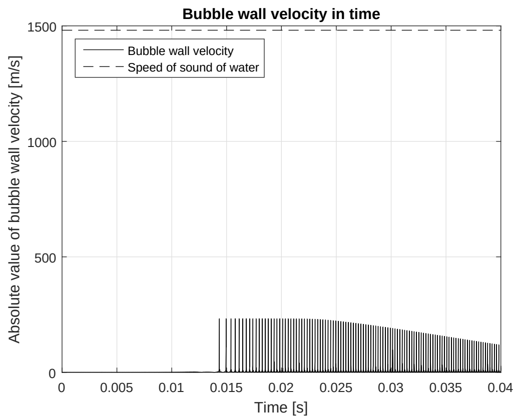

(d) Velocity of the wall in time

Figure 2.9: Behavior of the Rayleigh-Plesset equation in the flow field, not stopped by the body, $y_0 = 0.01$ and $\sigma_v = 0.4$.

Now the behavior of the general Keller-Herring equation is studied. The outcome can be seen in Figure 2.10.

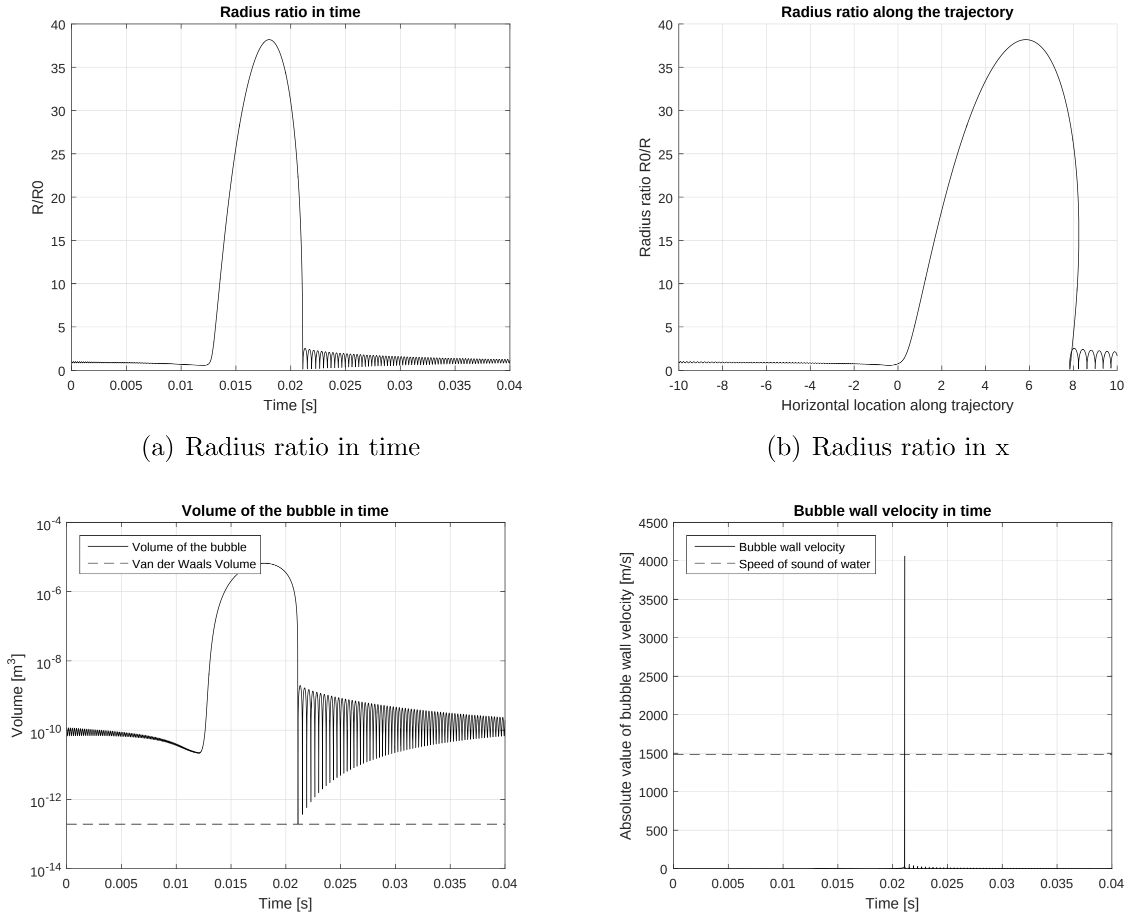

(a) Radius ratio in time

(b) Radius ratio in x

(c) Volume of the bubble in time

(d) Velocity of the wall in time

Figure 2.10: Behavior of the general Keller-Herring equation in the flow field, not stopped by the body, $y_0 = 0.01$ and $\sigma_v = 0.2$.

In Figure 2.10 it can be seen that the bubble radius strives more to its equilibrium size. The damping can clearly be seen, and the bubble wall velocity is significantly lower than the speed of sound after the first rebound. Still the bubble moves backwards due to the volume-changing force. The oscillation due to the initial condition is suppressed.

The same can be done with a higher cavitation number, see Figure 2.11.

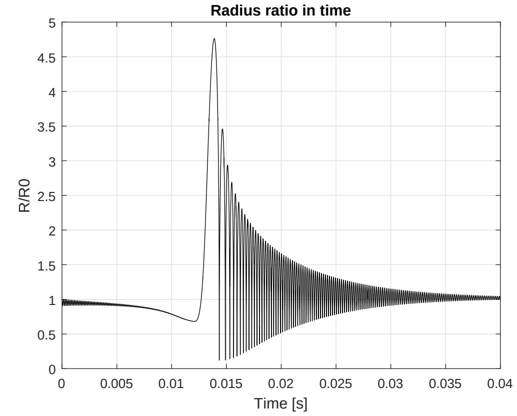

(a) Radius ratio in time

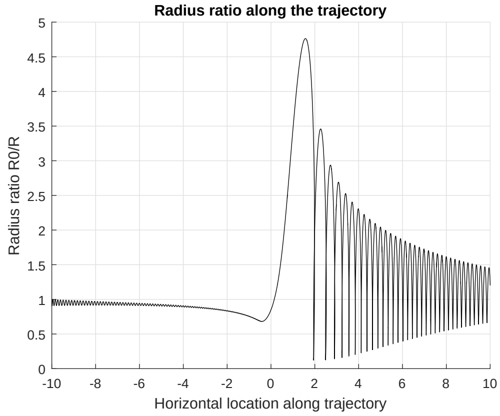

(b) Radius ratio in x

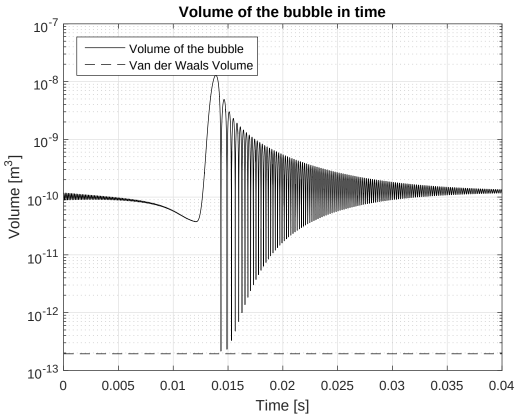

(c) Volume of the bubble in time

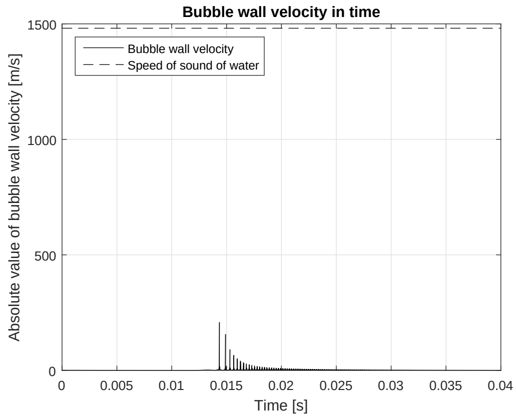

(d) Velocity of the wall in time

Figure 2.11: Behavior of the general Keller-Herring equation in the flow field, not stopped by the body, $y_0 = 0.01$ and $\sigma_v = 0.4$.

It can be seen that the bubble wall velocity stays very low. So all the damping comes from the $\frac{dp_g}{dt}$-term. The volume is now well above the van der Waals volume.

The stability of the bubble is only of physical importance if the bubble is still in the flow, because after the bubble hits the body contour the bubble “enters” the body. Therefore the calculation is stopped at the point where the bubble hits the body. The outcome of the bubble growth for the Rayleigh-Plesset equation can be seen in Figure 2.12.

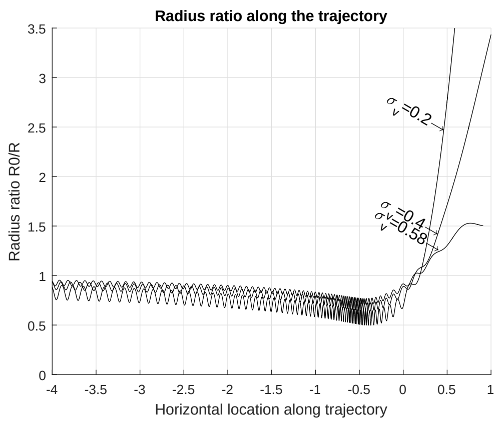

(a) Zoomed in like in [1]

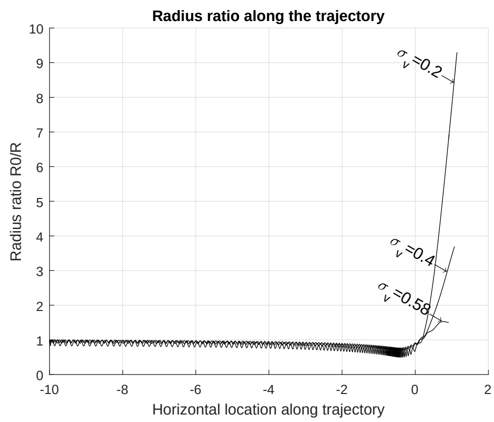

(b) Full range

Figure 2.12: Stability of the bubble along its trajectory with the Rayleigh-Plesset equation, the cavitation number increases with increasing steepness of the curve, with $\sigma_v = [0.2\ 0.4\ 0.58]$, $y_0 = 0.01$

In Figure 2.12 it can be seen that the initial oscillations only damp out when the bubble starts to grow. Furthermore it can be seen that the bubble does not get to the collapsing state. When the initial condition $y_0 = 0.05$ is taken the collapse of the bubble can be seen with $\sigma_v = 0.4$, see Figure 2.13.

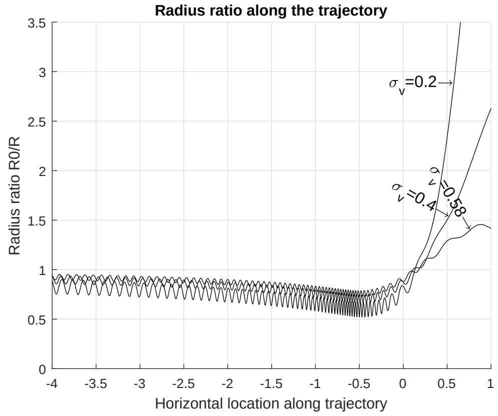

(a) Zoomed in like in the paper

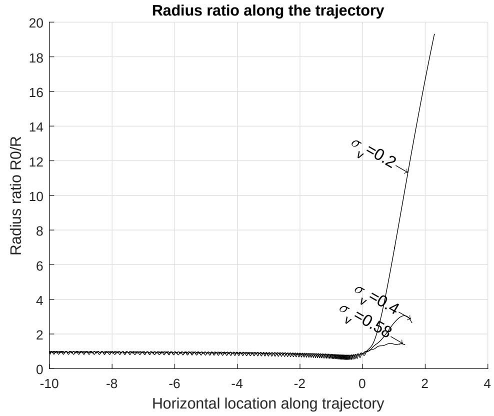

(b) Full range

Figure 2.13: Stability of the bubble along its trajectory with the Rayleigh-Plesset equation, the cavitation number increases with increasing steepness of the curve, with $\sigma_v = [0.2\ 0.4\ 0.58]$, $y_0 = 0.05$

The influence of the collapse of the bubble could also be seen in Figure 2.3(b).

The same bubble growth figures can also be made for the general Keller-Herring equation with $\lambda = 0$, see Figure 2.14.

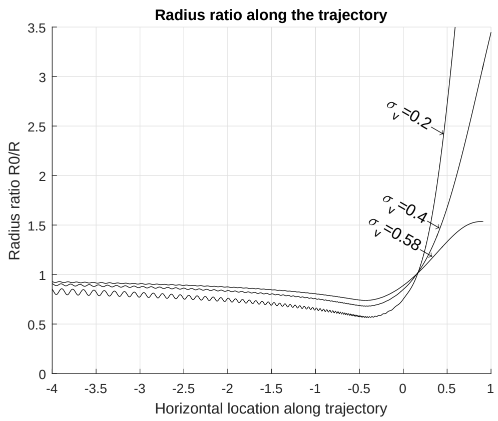

(a) Zoomed in like in the paper

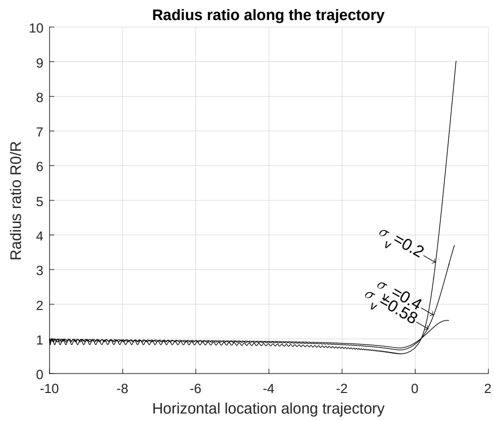

(b) Full range

Figure 2.14: Stability of the bubble along its trajectory with the general Keller-Herring equation ($\lambda = 0$), the cavitation number increases with increasing steepness of the curve, with $\sigma_v = [0.2\ 0.4\ 0.58]$, $y_0 = 0.01$

It can be seen that the Keller-Herring equation causes much smaller oscillations in the bubble radius, but the growth of the bubble radius is similar. For $y_0 = 0.05$, see Figure 2.15.

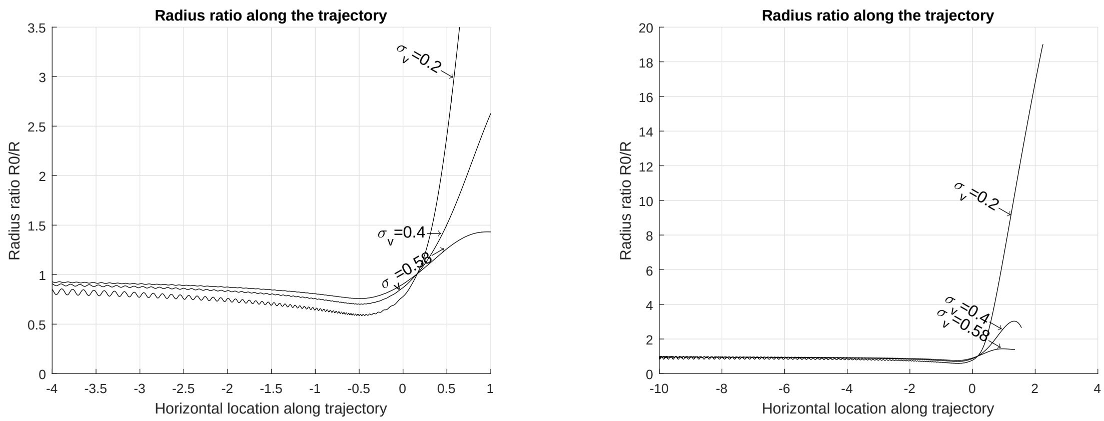

(a) Zoomed in like in the paper

(b) Full range

Figure 2.15: Stability of the bubble along its trajectory with the general Keller-Herring equation ($\lambda = 0$), the cavitation number increases with increasing steepness of the curve, with $\sigma_v = [0.2\ 0.4\ 0.58]$, $y_0 = 0.05$

Lastly it will be interesting to check the stability without gravity and volume-changing force, since the trajectories were in good agreement with [1] without these forces. The result can be seen in Figure 2.16.

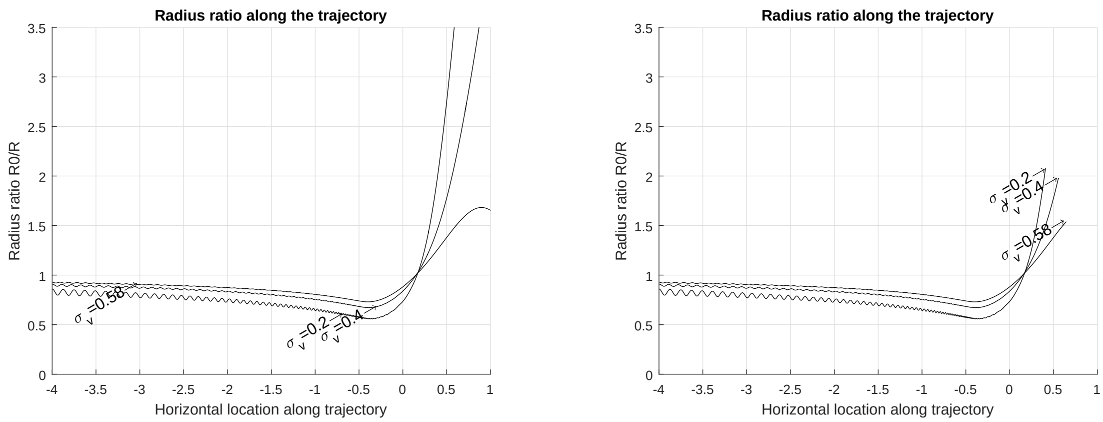

(a) Continue in body

(b) Stops when the body is hit

Figure 2.16: Stability of the bubble along its trajectory with the general Keller-Herring equation ($\lambda = 0$), the cavitation number increases with increasing steepness of the curve, with $\sigma_v = [0.2\ 0.4\ 0.58]$, $y_0 = 0.01$.

The bubble hits the body sooner because the bubble trajectory is closer to the body. Consequently, the ultimate bubble radius is smaller.

Discussion

In the discussion there will be looked at the results and the method. The terms in the equation of motion and the bubble growth will be discussed. Furthermore some extensions are discussed.

Equation of motion

The equation of motion is an extensive equation of motion under the assumption of steady potential flow. It is now interesting to see which forces are the most influential. In Figure 2.17 the forces can be seen on a log-scale (some extra damping is added to the Keller-Herring equation to disregard the vibration due to the initial condition). The force due to the mass of the bubble is not given.

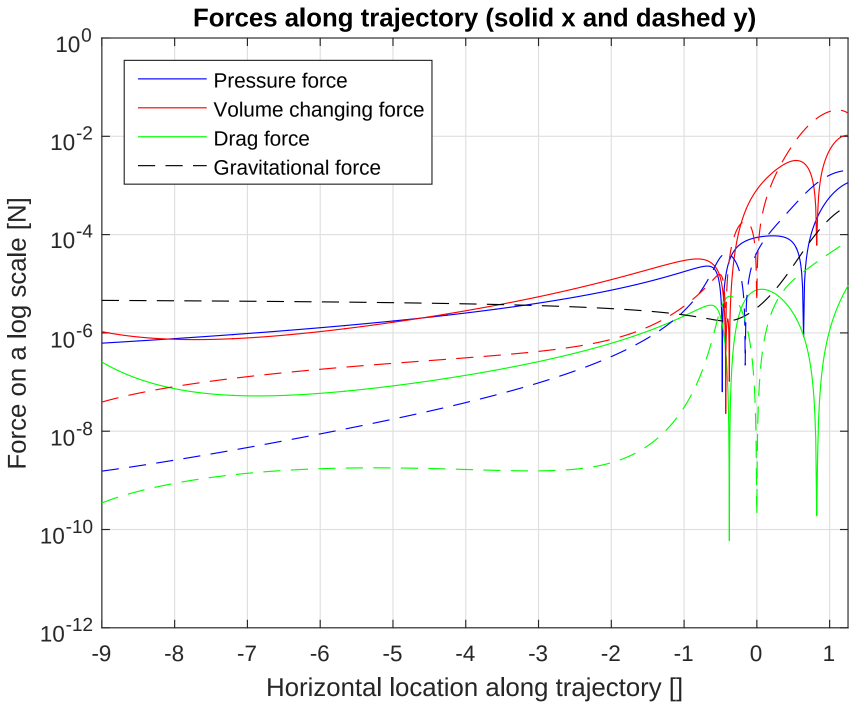

Figure 2.17: The absolute value of the forces along the trajectory, the solid lines are in the x-direction and the dashed lines are in the y-direction. $y_0 = 0.01$ and $\sigma_v = 0.4$

It can be seen that the gravitational force is the most influential in the beginning, leading to a rise of the bubble. The drag force is smaller than the pressure force, meaning that in the absence of the other forces the drag force is fully reactionary on the pressure force. As the body is approached the bubble shrinks, this leads to a lower body force (see the gravitational force). After the maximum pressure is passed the bubble grows, and the body force grows. It can be seen that the volume-changing force is the force with the highest magnitude. In most cases it is however in the direction of the trajectory since

the flow determines the trajectory of the bubble, and therefore the slip velocity of the bubble is in the direction of the trajectory. The bubble is not yet in the collapsing phase. In the collapsing phase (see Figure 2.14(b)) this force will become influential since a small difference in velocity direction between the bubble and the flow will be enlarged by the collapsing speed. In Figure 2.3(b) one can see the first minor effect of this force, since the bubble starts to shrink before hitting the body.
The added force which is the most influential is the gravitational force (buoyancy). This force namely couples the initial condition y_0 with the initial condition x_0.

Bubble growth

The bubble growth will be calculated in an accurate and physically relevant way by the general Keller-Herring equation. The Rayleigh-Plesset equation introduces oscillations in the presented model, and the oscillations require smaller time steps leading to higher computational times. The missing damping in the Rayleigh-Plesset equation will be a bigger problem when the bubble implodes before it hits the body. The presented method by Johnson and Hsieh is not very accurate in terms of bubble growth, but the gained accuracy in bubble growth can not be said to influence the bubble trajectories significantly.

Solid particle

The equations presented in this chapter can easily be used to let a solid particle approach the body. The bubble growth equation will be set to zero, so that the volume-changing force is zero. An example can be seen in Figure 2.18.

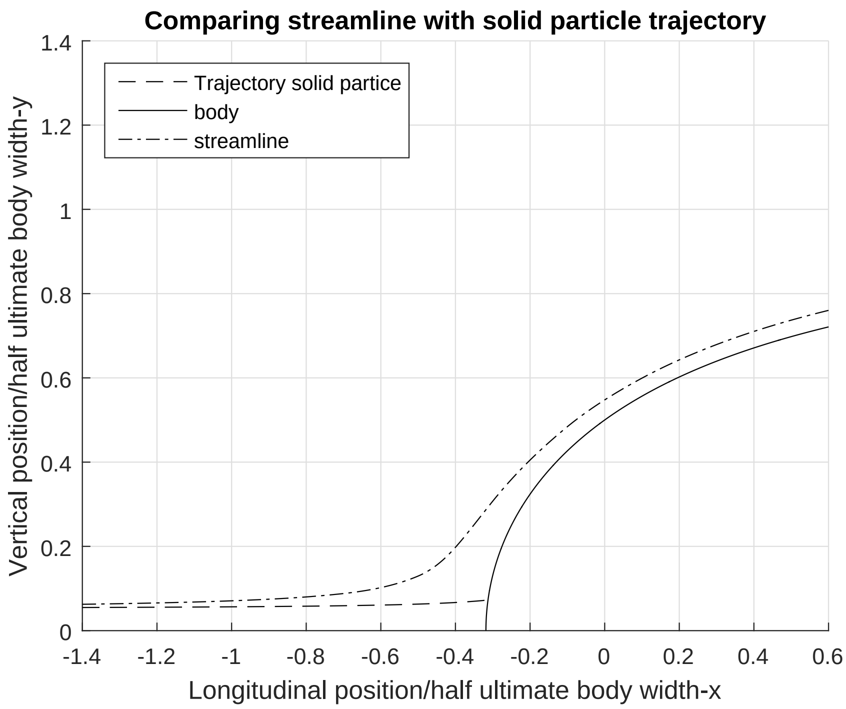

Figure 2.18: A solid particle with $y_0 = 0.05$ as initial condition, and density of $7800\,kgm^{-3}$

One sees the gravity pull the particle down, and the particle hits the body near the maximum pressure, this is possible since the particle is more dense than water.

History/Basset force

In this part the inclusion of the history force is being discussed, even though there are many ways in which to include the history force, the Basset force is taken. The history/Basset force is the force which accounts for the different time scales in the flow and that of the build up of the boundary layer of the bubble. The Basset force is based on the build up speed of the boundary layer of a flat plate, but can be used for nuclei. The Basset force is taken since this will be extendable easily. The equation from which will be started is given in Eq. 2.8.

$$\begin{aligned}\underbrace{\left(m_p + \frac{1}{2}m_f\right)\frac{dW_i}{dt}}_{\text{Accelaration force}} + \underbrace{\frac{1}{2}4\pi\rho_f a^2\frac{da}{dt}W_i}_{\text{Changing volume force}} + \underbrace{6\pi a^2\mu\int_{-\infty}^{t}\frac{dW_i}{d\tau}\left[\pi\nu(t-\tau)\right]^{-1/2}d\tau}_{\text{History force}} = \\ -\underbrace{\frac{1}{2}\rho_f C_D\pi a^2 W_i^2}_{\text{Drag force}} - \underbrace{\frac{3}{2}\frac{4\pi}{3}a^3\boldsymbol{\nabla}p}_{\text{Pressure force}} + \underbrace{\left(m_p - m_f\right)g_i}_{\text{Buoyancy force}} - \underbrace{m_p\frac{d\boldsymbol{w}}{dt}}_{\text{Acceleration force}}\end{aligned} \tag{2.8}$$

This equation can be written as Eq. 2.9.

$$
\underbrace{\left(m_p + \frac{1}{2}m_f\right)\frac{d\boldsymbol{w_b}}{dt}}_{\text{Accelaration force}} = \underbrace{\frac{1}{2}4\pi\rho_f R'^2 \frac{dR'}{dt}(\boldsymbol{w} - \boldsymbol{w_b})}_{\text{Changing volume force}} + \underbrace{6\pi R'^2 \mu \int_{-\infty}^{t} \frac{d\boldsymbol{w} - \boldsymbol{w_b}}{d\tau}\left[\pi\nu(t-\tau)\right]^{-1/2} d\tau}_{\text{History force}}
$$

$$
+ \underbrace{\frac{1}{2}\rho_f C_D \pi R'^2 (\boldsymbol{w} - \boldsymbol{w_b})|\boldsymbol{w} - \boldsymbol{w_b}|}_{\text{Drag force}} - \underbrace{2\pi R'^3 \boldsymbol{\nabla} p}_{\text{Pressure force}} + \underbrace{(m_p - m_f)\, g_i'}_{\text{Buoyancy force}} + \underbrace{\frac{1}{2}m_f \frac{d\boldsymbol{w}}{dt}}_{\text{Acceleration force}} \tag{2.9}
$$

In dimensionless form this leads to Eq. 2.10.

$$
\begin{aligned}
\frac{d\boldsymbol{w_b}}{d\tau} =& \beta g_i - \frac{3}{4}\alpha \boldsymbol{\nabla} C_p + \frac{1}{2}\alpha \frac{d\boldsymbol{w}}{d\tau} + \frac{3}{2}\alpha \frac{1}{R}\frac{dR}{d\tau}(\boldsymbol{w} - \boldsymbol{w_b}) + \frac{3}{8}\alpha C_D \frac{1}{R}(\boldsymbol{w} - \boldsymbol{w_b})|\boldsymbol{w} - \boldsymbol{w_b}| \\
& \frac{9}{2}\alpha \frac{\frac{\nu}{\sqrt{\pi\nu\frac{h}{U}}}}{U}\frac{1}{R}\int_{-\infty}^{\tau} \frac{d(\boldsymbol{w} - \boldsymbol{w_b})}{d\tau'}(\tau - \tau')^{-\frac{1}{2}} d\tau'
\end{aligned} \tag{2.10}
$$

The integral of the history force can be written as:
$\int_{-\infty}^{\tau} \frac{d(\boldsymbol{w}-\boldsymbol{w_b})}{d\tau'} K(\tau-\tau')d\tau' = \int_{-\infty}^{\tau_0} \frac{d(\boldsymbol{w}-\boldsymbol{w_b})}{d\tau'} K(\tau-\tau')d\tau' + \int_{\tau_0}^{\tau} \frac{d(\boldsymbol{w}-\boldsymbol{w_b})}{d\tau'} K(\tau-\tau')d\tau'$

If it is assumed that the relative acceleration prior to and at the initial time τ_0 is zero, then the integral can be written as: $\int_{-\infty}^{\tau} \frac{d(\boldsymbol{w}-\boldsymbol{w_b})}{d\tau'} K(\tau-\tau')d\tau' = \int_{\tau_0}^{\tau} \frac{d(\boldsymbol{w}-\boldsymbol{w_b})}{d\tau'} K(\tau-\tau')d\tau'$

Note that from now on therefore the initial condition on the velocities is no longer zero, but the same as that of the flow (this makes the derivation more easy, and the result still useful). The integral presented goes to infinity when τ is filled in for τ'. This needs to be solved and will be done by splitting the integral once more: $\int_{-\infty}^{\tau} \frac{d(\boldsymbol{w}-\boldsymbol{w_b})}{d\tau'} K(\tau-\tau')d\tau' = \int_{\tau_0}^{\tau-\Delta\tau} \frac{d(\boldsymbol{w}-\boldsymbol{w_b})}{d\tau'} K(\tau-\tau')d\tau' + \int_{\tau-\Delta\tau}^{\tau} \frac{d(\boldsymbol{w}-\boldsymbol{w_b})}{d\tau'} K(\tau-\tau')d\tau'$.

If it is now assumed that the relative dimensionless acceleration is constant during the last time step, $\Delta\tau$. The integral can be written as: $\int_{-\infty}^{\tau} \frac{d(\boldsymbol{w}-\boldsymbol{w_b})}{d\tau'} K(\tau-\tau')d\tau' \approx \int_{\tau_0}^{\tau-\Delta\tau} \frac{d(\boldsymbol{w}-\boldsymbol{w_b})}{d\tau'} K(\tau-\tau')d\tau' + \frac{d(\boldsymbol{w}-\boldsymbol{w_b})}{d\tau'}|_{\tau-\frac{1}{2}\Delta\tau} \int_{\tau-\Delta\tau}^{\tau} K(\tau-\tau')d\tau'$. The integral over the Basset kernel can be found to be: $\int_{\tau-\Delta\tau}^{\tau} (\tau-\tau')^{-\frac{1}{2}} d\tau' = 2\sqrt{\Delta\tau}$. If then the acceleration at $\tau - \frac{1}{2}\Delta\tau$ is taken to be the average over the two points one finds: $\frac{d(\boldsymbol{w}-\boldsymbol{w_b})}{d\tau'}|_{\tau-\frac{1}{2}\Delta\tau} \approx \frac{1}{2}\left(\frac{d(\boldsymbol{w}-\boldsymbol{w_b})}{d\tau'}|_{\tau-\Delta\tau} + \frac{d(\boldsymbol{w}-\boldsymbol{w_b})}{d\tau'}|_{\tau}\right)$. So the conclusion on the integral can be seen in Eq. 2.11.

$$
\begin{aligned}
&\int_{-\infty}^{\tau} \frac{d(\boldsymbol{w} - \boldsymbol{w_b})}{d\tau'} K(\tau - \tau')d\tau' \approx \\
&\int_{\tau_0}^{\tau-\Delta\tau} \frac{d(\boldsymbol{w} - \boldsymbol{w_b})}{d\tau'}(\tau - \tau')^{-\frac{1}{2}} d\tau' + \left(\frac{d(\boldsymbol{w} - \boldsymbol{w_b})}{d\tau'}|_{\tau-\Delta\tau} + \frac{d(\boldsymbol{w} - \boldsymbol{w_b})}{d\tau'}|_{\tau}\right)\sqrt{\Delta\tau}
\end{aligned} \tag{2.11}
$$

In this way the history force is found in terms of the relative acceleration and in terms of the time step.
The focus is therefore now on finding the relative dimensionless acceleration of the bubble. This acceleration can be found by reusing the force balance. The procedure of implementing the history force is given below.

1. Calculate the trajectory of the bubble without using any history force.
2. Calculate the relative acceleration of the bubble and use this to calculate the history force.
3. Use the found history force as an input for the new trajectory calculation.
4. Then calculate the relative acceleration again based on all the forces including the prior used history force to find the new history force.
5. Repeat 3 and 4 until a certain convergence has been reached.

The convergence of this scheme is not that great, and will in practice depend on interpolation accuracy and ODE solver accuracy. This makes the history force inclusion hard. Errors of up to 0.01% can be reached, but after this there will not be much improvement, since always one or the other accuracy of the interpolation or the grid will come in to play. This can of course be altered, but that will mean having to decrease the time step such that this is not computationally efficient anymore. Therefore the reached error will be seen as sufficiently small. Another reason of this accuracy is the stiffness introduced by the introduction of the history force to the set of equations. This makes solving the system less accurate.

Falling sphere

To test the implementation of the history force in the way described above a test case of a falling sphere is used. This test case is also used in the paper by D.F. van Eijkeren [7] and can therefore be used as reference. The history force found after iteration can be seen in Figure 2.19, in the same Figure the reference plot can be seen.

As can be seen the forces are of the same order of magnitude, and are similar in shape and in final value, the peak value however is a bit higher in the iterative case. This might be due to the fact that not exactly the same model has been used for the drag force, or due to the fact that the model used in the iterative test case was more simplistic than the model used in the literature. Lastly it can be seen that the Basset force overestimates the history force significantly, as compared to the other history kernels (different functions for $K(\tau - \tau')$), see Figure 2.19(b).
A zoomed in version of the history/Basset force is shown in Figure 2.20. It can be seen that the history force converges, and that it is not completely smooth. This is due to the assumption of constant acceleration of the bubble during the last time step.

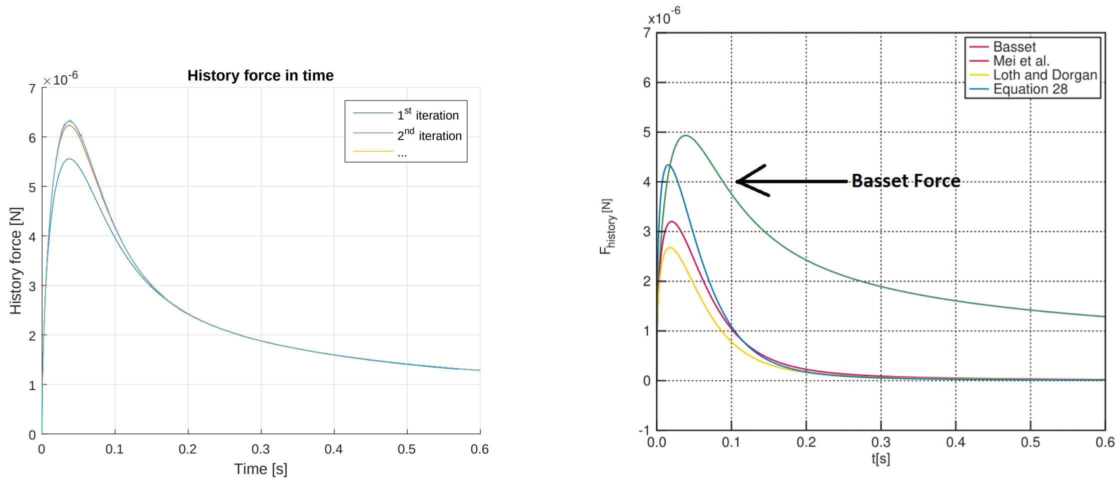

(a) Iterative calculation result (b) Result from literature [7]

Figure 2.19: Resulting History force found by iteration and discussed in literature

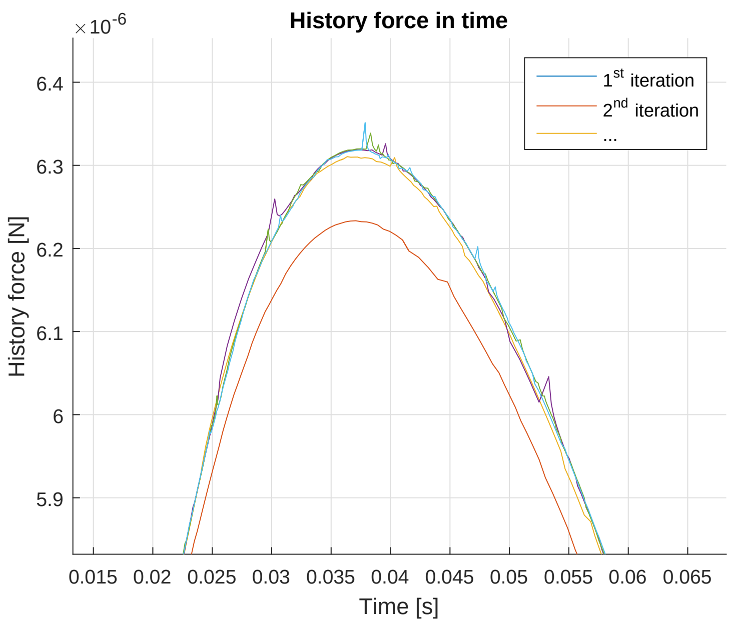

Figure 2.20: Zoomed in history force

The velocity in time is also shown in the reference literature. The comparison can be found in Figure 2.21.

Again it can be seen that the iterative procedure overestimates the velocity slightly, the possible explanations have been given. The end result is similar.

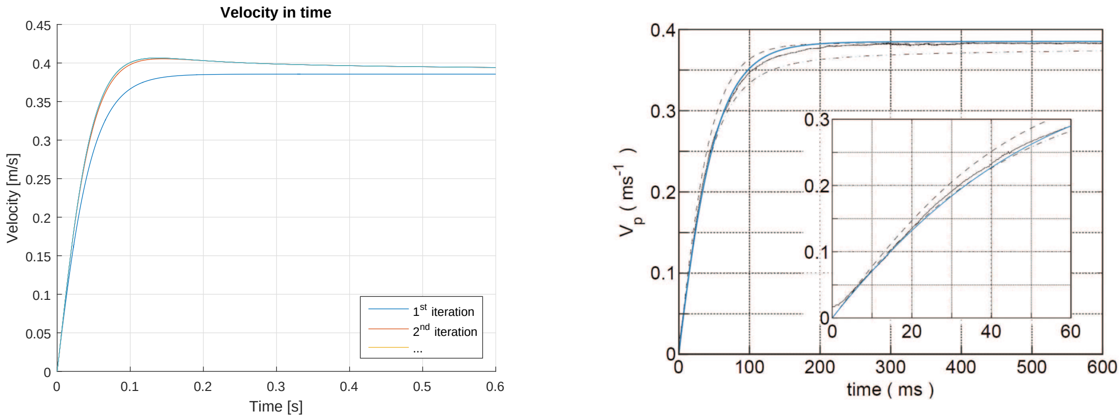

(a) Iterative calculation result (b) Result from literature [7]

Figure 2.21: Resulting vertical velocity found by iteration and discussed in literature

Application to the bubble trajectory

The history force can be implemented, in the same way as discussed for the falling sphere in the calculation of the particle trajectory. The outcome can be seen in Figure 2.22.

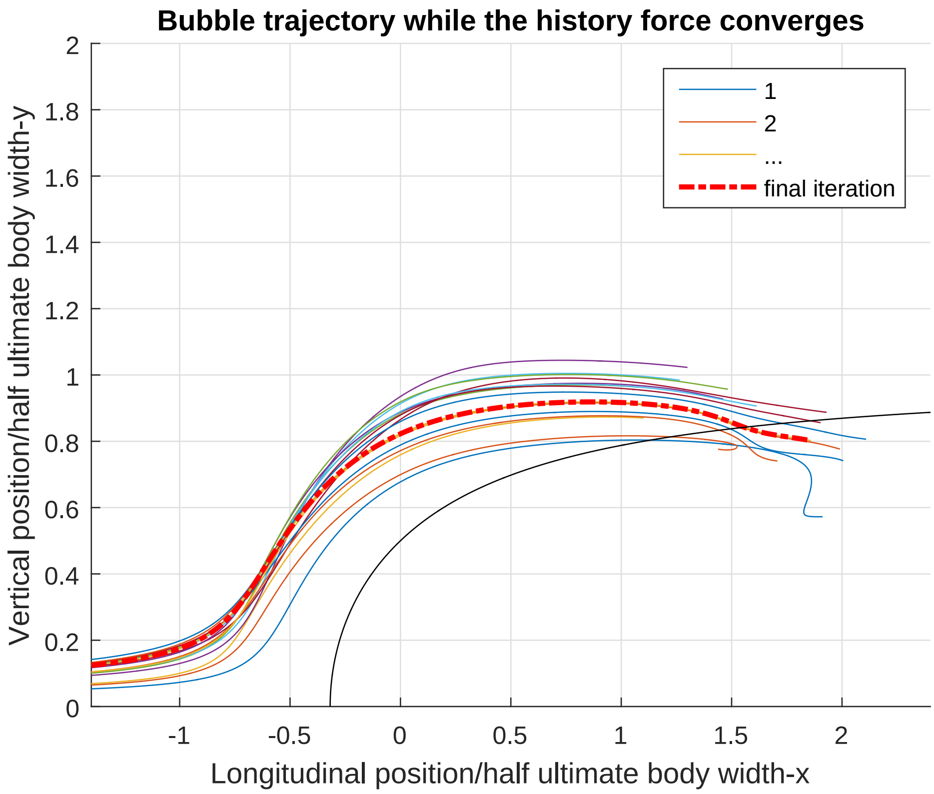

Figure 2.22: The trajectories of the bubble as the history force converges, the first iteration is the lowest blue line and the red dashed-dotted line is the final trajectory.

A new problem arises, namely when the history force is added the trajectory is altered, and therefore altered flow conditions will be encountered. This will make the convergence harder. Luckily the flow field is a potential flow field, so that boundary layers are not a problem, and the flow field will not be much different when the trajectory is shifted.

The final history force in both directions is shown in Figure 2.23.

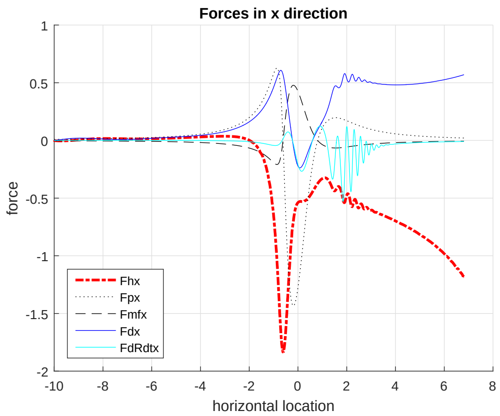

(a) Iterative calculation result

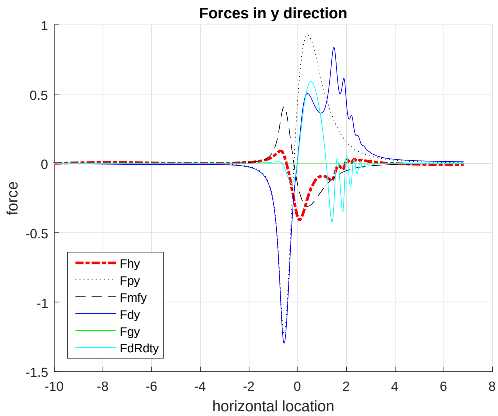

(b) Result from literature

Figure 2.23: Resulting forces in both directions, the history force is the red striped line

In Figure 2.23(a) it can be seen that the history force in the x-direction is not correct far along the trajectory. What can also be seen is that the history force is the main force, and therefore determines the relative acceleration, which in term determines the history force. This makes that the history/Basset force increase exponentially in time. That problem could be solved using a better definition of the history force kernel. In Figure 2.19(b), it could be seen that history kernels exist, which overestimate the actual history force for larger times significantly less. The Basset force can in this case however still be useful as the large deviations happen within the body (the calculation was not stopped when the bubble hits the body since the influence of the history force on unsteady behavior, which happens within the body, was of interest. A practical reason is that stopping the calculation means stopping the bubble, which gives huge spikes in the history force, leading to a not converging system, this could be solved by stopping the calculation at a different estimated time). It can be seen that the history force smears out the initial trajectory, and that the effect of the collapsing bubble is almost fully canceled, so the most unsteady force is counteracted the most by the history force. This is expected, since the Basset force is based on the time it takes to build up a boundary layer.

Conclusions

The aim of this chapter was to expand the basic model. This has been done by both changing the bubble dynamics equation and by expanding the equation of motion.

The general Keller-Herring equation has physically relevant features for the description of the bubble growth, such as damping depending on the speed of sound. These features can be used for future extensions, such as predicting the sound emitted by this form of cavitation.

The prediction of the bubble growth has improved as compared to the quasi-steady bubble growth description. The bubble growth did not influence the trajectory significantly however.

It seems that the equation of motion is far more important in terms of the trajectory than the actual bubble growth. This was shown by consequently adding forces to the equations being solved, and their outcome with respect to the trajectories.

The most significant added force was the buoyancy force. The magnitude of the volume changing force was only significant when the bubble changed its volume noticeable.

The used way of solving is very general, which makes it easy to change the kind of problem solved. As an example the trajectory of a solid particle has been shown.

Finally, the Basset force as an estimate of the history force was added. The implementation of this force and the mathematical description of this force did not yield good results. The force is overestimated by the Basset kernel. And the iterative implementation of the Basset force only works in uniform flows.

3. Validation of expanded model in a RANS solution

In this chapter an equation of motion coupled with an equation for the bubble dynamics will be solved in a RANS solution which was used by Martijn van Rijsbergen [8]. The 3D flow was calculated around a NACA-0015 foil with a chord length of $0.06\,m$ at an angle of attack of $6°$. Two 2D section of the foil have been examined, namely one without the roughness element (smooth) and one with a roughness element. An impression of the flow field and an impression of the foil with and without the roughness element can be seen in Figure 3.1.

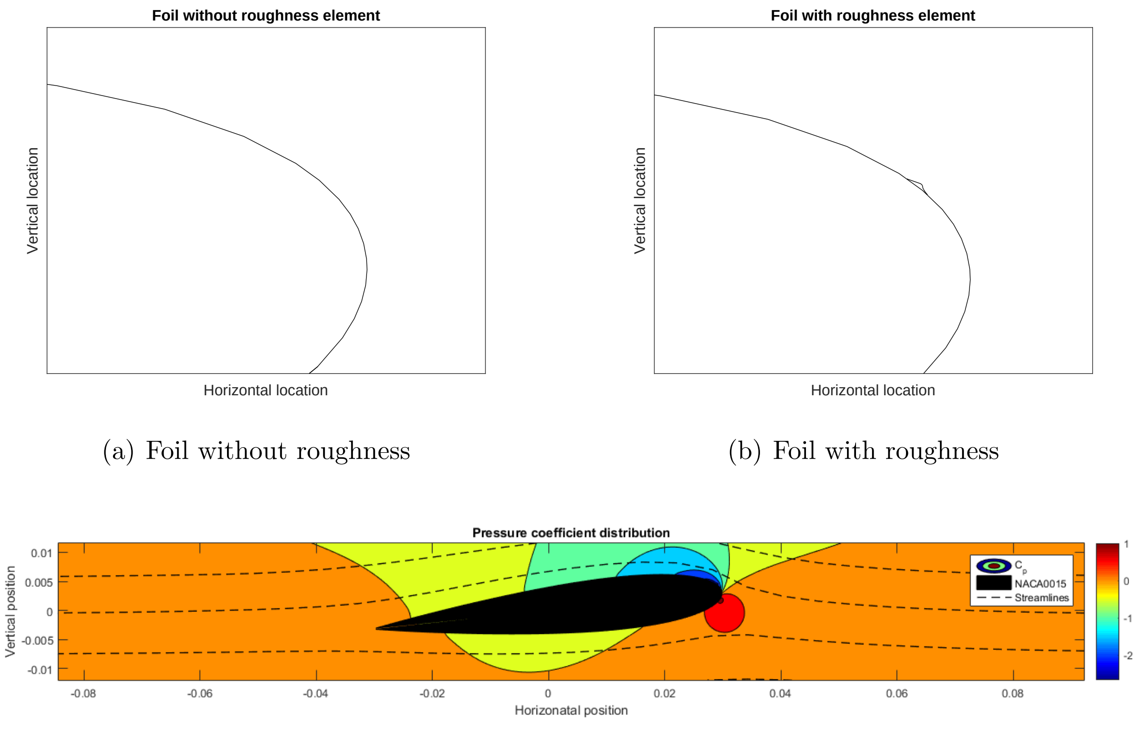

(a) Foil without roughness

(b) Foil with roughness

(c) Pressure coefficient plot with $C_{p,min} \approx -3.62$ and $C_{p,max} \approx 1.08$

Figure 3.1: An overview of the flow field and the different grids

Used equations

The equations which will be solved in this given flow field will be discussed briefly, the equations have (partly) been mentioned before, so they will not be derived. They are named because they will be used in their dimensionfull form.

Equations of motion

The equation of motion used is given in Eq. 3.1.

$$\underbrace{\frac{4}{3}\pi R'^3\left(\rho_b+\frac{1}{2}\rho_f\right)\frac{d\boldsymbol{w}_b}{dt}}_{\text{Acceleration force}}=\underbrace{\frac{1}{2}\rho_f(\boldsymbol{w}-\boldsymbol{w}_b)|\boldsymbol{w}-\boldsymbol{w}_b|C_D\pi R'^2}_{\text{Drag force}}-\underbrace{\frac{3}{2}\frac{4}{3}\pi R'^3\boldsymbol{\nabla}p}_{\text{Pressure force}} \tag{3.1}$$

It can be seen that the driving forces are only the drag force and the pressure force. These forces are chosen for now since it seemed in the potential flow case like these two were enough to describe the bubble trajectory. Furthermore it can be seen that the mass of the bubble is not neglected. This is done to make the code suitable for solid particles.

Bubble dynamics equation

To describe the bubble dynamics the general Keller-Herring equation is used (see Eq. 2.3). The general Keller-Herring equation is chosen since it has damping properties, this potentially reduces the amount of temporal steps. $\lambda = 0$ will be chosen, the equation of state used is that of a perfect gas.

Data handling

The data used in these simulations is retrieved from a 3D RANS simulation. The 3D simulation was meant to test the effect of one roughness element on the foil. Therefore two planes have been chosen, namely one over the symmetry line of the roughness element, and one far away from the roughness element. Both choices have been made so that the assumption of a 2D flow is reasonable.

Grid

The grid that is used in 2D is a structured grid (see Figure 3.1). On the nodes in the grid the velocity in three directions, and the pressure is defined. The node itself is defined by its 3D Cartesian coordinate, the origin is in the middle of the foil.

Interpolation

The particle trajectory will not be bound to the grid points, meaning that a point can be in a cell and not only on its nodes. This creates the need for interpolating. The interpolation needs to capture the physics of the flow properties. In flow fields local effects, like a boundary layers, lead to the need for local interpolation. The interpolation function used for the velocity components in x and y-direction and for the pressure is given in Eq. 3.2.

$$q_p = \frac{\sum_k q_{c,k} R_{c,k}^{-1}}{\sum_k R_{c,k}^{-1}} \tag{3.2}$$

Where q_p is the value of the flow property at the point $p = (x_b, y_b)$, $R_{c,k}$ is the distance from the point p to the k^{th} closest point, and finally $q_{c,k}$ is the flow property in the k^{th} closest point. So basically this is a weighted average. The amount of closest points used, k, influences the capturing of local effects, and the continuity of the resulting flow properties. A different way of interpolation is shown in Eq. 3.3.

$$q_p = \frac{\sum_t q_{c,t} R_{c,t}^{-2}}{\sum_t R_{c,t}^{-2}} \tag{3.3}$$

Where in this case the summing index t is over all points. The result is a continuous function for the flow variables, which still captures the local effects. The downside is that a whole set of distances (R) needs to be used at every time step in stead of just the first few. Clearly the interpolation can be done with even higher orders, but is not expected to give better results. For practical applications the interpolation of Eq. 3.2 will be used, since this is more efficient in terms of computational time.

Spatial derivatives

Spatial derivatives play an important role in the equation of motion for the bubble. In the simple equation of motion given in Eq. 3.1 only the pressure gradient is of importance, but in more complex equations of motion the spatial derivative of the velocity can be of importance. The used derivative is calculated as in Eq. 3.4.

$$\frac{\partial q_p}{\partial x_i} = \frac{q_{p+\delta x_i} - q_{p-\delta x_i}}{2\delta x_i} \quad \text{Where:} \quad \delta x_i = C\frac{\sum_k \Delta x_{i,k}}{k} \tag{3.4}$$

In Eq. 3.4 the derivative can be in two directions depending on i. The δx_i depends on the average distance in the x_i-direction and on a constant C which can be chosen freely. The constant C will determine how local the pressure gradient is being calculated. It could make sense to calculate the derivatives with δx_i being related to the radius of the bubble, because this will take the fact that there is no flow inside the bubble into account. This is however not done. The derivative is taken very locally, since the bubble is assumed to be a point mass, this assumption needs(!) local information. $C = \frac{1}{100}$ will be taken. A low value for C will also decrease the chance of having other points as the closest point, preventing jumps in these derivatives.

Results

In this section the results will be shown. The results will be compared with [8] in the conclusion, the data set used is namely the same. In [8] a streamline is taken as the (local) bubble trajectory. In this report the bubble trajectory is the result of an equation of motion. The results will all be shown on the full scale of the solution, and on a zoomed scale. The zoomed scale is the same in time as in space.

Trajectory

The trajectory of a bubble depends on the flow field properties, and on the properties of the bubble itself. The most important property of the bubble is the size. Other properties that play a role are mostly dependent on the type of gas used (like gas density and surface tension). Some other factors, like the minimum pressure in the bubble, namely the vapor pressure, are taken into account as well. The most important factor not taken into account is the shape of the bubble. A larger bubble will react stronger to the pressure force. This yields different trajectories for different initial radii of the bubble. Two initial bubble sizes have been investigated, namely $R_0 = 18.5\,\mu m$ and $R_0 = 43\,\mu m$.
The trajectory over the roughness element of the bubble with an initial radius of $R_0 = 18.5\mu m$ can be seen in Figure 3.2.

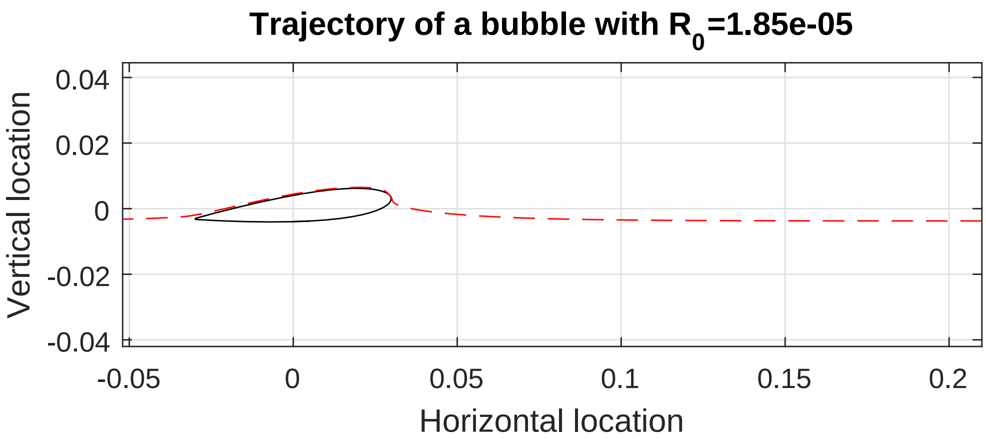

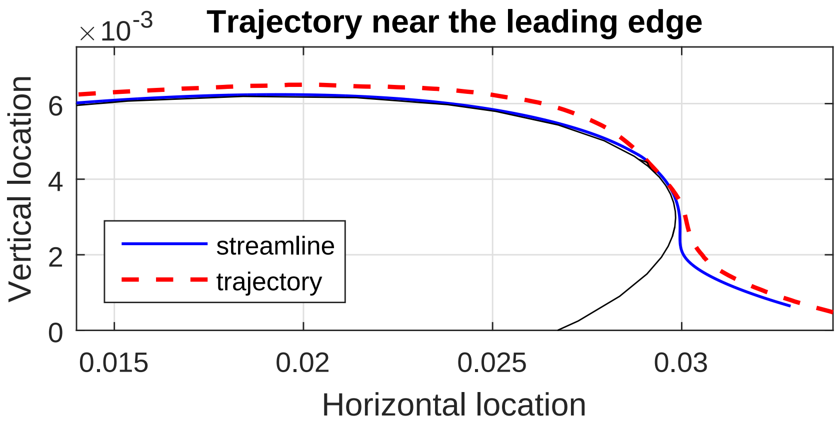

Figure 3.2: Trajectory around the foil with roughness element of a bubble with $R_0 = 18.5\,\mu m$ and $y_0 = -0.00375\,m$

The bubble nearly hits the roughness element, as intended (the trail and error method has been used to find a suitable initial condition). The trajectory with the same initial conditions can also be found on the foil without roughness, see Figure 3.3.

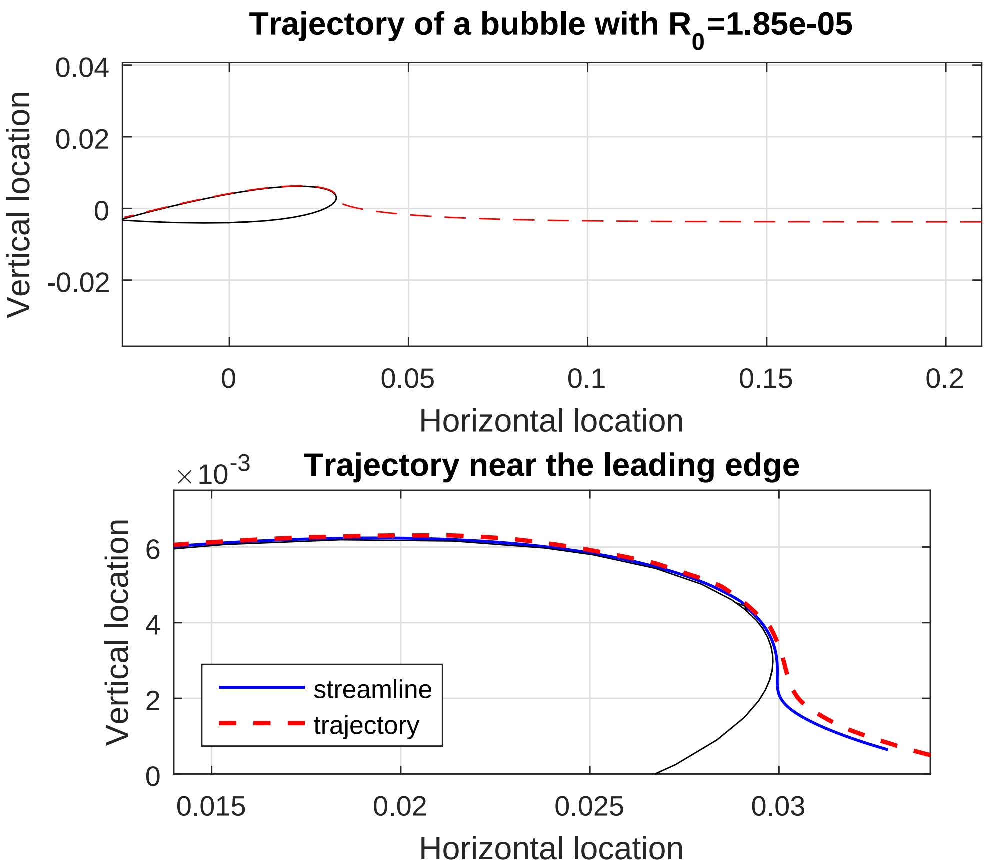

Figure 3.3: Trajectory around the foil without roughness element of a bubble with $R_0 = 18.5\,\mu m$ and $y_0 = -0.00375\,m$

The trajectory of the bubble with an initial radius of $R_0 = 43\,\mu m$ can be seen in Figure 3.4.

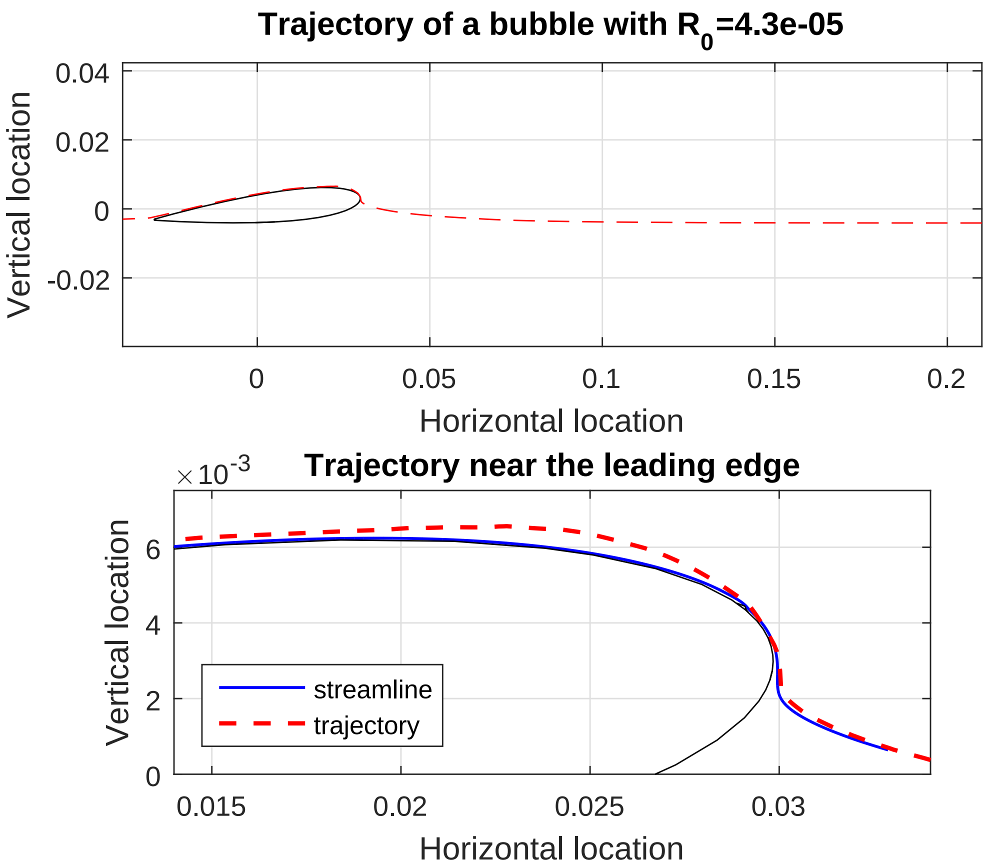

Figure 3.4: Trajectory around the foil with roughness element of a bubble with $R_0 = 43\,\mu m$ and $y_0 = -0.00409\,m$

Again the trajectory without the roughness can be found and can be seen in Figure 3.5.

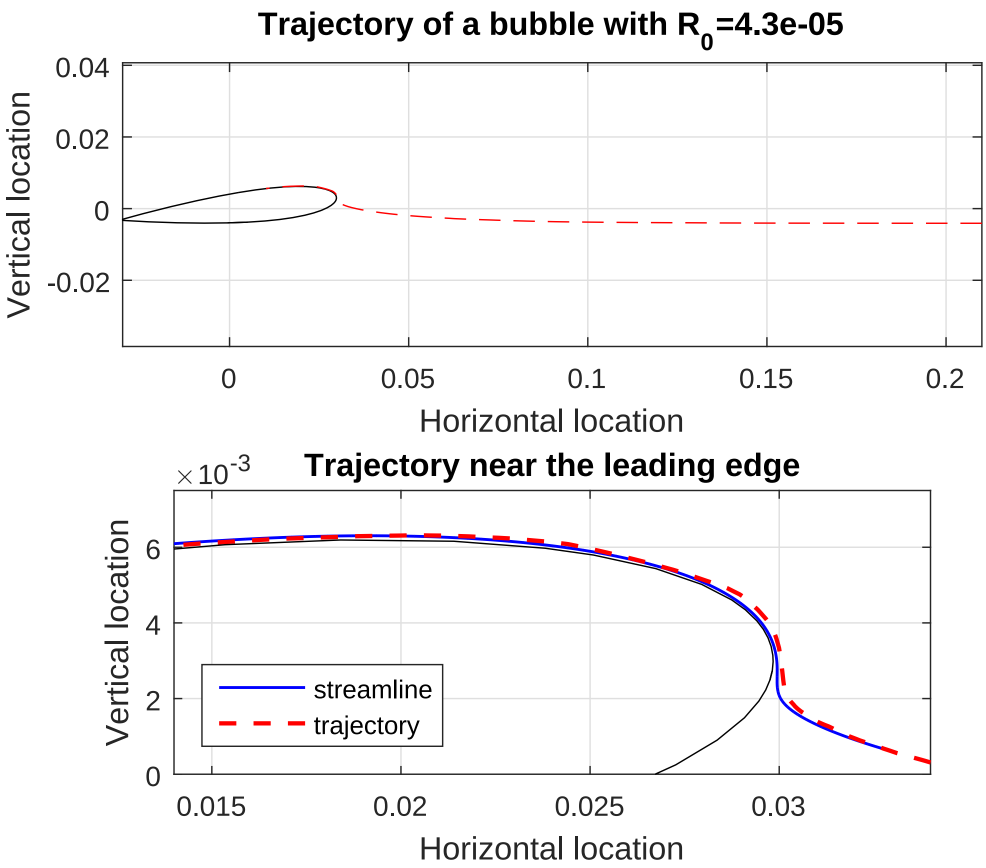

Figure 3.5: Trajectory around the foil without roughness element of a bubble with $R_0 = 43\,\mu m$ and $y_0 = -0.00409\,m$

The trajectories are sensitive for the relative solving tolerance, which was 10^{-4} in this case. This tolerance has been chosen as such since it is reasonably fast in terms of computational time, and the interpolation tolerance will not be bigger than this value. The shooting method is used for finding the initial condition which yields these trajectories.

Pressure along trajectory

The pressure along a trajectory is of importance for the bubble dynamics equation. The bubble size depends namely on the local pressure.

The pressure coefficient along the bubble trajectory depends on the initial bubble size, since this is an important factor in the trajectory. The different pressure coefficients can be seen in Figures 3.6-3.7.

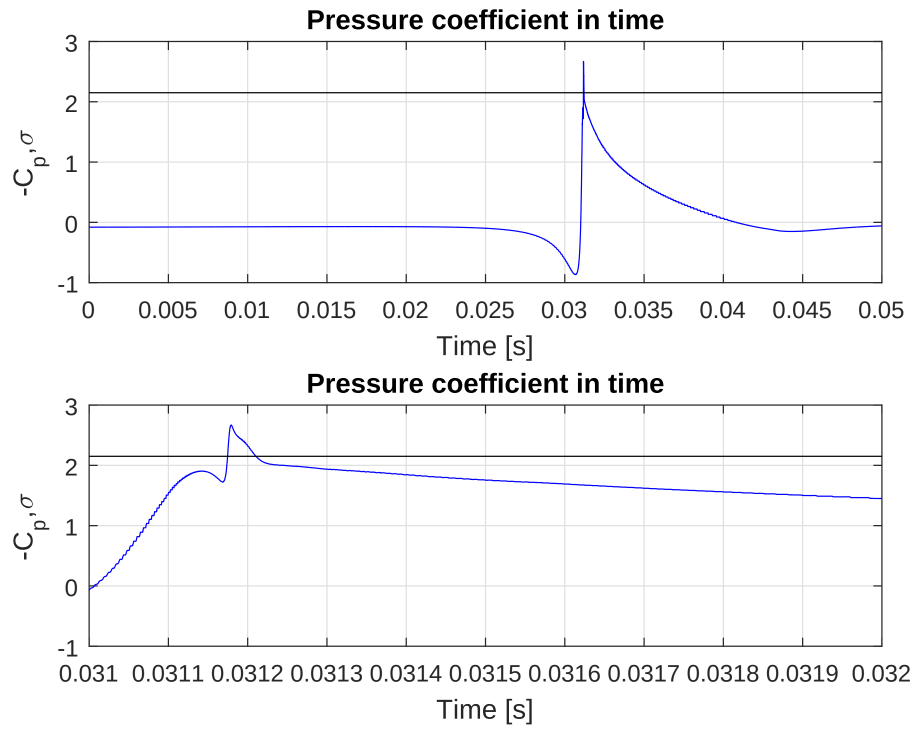

(a) With roughness element

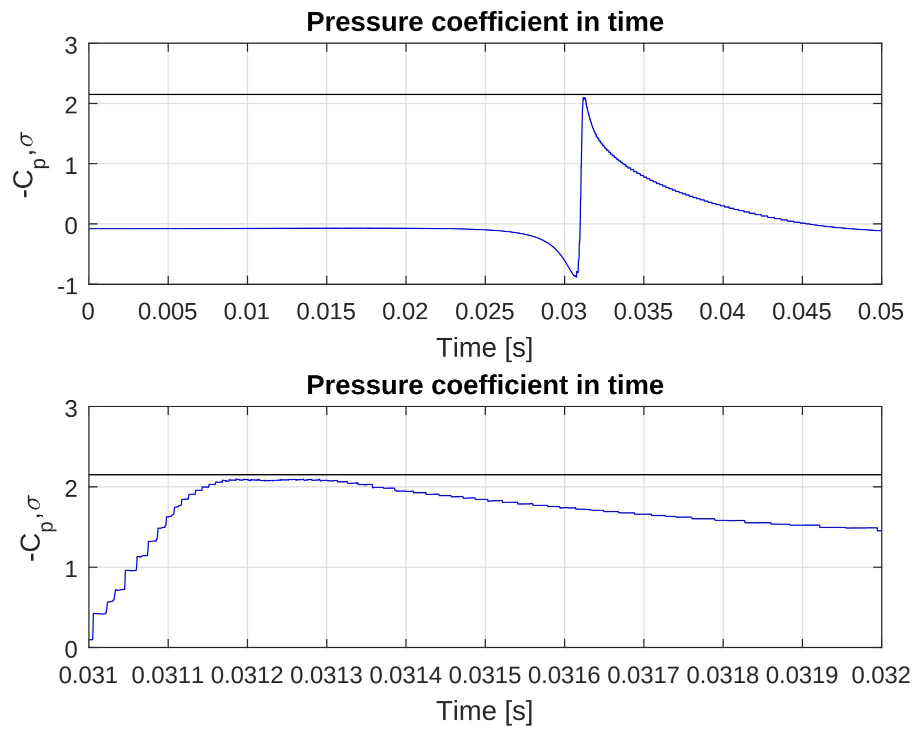

(b) Without roughness element

Figure 3.6: Pressure coefficient in time with $R_0 = 18.5\,\mu m$ and $y_0 = -0.00375\,m$

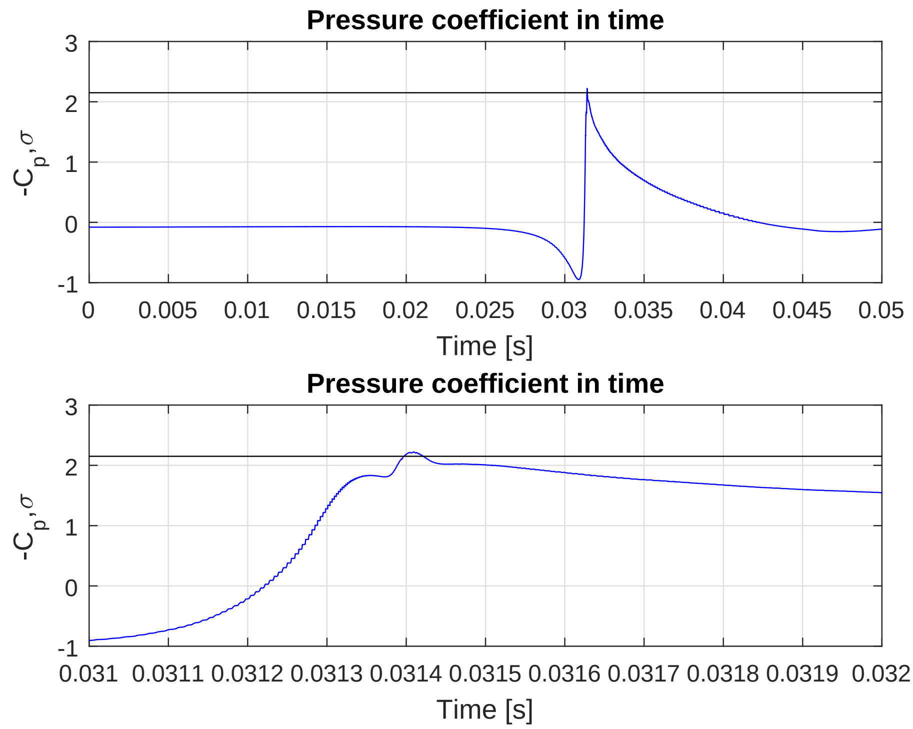

(a) With roughness element

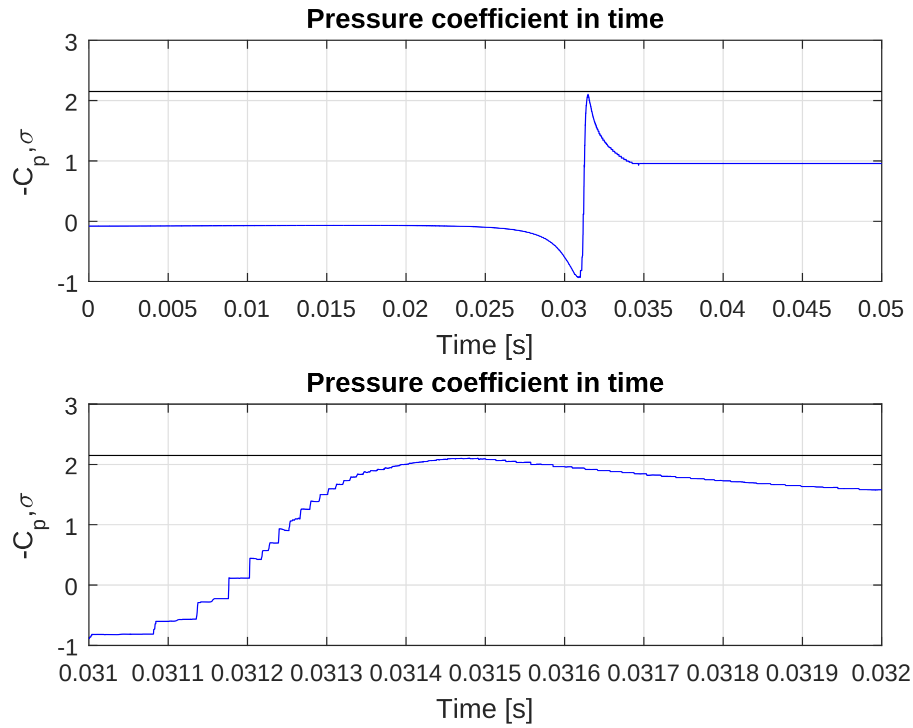

(b) Without roughness element

Figure 3.7: Pressure coefficient in time with $R_0 = 43\,\mu m$ and $y_0 = -0.00409\,m$

In both Figures 3.6-3.7 the interpolation can be seen not to be smooth. The influence of the roughness element can also be seen. The minimum pressure coefficient becomes locally lower. The peak in the negative pressure coefficient can therefore be ascribed to the roughness element. The trajectories do not pass the roughness element at the exact same height, this might be the reason for the different type of peak for the different initial bubble radii.

The "local flatness" of the curve in Figure 3.6(b) can be explained, since the bubble is at that time closest to the boundary layer (see Figure 3.3), in the boundary layer the pressure is higher and therefore the pressure coefficient is flatter.

Radius along trajectory

The radius along the trajectory shows the bubble dynamics which is dependent on the bubble trajectory, see Figures 3.8-3.9.

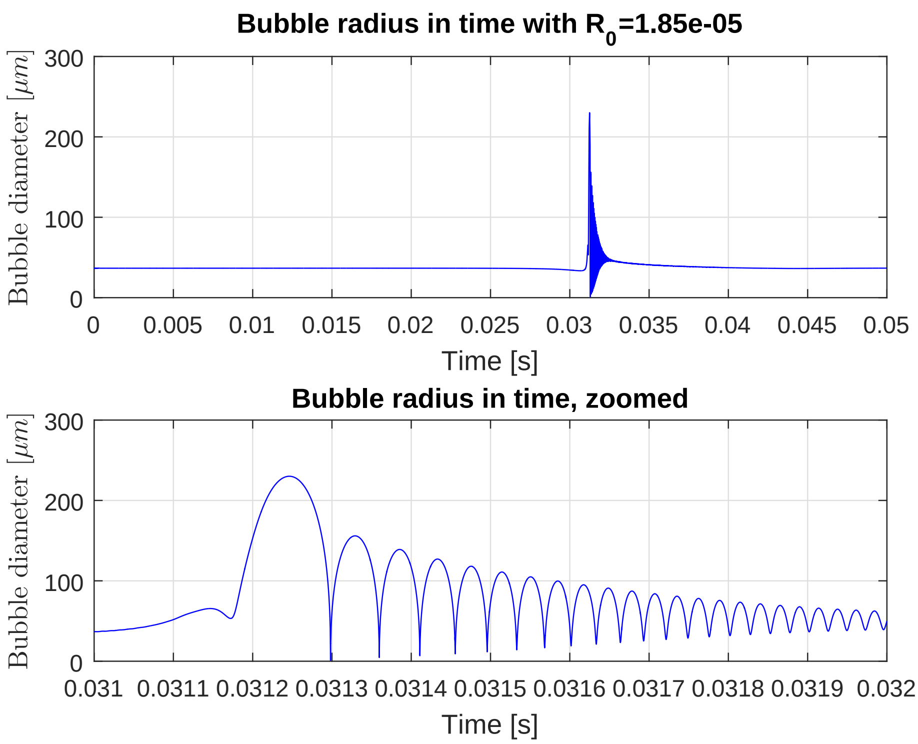

(a) With roughness element

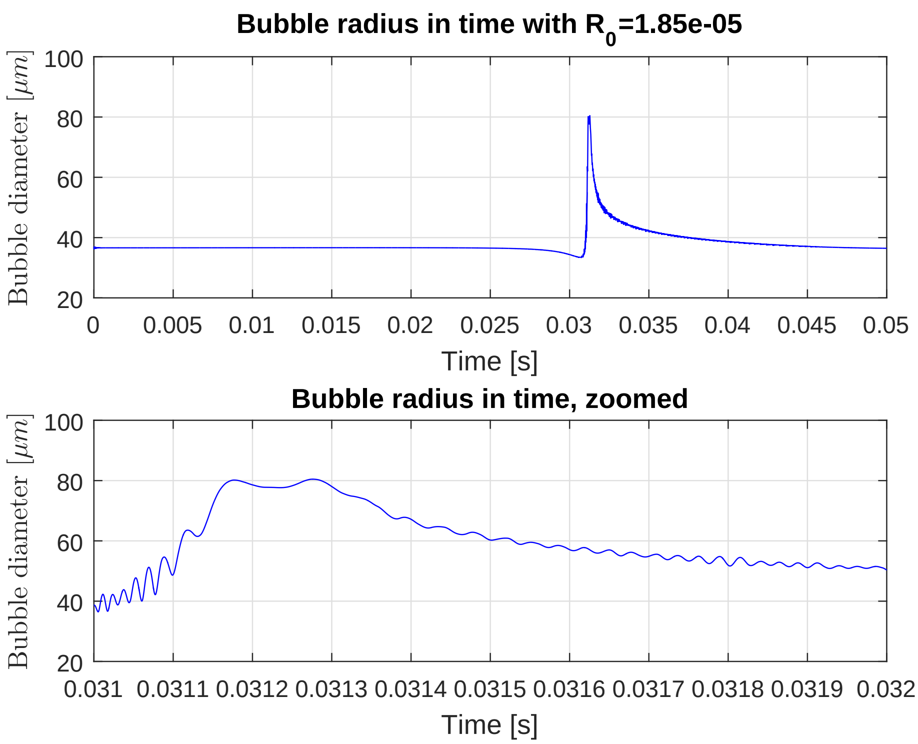

(b) Without roughness element

Figure 3.8: Bubble diameter in time with $R_0 = 18.5\,\mu m$ and $y_0 = -0.00375\,m$

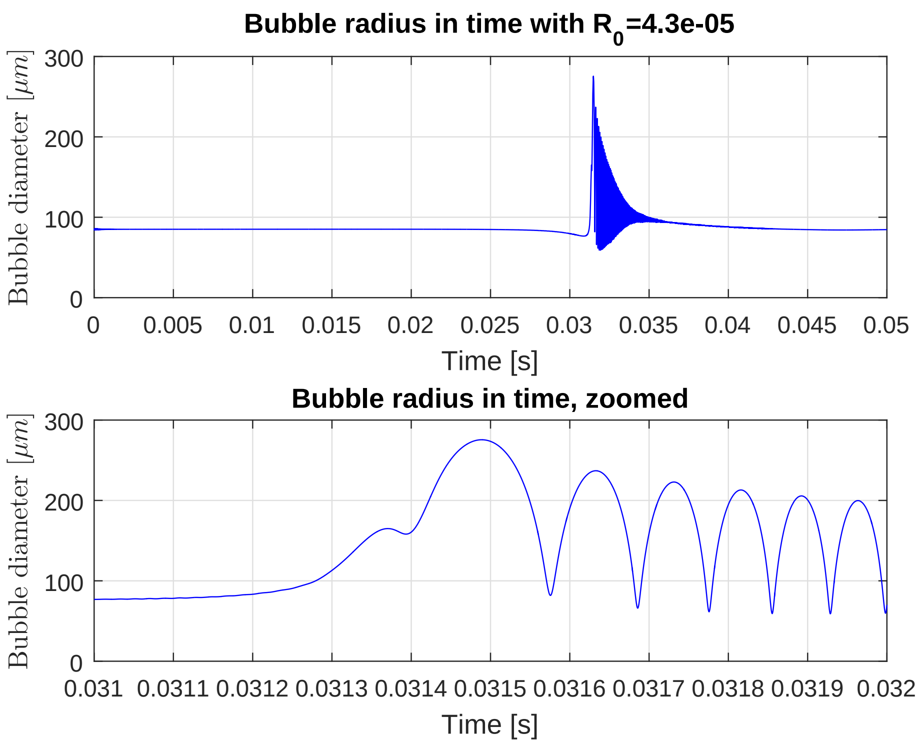

(a) With roughness element

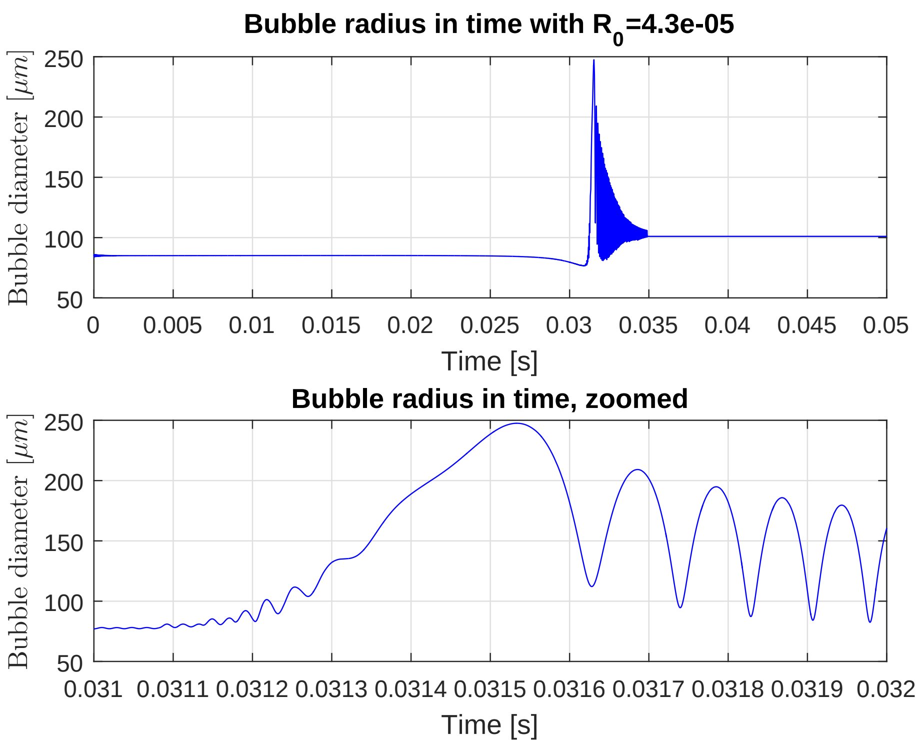

(b) Without roughness element

Figure 3.9: Bubble diameter in time with $R_0 = 43\,\mu m$ and $y_0 = -0.00409\,m$

As can be seen the bubble diameter reacts to the roughness element. The small bubble collapses repeatedly with the roughness element, without the roughness element, the bubble only grows slightly. The larger bubble in both cases shows significant grow, still the effect of the roughness element can be observed. The bubble radius with the roughness element decreases more in size.

Comparison with experiments

The simulations can be validated by comparing the found results with experiments. The experimental data is however not available under the exact same circumstances. The inlet velocity assumed in the simulations was $U = 6\,m/s$, where as in the experiments the inlet velocity was $U = 8\,m/s$. The difference in inlet velocity results in a different flow field. The foil and the angle of attack of the foil were the same.
All experimental results are near the roughness element, therefore two cases have been examined for both the initial radii $R_0 = 18.5\,\mu m$ and $R_0 = 43\,\mu m$.

The first case is trying to find a simulation which has been done previously and compare with the experimental results, see Figures 3.10-3.11 (it should be noted that the error taken for the bubble radius is only the camera accuracy). It can be seen that for $R_0 = 18.5\,\mu m$ the trajectory is not accurate. This can be due to the fact that no other simulation was available at for example $y_0 = -0.0036\,m$, still the trajectory is reasonably close to the experimental results with normal uncertainty (blue). Another reason why the trajectory is not that close is the different circumstances for the simulation and the experiment described above. The diameter of the bubble can be seen to be reasonable accurate. The frequency of the camera is too low to capture the influence of the roughness element, especially just before the last experimental result it would have been nice to have more data.
For $R_0 = 43\,\mu m$ the trajectory is close to that of the experiments. The bubble diameter is with this initial radius not comparable. This might be an effect of the estimation of the radius as done in the experiments. The shape of the bubble is namely far from spherical, especially for the last result. Furthermore it can again not be ruled out that the different circumstances influence the bubble growth significantly.

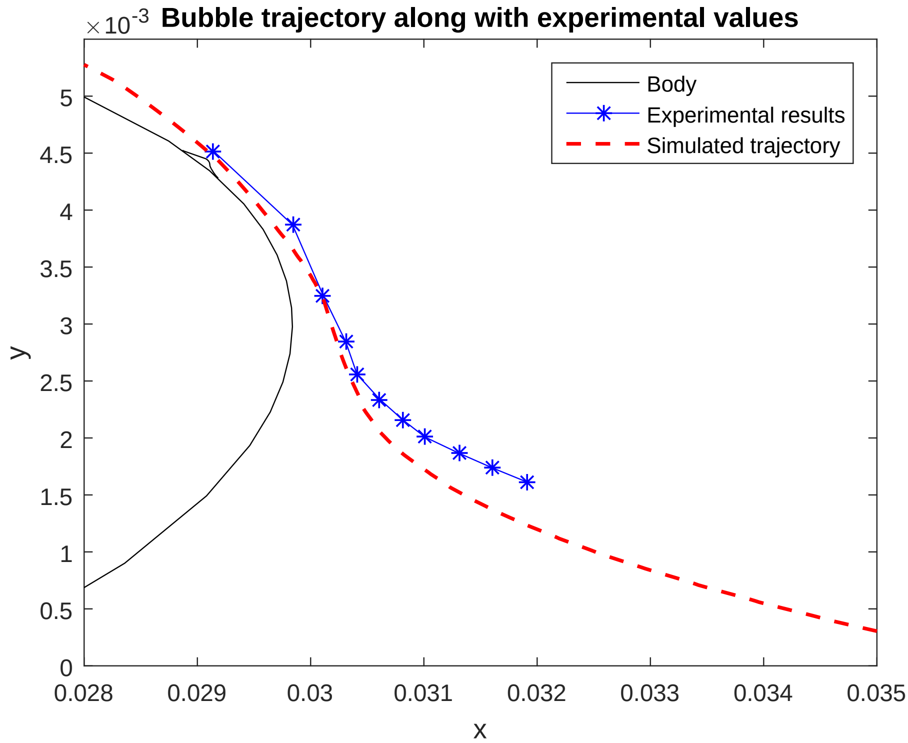

(a) Trajecory of the bubble

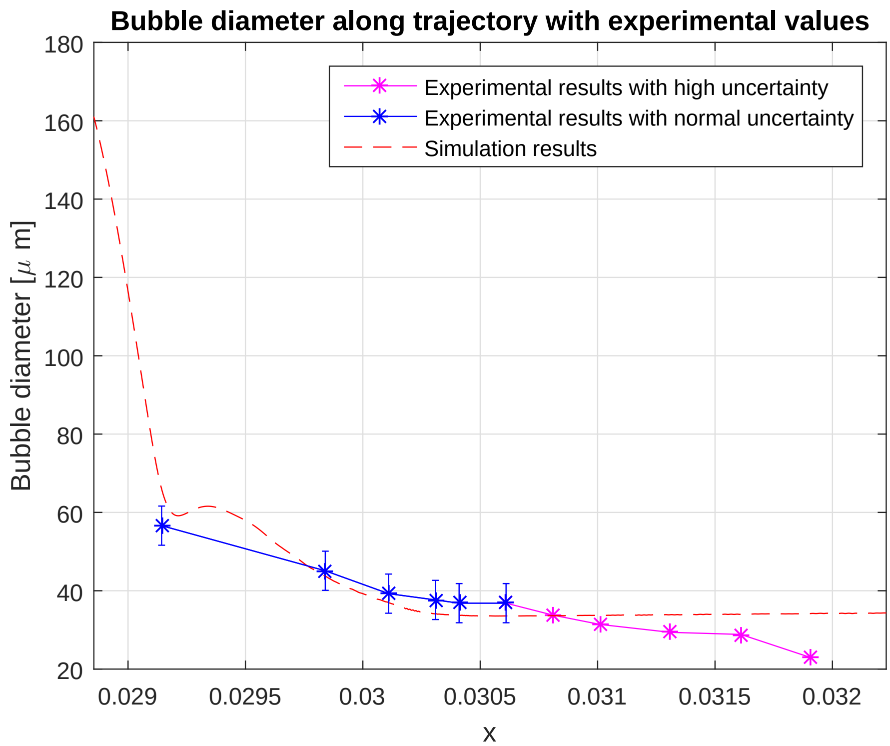

(b) Radius of the bubble

Figure 3.10: The bubbles experimental results with the simulated result for $y_0 = -0.0037\, m$ and $R_0 = 18.5\, \mu m$

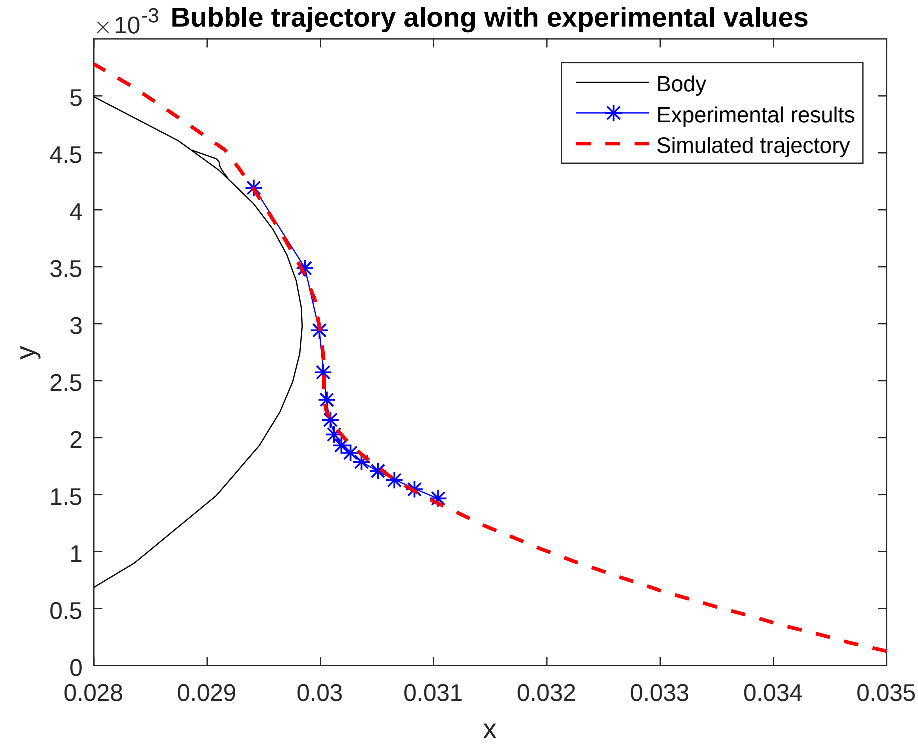

(a) Trajecory of the bubble

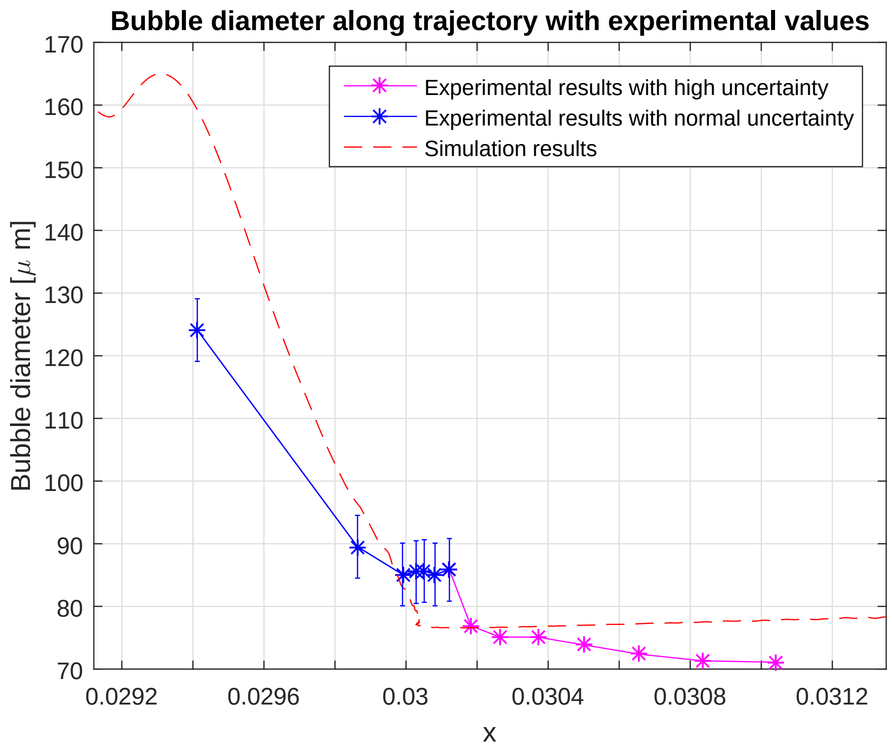

(b) Radius of the bubble

Figure 3.11: The bubbles experimental results with the simulated result for $y_0 = -0.00409\,m$ and $R_0 = 43\,\mu m$

The second case is trying to use the experimental data as an initial condition and then compare results, see Figures 3.12-3.13. It can be seen that for $R_0 = 18.5\,\mu m$ the trajectory is not comparable. The initial condition on the velocity has been scaled by $\frac{3}{4}$, since this accounts for the different inlet velocity. The second point experimental point has been used as an initial condition since at that point an estimate for the velocity is available. The initial condition on the radius is taken as the first radius in the more accurate experimental results. The bubble diameter is pretty accurate, and is nearly everywhere within the experimental error.
For $R_0 = 43\,\mu m$ the trajectory is close. The initial condition on the velocity has again been scaled by $\frac{3}{4}$, and the second experimental point is used. The bubble diameter deviates significantly, but this might be the error of determining the effective bubble diameter. The bubble is less spherical towards the end of the measurements.

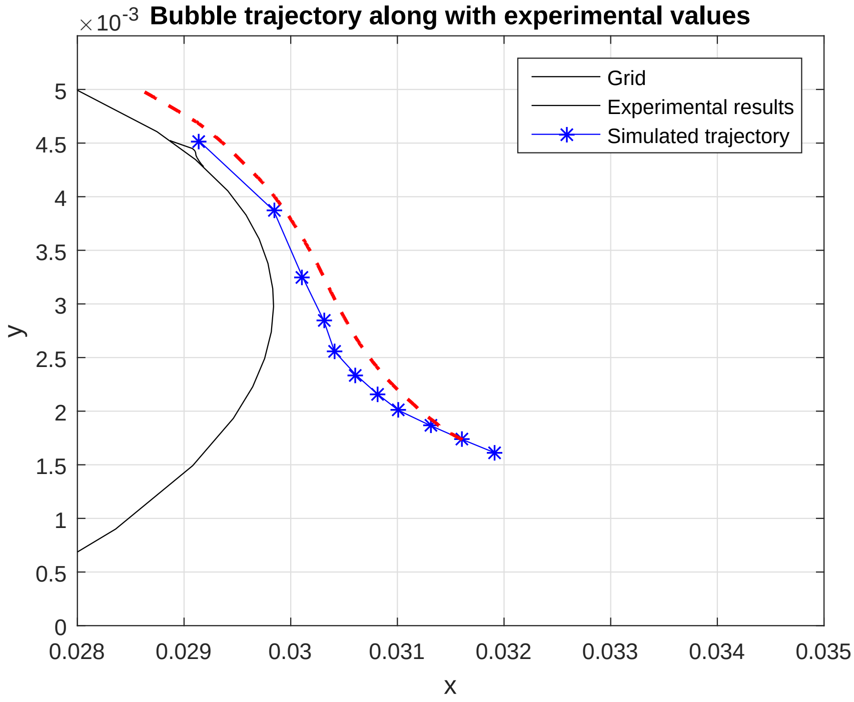

(a) Trajecory of the bubble

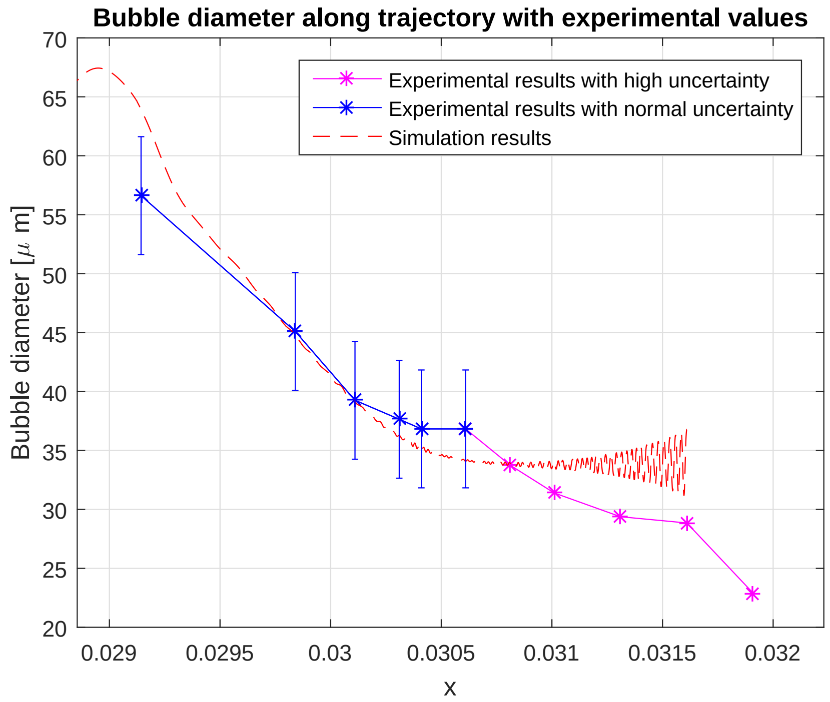

(b) Radius of the bubble

Figure 3.12: The bubbles experimental results with the simulated result with the first result as initial condition

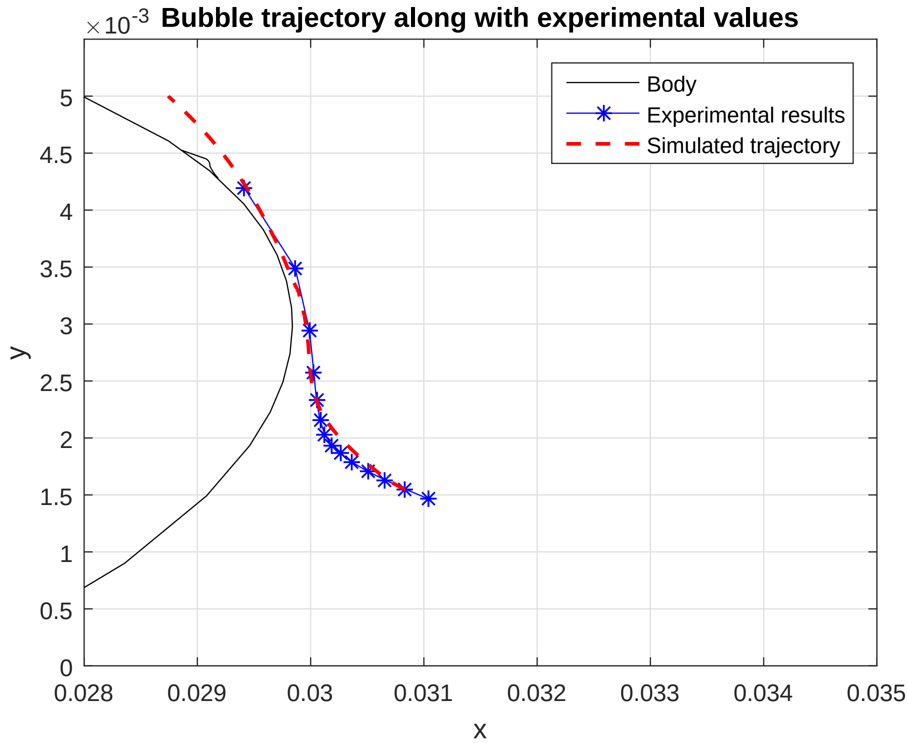

(a) Trajecory of the bubble

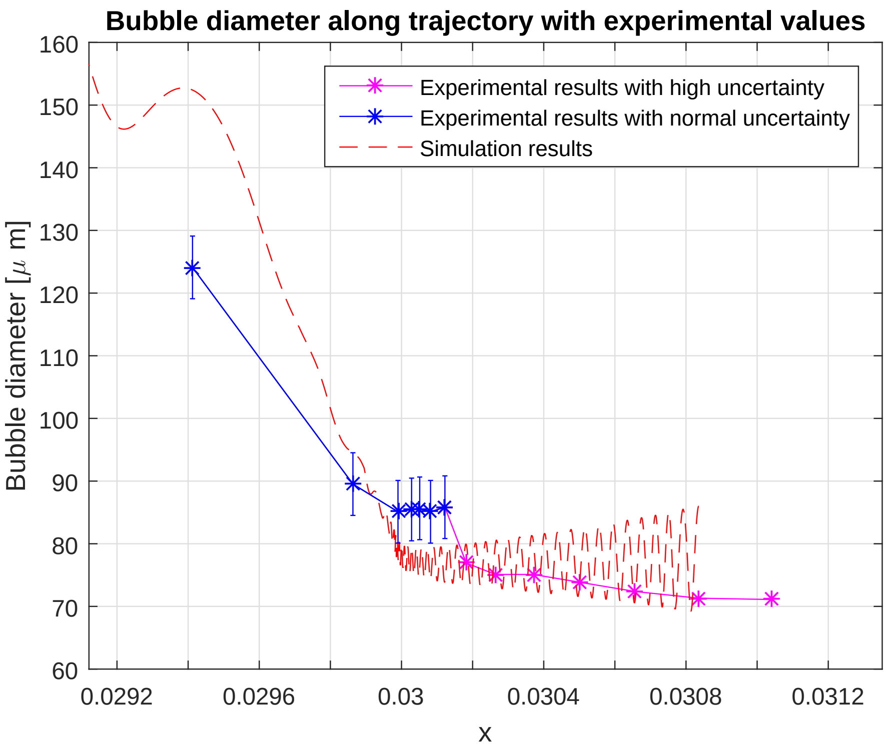

(b) Radius of the bubble

Figure 3.13: The bubbles experimental results with the simulated result with the first result as initial condition

Conclusions

The objective of this chapter was to use a RANS flow solution instead of potential flow as the input for the bubble dynamics and the equation of motion.

Interpolation of the flow properties has been done on the basis of distance. This gives acceptable results, but it causes discontinuities and in stretched cells the interpolation might only take points on a line of cells. This might lead to less accurate results, especially in the boundary layer.

The assumption of spherical bubbles is not accurate, when large pressure gradients are involved.

The bubble can become larger than the spacing between the grid cells. This means that taking the bubble as a point mass is not accurate. This is however required for the equation of motion.

The simulated trajectories deviate significantly from the streamline, especially when the foil with the roughness element is considered. So the roughness element influences the trajectory significantly.

The computational time is significant; up to 2 hours with high tolerances. This can be ascribed to the large data set and the inefficient interpolation in this data set.

The pressure along the trajectory shows that the assumption of taking the streamline locally as done in [8] is reasonable to use as an input to a bubble dynamics equation. Even though the trajectory does not correspond very well with the streamline, the pressure input is very similar.

The bubble grows under similar circumstances more when the foil has a roughness element. The lower pressure at the roughness element causes this. The small bubble collapses repeatedly, where the larger bubble shrinks in size but does not shrink violent enough to call it a collapse. Both bubbles oscillate after having reached their maximum size.

The experiments and the simulations have different inlet velocities. Therefore the trajectories can only be compared qualitatively. The trajectories show that the same type of trajectory shape is found. To compare the results more quantitatively the flow conditions should be the same in the simulations and the experiments.

4. Conclusions and Recommendations

The conclusions have shortly been discussed after each chapter. The final conclusions and recommendations are summarized in this chapter.

Conclusion

The aim was to make a model which solves the bubble trajectory and the bubble growth at the same time. This has been done in steps.

- The model as described by Johnson and Hsieh has been used as a basic model. This model couples quasi-steady bubble growth to a simple equation of motion in potential flow. The model is computationally efficient, but the results were not fully reproducible. The model is adequate in giving insight in the trajectories of cavitation nuclei.
- The basic model was expanded by using a bubble dynamics equation. Both the Rayleigh-Plesset equation and the general Keller-Herring equation have been used. The latter has damping properties which gives a physically more accurate description and makes a code using this equation computationally more efficient.
- More forces were included in the equation of motion. The most influential force was the buoyancy force. The expanded model gives more relevant results in terms of the bubble growth. The trajectories did not change much when the buoyancy force was not taken into account.
- The history force was implemented in the equation of motion, using the Basset force. The Basset force overestimates the history force, which is not physical. The iterative implementation only works in uniform flow fields.
- Using a RANS solution as the flow field showed that the trajectory and the streamline deviate. This effect was exaggerated by the roughness element.

Recommendations

- The simple equation of motion used by Johnson and Hsieh is a good option for an initial calculation.
- The general Keller-Herring equation should be used when violent collapses are expected, since the damping properties will benefit the computational time and the relevance of the results.
- If a force is added to the equation of motion but a force of approximately the same magnitude is neglected the result will not improve, but worsen. Therefore the added forces in the equation of motion should be examined.
- The Basset force should not be used as the history force, since this overestimates this force.
- Iterative implementation of the history force should not be used.
- The interpolation and data handling should be examined further for the case of a given flow field.
- Comparison between the simulations and experiments should be made with similar flow conditions.
- For better results the assumption of a spherical bubble should be abandoned.
- In general, the one-way coupling is not realistic when cavitation occurs on a large scale. This might be a limitation of the presented model, which needs further investigation.

Bibliography

[1] Virgil E. Johnson, Jr., and Tsuying Hsieh, 1966 *The influence of the trajectories of gas nuclei on cavitation inception*, 6th Symposium on Naval Hydrodynamics 1966

[2] Michael P. Brenner, Sacha Hilgenfeldt and Detlef Lohse, 2002 *Single-bubble sonoluminescence*, Reviews of modern physics, volume 74, april 2002

[3] Andrea Prosperetti, *Bubble dynamics: Some things we did not know 10 years ago*

[4] Michael P. Brenner, Detlef Lohse and T.F. Dupont, 1995 *Bubble shape oscillations and the onset of sonoluminescence*, april 4, 1995

[5] Martin R. Maxey and James J. Riley, 1983 *Equation of motion for a small rigid sphere in a nonuniform flow*, Phys. of fluids, **26**, 883-889

[6] Kevin J. Farrell, 2001 *Eulerian/Lagrangian Analysis for the Prediction of Cavitation Inception*, CAV2001:sessionA1.003

[7] Dirk F. van Eijkeren and Harry W. M. Hoeijmakers *The influence of the history force in Lagrangian particle tracking applied to swirling flow produced water treatment*, 8th international conference on multiphase flow, May 26-31 2013

[8] Martijn van Rijsbergen and Jesse Slot, 2015 *Bubble-induced sheet cavitation inception on an isolated roughness element*, Journal of Physics, Conference Series 656, 2015

Appendices

A. Static stability of spherical gas bubbles

First a look will be taken at the bubble related equations. The assumptions made to support the first part of the derivation are as follows:

- The bubble is assumed to be spherical regardless of the flow features.
- Gravity is assumed not to play a role, therefore the buoyancy of the bubble is not taken into account.
- It is assumed that pressure changes slowly so that mechanical equilibrium is still satisfied.
- The fluid inside the bubble is isothermal.
- The bubble is small enough to feel no pressure difference inside the flow. So in practice the bubbles should not enter the boundary layer or become too large.

Having these assumptions the sketch shown in Figure A.1 can be made of the situation. In which p is the surrounding pressure for the bubble, so the pressure determined by the flow field. p_v is the vapor pressure of the liquid and p_g is the partial gas pressure.

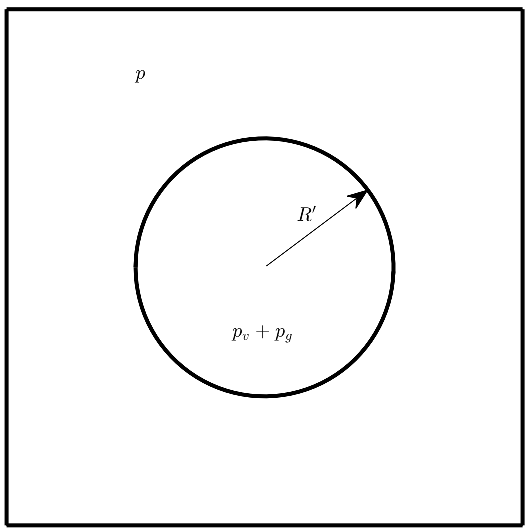

Figure A.1: Sketch of a bubble with radius R' in a liquid

To get static stability the sum of the forces acting on any point in the bubble needs to be zero. This will in general not yet be the case since the surface tension is not included. So now the surface tension needs to be included. The surface tension will account for the difference in pressure over the boundary of the bubble. Imagine to cut the bubble in half, so the cut should go along the middle of the sphere. Then the force that is exerted by the pressure difference felt by the boundary of the cut is equal to the pressure difference times the projected area (a circle with radius R'). This projected area is the effective area on which the pressure works in a force balance in any direction, since the cut of a sphere is not direction dependent. The surface tension now works on the edge of the cut of the sphere, and has therefore a work line described by the circumference of a circle. In equations we get the force balance shown in Eq. A.1.

$$F_{\Delta p} = F_\gamma \tag{A.1}$$

In which $F_{\Delta p}$ stands for the force exerted by the pressure difference and F_γ stands for the force exerted by the surface tension. Since this force balance has a direction the pressure difference force is given by $F_{\Delta p} = \Delta p A_{proj}$. In which A_{proj} is the projected area of a sphere in any direction, so a circle with area $A_{proj} = \pi R'^2$. The surface tension works on the circumference of the projected area since the normal of the projected area is in the direction of the force balance, and therefore the surface tension has to work on this line. Thus the surface tension force is given by: $F_\gamma = \gamma S_{circ}$, where S_{circ} is the circumfurence of a circle, which is $S_{circ} = 2\pi R'$ and γ is the surface tension. Filling this in one finds Eq. A.2.

$$\Delta p \pi R'^2 = \gamma 2\pi R' \quad \rightarrow \quad \Delta p = \frac{2\gamma}{R'} \tag{A.2}$$

The pressure difference is positive if the pressure inside the bubble is larger then the pressure outside the bubble. Using this Eq. A.3 is derived.

$$p_g + p_v - p = \frac{2\gamma}{R'} \quad \rightarrow \quad p = p_g + p_v - \frac{2\gamma}{R'} \tag{A.3}$$

Eq. A.3 is the equation for static stability of a bubble. This equation will now be rewritten into a more usable form. Eq. A.3 holds at any point in a flow field, and therefore also holds at a chosen reference point. Therefore Eq. A.4 holds as well.

$$p_0 = p_{g0} + p_v - \frac{2\gamma}{R'_0} \tag{A.4}$$

Where p_0 is the reference pressure at a point where the bubble has a radius of R'_0. The vapor pressure is not dependent on the place in the flow field since the composition of the liquid does not change, so $p_{v0} = p_v$. Furthermore the partial gas pressure at any point can be related by using the prefect gas law, since the temperature does not change one finds $p_{g0}V_0 = p_g V$. This in turn gives $p_g = p_{g0}\frac{R_0'^3}{R'^3}$. Filling this in in Eq. A.3 Eq. A.5 is found.

$$p = p_{g0}\left[\frac{R'_0}{R'}\right]^3 + p_v - \frac{2\gamma}{R'} \tag{A.5}$$

By rewriting Eq. A.5 and dividing by $p_0 - p_v$ Eq. A.6 can be found.

$$\frac{p - p_v}{p_0 - p_v} = \frac{1}{p_0 - p_v}\left(p_{g0}\left[\frac{R'_0}{R'}\right]^3 - \frac{2\gamma}{R'}\right) \tag{A.6}$$

To get rid of the partial gas pressure Eq. A.4 is used once more leading to Eq. A.7.

$$\frac{p - p_v}{p_0 - p_v} = \frac{1}{p_0 - p_v}\left(\left[p_0 - p_v + \frac{2\gamma}{R'_0}\right]\left(\frac{R'_0}{R'}\right)^3 - \frac{2\gamma}{R'}\right) \tag{A.7}$$

If Eq. A.7 is rewritten conveniently one gets Eq. A.8.

$$\frac{p - p_v}{p_0 - p_v} = \left(\frac{R'_0}{R'}\right)^3\left[1 + \frac{2\gamma}{(p_0 - p_v)R'_0}\left(1 - \frac{R'^2}{R'^2_0}\right)\right] \tag{A.8}$$

Now the vapor cavitation number is introduced as:

$$\sigma_v = \frac{p_0 - p_v}{\frac{1}{2}\rho U^2} \tag{A.9}$$

and the Weber number as:

$$W = \frac{2\rho U^2 R'_0}{\gamma} \tag{A.10}$$

When both the vapor cavitation number (Eq. A.9) and the Weber number (Eq. A.10) are used in Eq. A.8, Eq. A.11 can be found.

$$\boxed{\frac{p - p_v}{p_0 - p_v} = \left(\frac{R'_0}{R'}\right)^3\left[1 + \frac{8}{\sigma_v W}\left(1 - \frac{R'^2}{R'^2_0}\right)\right]} \tag{A.11}$$

Eq. A.11 is the first equation in the paper. The second equation in the paper will now be derived from the first equation. To write this dimensionless equation (Eq. A.11) in a more convenient form, more dimensionless numbers will be introduced. The vapor cavitation number (Eq. A.9) and the Weber number (Eq. A.10) are both already dimensionless. Next the radius ratio r is introduced as $r = \frac{R'_0}{R'}$ and the pressure coefficient C_p is introduced to be the ratio of the relative pressure over the dynamic pressure $C_p = \frac{p-p_0}{\frac{1}{2}\rho U^2}$. Eq. A.11 can now be rewritten using:

$$\frac{C_p + \sigma_v}{\sigma_v} = \frac{p - p_v}{p_0 - p_v} \tag{A.12}$$

into Eq. A.13.

$$\frac{C_p + \sigma_v}{\sigma_v} = r^3 \left[1 + \frac{8}{\sigma_v W}\left(1 - r^{-2}\right)\right] \tag{A.13}$$

Rewriting Eq. A.13 gives Eq. A.14.

$$r^3 - \frac{\frac{8}{\sigma_v W}}{\left(1 + \frac{8}{\sigma_v W}\right)} r - \frac{\frac{C_p + \sigma_v}{\sigma_v}}{\left(1 + \frac{8}{\sigma_v W}\right)} = 0 \tag{A.14}$$

Which leads to Eq. A.15.

$$\boxed{r^3 - \frac{\frac{8}{W}}{\sigma_v + \frac{8}{W}} r - \frac{C_p + \sigma_v}{\sigma_v + \frac{8}{W}} = 0} \tag{A.15}$$

Eq. A.15 is the same equation as Eq. A.11 but written in a solvable form when r is sought. Eq. A.15 is written shortly as: $r^3 - Pr - Q = 0$. A third degree polynomial can be solved, the solution depends on the discriminant. The discriminant of a third degree function of the form $ax^3 + bx^2 + cx + d$ is given by $\Delta = 18abcd - 4b^3d + b^2c^2 - 4ac^3 - 27a^2d^2$. In the case of Eq. A.15 the discriminant becomes: $\Delta = 4P^3 - 27Q^2$. By using the discriminant three cases can be distinguished, namely:

1. if $\Delta > 0$, then the equation has 3 distinct real roots
2. if $\Delta = 0$, then the equation has a multiple root and all of its roots are real
3. if $\Delta < 0$, then the equation has one real root and two complex roots

First the case in which the local pressure p is greater then the vapor pressure p_v is considered. This means that $C_p + \sigma_v > 0$. If this is the case then Q will be positive just as P which is always positive. If then the case in which $Q^2 > \frac{4}{27}P^3$ is considered the discriminant will be negative($\Delta < 0$, case 3). When a third degree polynominal in the form of Eq. A.15 has one real root, this root can be found by Cardano's method. This gives as a solution Eq. A.16. Of course only real solutions are interesting since this problem is physical.

$$\boxed{r = \sqrt[3]{\frac{1}{2}Q + \frac{1}{2}\sqrt{Q^2 - \frac{4}{27}P^3}} + \sqrt[3]{\frac{1}{2}Q - \frac{1}{2}\sqrt{Q^2 - \frac{4}{27}P^3}}} \tag{A.16}$$

Realizing $r = \frac{R_0'}{R'}$ the first equation of the third equation (3a) of the paper has been found. Note that $\frac{1}{2}Q$ has been forgotten in the paper.

If now the case $C_p + \sigma_v > 0$ and $Q^2 < \frac{4}{27}P^3$ is considered the determinant becomes positive($\Delta > 0$, case 1), meaning 3 real solutions. The solution which will be relevant however needs to be positive since the radius of the bubble will always be positive. The solutions for this case can be found by Viète's method the only positive solution is found in the case where $k = 0$. This gives Eq. A.17.

$$\boxed{r = 2\sqrt{\frac{P}{3}}\cos\theta \quad \text{Where} \quad \theta = \frac{1}{3}\cos^{-1}\left(\frac{Q}{\sqrt{\frac{4}{27}P^3}}\right)} \tag{A.17}$$

Eq. A.17 is the second part of the third formula (3b) in the paper. Note that the division is missing in the paper.

Lastly the case where $C_p + \sigma_v < 0$ and $Q^2 < \frac{4}{27}P^3$ is considered. This means that the surrounding pressure is smaller than the vapor pressure. In that case the determinant is again positive and the solution to the problem has therefore three real roots. In this case two positive solution can be found when, namely when $k = 0$ or $k = 1$ is taken. Only in the case where $k = 1$ r is smaller than 1, meaning that the bubble has grown which it should do since the surrounding pressure is lower than the vapor pressure. Similar to the previous case one can find Eq. A.18.

$$\boxed{r = 2\sqrt{\frac{P}{3}}\cos\frac{\pi - \theta'}{3} \quad \text{Where} \quad \theta' = \cos^{-1}\left(\frac{Q}{\sqrt{\frac{4}{27}P^3}}\right)} \tag{A.18}$$

Eq. A.18 is the last part of the third formula (3c) in the paper. Note that the division is again missing in the paper.

With Eqs A.16-A.17-A.18 the third equation in the paper is reproduced.

One special case has not been investigated yet, namely the case where $Q^2 = \frac{4P^3}{27}$. This case is only of interest when $C_p + \sigma_v < 0$ so that the surrounding pressure is lower then the vapor pressure because only then this critical point will lead to massive growth of the initial bubbles. This phenoma is known as cavitation inception since the bubbles will become visible after/shortly after this point. One could find a critical pressure coefficient by simply working out $Q^2 = \frac{4P^3}{27}$ but to get a better understanding of the meaning of this critical point a plot of the outcome of Eq. A.11 is given in Figure A.2.

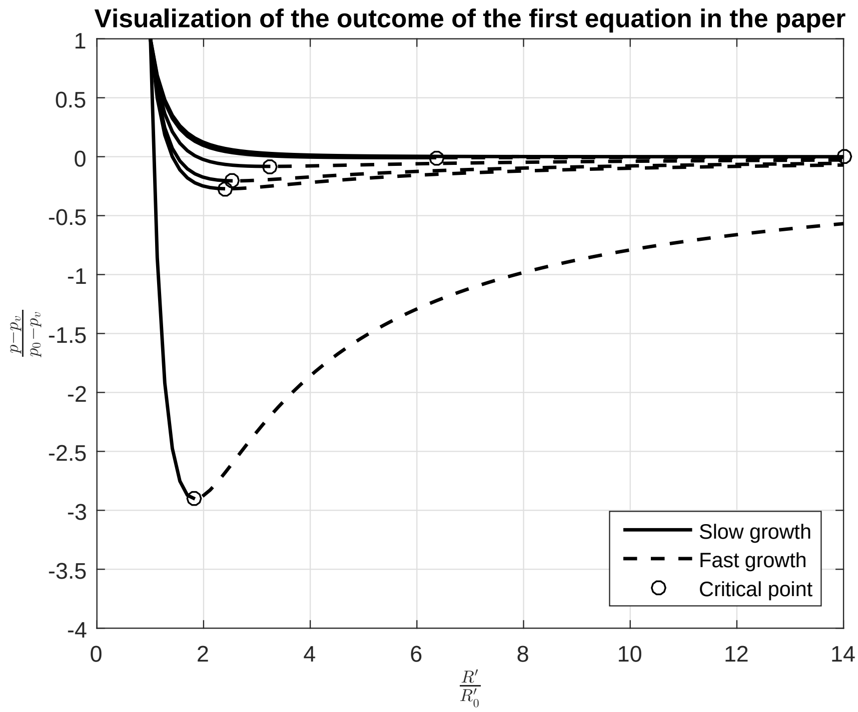

Figure A.2: The function given in Eq. A.11 plotted for different values of $\sigma_v W$. The values used for $\sigma_v W$ are 1,8,10,20,100 and 1000, the higher this value the higher the critical point.

As can be seen in Figure A.2 there is a minimum pressure after which the particle begins to grow very fast. This point is called the critical point. It can be seen that all functions head towards the $\frac{p-p_v}{p_0-p_v} = 0$-line, meaning that the surrounding pressure moves towards the vapor pressure due to the bubble expanding.
To find the minima observed in Figure A.2 and to create decent understanding of the phenoma Eq. A.5 is used. Cavitation inception occurs at the minimal surrounding pressure reached, this point can be found by setting the derivative to zero, see Eq. A.19.

$$\frac{\partial p}{\partial R'} = -3\frac{p_{g0}R_0'^3}{R'^4} + \frac{2\gamma}{R'^2} \tag{A.19}$$

After setting the derivative to zero and some convenient rewriting Eq. A.20 is found.

$$R'_c = R'_0\sqrt{\frac{3p_{g0}}{\frac{2\gamma}{R'_0}}} \tag{A.20}$$

In Eq. A.20 R'_c is the critical radius. Using this critical radius the critical pressure can be found by using Eq. A.5 again. This leads to Eq. A.21.

$$p_c = p_{g0}\left(\frac{\frac{2\gamma}{R_0'}}{3p_{g0}}\right)^{3/2} + p_v - \frac{2\gamma}{R_c'} \tag{A.21}$$

Rewriting Eq. A.21 gives Eq. A.22.

$$p_c = \frac{2\gamma}{3R_0'}\frac{R_0'}{R_c'} + p_v - \frac{2\gamma}{R_c'} = p_v - \frac{4\gamma}{3R_c'} \tag{A.22}$$

So the critical pressure is known. Writing Eq. A.22 in dimensionless form requires the dimensionless critical radius. This can be found by using Eq. A.4 and using the cavitation and Weber number. This gives Eq. A.23.

$$R_c' = R_0'\sqrt{3}\sqrt{\frac{W\sigma_v}{8}+1} \tag{A.23}$$

Filling in the critical radius found in Eq. A.23 into Eq. A.22 one finds Eq. A.24.

$$p_c - p_v = -\frac{4\gamma}{3\sqrt{3}R_0'\sqrt{\frac{W\sigma_v}{8}+1}} \tag{A.24}$$

Introducing the critical pressure coefficient as: $C_p^* = \frac{p_c - p_0}{\frac{1}{2}\rho U^2}$ one can find Eq. A.25.

$$C_p^* + \sigma_v = -\frac{\frac{16}{W}}{3\sqrt{3}\sqrt{\frac{W\sigma_v}{8}+1}} \tag{A.25}$$

Rewriting Eq. A.25 gives Eq. A.26.

$$\boxed{C_p^* + \sigma_v = -\frac{2\sigma_v\left(\frac{8}{\sigma_v W}\right)^{3/2}}{3\sqrt{3}\left(1+\frac{8}{\sigma_v W}\right)^{1/2}}} \tag{A.26}$$

This found equation (Eq. A.26) could also be found by equating $4Q^2 = 27p^3$, and is the same equation as the fourth equation in the paper.

B. Bubble trajectory

The bubble trajectory will be constructed by using the second law of Newton. Therefore the force balance is needed. The forces which could be relevant are the following:

- F_D, Drag force
- F_p, Pressure force
- F_f, Added mass force
- F_G, Force due to growth
- F_b, Buoyancy force
- F_μ, Viscous forces

The drag force on any particle in any direction could be written in the form given in Eq. B.1.

$$F_D = \frac{1}{2}\rho \boldsymbol{w}_{rel}|\boldsymbol{w}_{rel}|C_D A_{frontal} \tag{B.1}$$

In which C_D is the drag coefficient, $\boldsymbol{w}_{rel}$ is the relative velocity vector, and $A_{frontal}$ is the frontal area of the particle. A spherical bubble has a frontal area of $A_{frontal} = \pi R'^2$. The relative velocity is the difference between the flow velocity and the bubbles velocity, so $\boldsymbol{w}_{rel} = \boldsymbol{w} - \boldsymbol{w}_b$.

The pressure force is given by $\frac{3}{2}$ of the volume of the bubble times the pressure gradient, when it is assumed that the bubble is a point mass. The factor $\frac{3}{2}$ accounts for the added mass of the sphere, the added mass adds up to half the volume of the bubble. To take the pressure gradient instead of an integral of the pressure over the surface of the bubble means that the bubble is considered to be a point mass. Lastly a positive gradient in the pressure field means a negative force on the bubble since the pressure is then higher on the front of the bubble. So the pressure force is as in Eq. B.2.

$$F_p = -\frac{3}{2}\frac{4}{3}\pi R'^3 \boldsymbol{\nabla} p \tag{B.2}$$

The added mass force is the force due to the fact that the bubble will transport a bit of surrounding fluid. This fluid will just as the bubble have to be accelerated. This force is defined as the mass of half (exact outcome of potential theory) the volume bubble in the surrounding fluid times the accelaration of the bubble. This leads to Eq. B.3.

$$F_f = -\frac{1}{2}\frac{4}{3}\pi R'^3 \rho \frac{d\boldsymbol{w}_b}{dt} \tag{B.3}$$

The forces due to growth is a force which can be seen as the force due to the moving of a wall. Imagine a wall in quiescent water, which is then moved in the direction of the water. A force would be felt by the wall, in the opposite direction of its movement. In this case however the wall is not at rest at first but it has just as the example a velocity difference. This force is defined in Eq. B.4.

$$F_G = 2\pi\rho R'^2 \boldsymbol{w}_{rel} \frac{dR'}{dt} \tag{B.4}$$

This force will be limited due to the fact that initially the calculation will be stopped after the critical point, so the time derivative of the radius will never be large. Therefore this force will be neglected.

The buoyancy force will be zero since gravity is set to zero.

The viscous forces are not incorporated since the flow will be taken to be potential flow, in which the viscosity will not be playing a role.

The force balance will thus become as in Eq. B.5.

$$m_b \frac{d\boldsymbol{w}_b}{dt} = -\frac{1}{2}\frac{4}{3}\pi R'^3 \rho \frac{d\boldsymbol{w}_b}{dt} + \frac{1}{2}\rho(\boldsymbol{w} - \boldsymbol{w}_b)|\boldsymbol{w} - \boldsymbol{w}_b| C_D \pi R'^2 - \frac{3}{2}\frac{4}{3}\pi R'^3 \boldsymbol{\nabla} p \tag{B.5}$$

Since the mass of the bubble (m_b) will be significantly smaller than the added mass by the surrounding fluid the mass of the bubble will be neglected initially, this leads to Eq. B.6.

$$\boxed{\frac{1}{2}\frac{4}{3}\pi R'^3 \rho \frac{d\boldsymbol{w}_b}{dt} = \frac{1}{2}\rho(\boldsymbol{w} - \boldsymbol{w}_b)|\boldsymbol{w} - \boldsymbol{w}_b| C_D \pi R'^2 - \frac{3}{2}\frac{4}{3}\pi R'^3 \boldsymbol{\nabla} p} \tag{B.6}$$

Eq. B.6 is the same equation as equation 5 from the paper where only the inertia force is already neglected.

The drag coefficient, C_D, is related to the Reynolds number of the sphere R_b by the relation given in Eq. B.7.

$$\boxed{\frac{C_D R_b}{24} = 1 + 0.197 R_b^{0.63} + 2.6 \cdot 10^{-4} R_b^{1.38}} \tag{B.7}$$

Eq. B.7 was obtained by fitting experimental data of rigid spheres. The part which can be extracted with $\frac{24}{R_b}$ is the normal drag relation for Stokes flow. The other terms are there to account for the higher Reynolds number regimes. The definition of the bubble Reynolds number is given in Eq. B.8.

$$R_b = \frac{2R'|\boldsymbol{w} - \boldsymbol{w}_b|}{\nu} \tag{B.8}$$

Eq. B.6 can be made dimensionless, this is convenient for solving them since then the outcomes are more general. First Eq. B.6 will be written as separate formulas for velocity components u' and v', see Eq. B.9.

$$\begin{aligned}
\frac{1}{2}\frac{4}{3}\pi R'^3 \rho \frac{du'_b}{dt} &= \frac{1}{2}\rho(u' - u'_b)\left[(u' - u'_b)^2 + (v' - v'_b)^2\right]^{1/2} C_D \pi R'^2 - \frac{3}{2}\frac{4}{3}\pi R'^3 \frac{\partial p}{\partial x'} \\
\frac{1}{2}\frac{4}{3}\pi R'^3 \rho \frac{dv'_b}{dt} &= \frac{1}{2}\rho(v' - v'_b)\left[(u' - u'_b)^2 + (v' - v'_b)^2\right]^{1/2} C_D \pi R'^2 - \frac{3}{2}\frac{4}{3}\pi R'^3 \frac{\partial p}{\partial y'}
\end{aligned} \tag{B.9}$$

It will be shown how to make the first equation of Eq. B.9 dimensionless since the process for the other equation is similar. First the equation is rewritten to Eq. B.10.

$$\frac{du'_b}{dt} = \frac{3C_D}{4R'}(u' - u'_b)\left[(u' - u'_b)^2 + (v' - v'_b)^2\right]^{1/2} - \frac{3}{\rho}\frac{\partial p}{\partial x'} \tag{B.10}$$

If now the following dimensionless variables are introduced: $\tau = \frac{Ut}{h}$, $u = \frac{u'}{U}$, $u_b = \frac{u'_b}{U}$, $v = \frac{v'}{U}$, $v_b = \frac{v'_b}{U}$, $x = \frac{x'}{h}$, $y = \frac{y'}{h}$ and $R = \frac{R'}{h}$ where U is the free stream velocity and h the body size, Eq. B.11 is found.

$$\frac{du_b}{d\tau} = \frac{3C_D}{4R}(u - u_b)\left[(u - u_b)^2 + (v - v_b)^2\right]^{1/2} - \frac{3}{\rho U^2}\frac{\partial p}{\partial x} \tag{B.11}$$

Now by using the definition of the bubble Reynolds number(Eq. B.8) and using the fact that the derivative to the pressure over the dynamic pressure is the same as the derivative of the pressure coefficient since there is only a constant added to the pressure coefficient, Eq. B.12 is found.

$$\frac{du_b}{d\tau} = \frac{18}{R_b R}\frac{R_b C_D}{24}(u - u_b)\left[(u - u_b)^2 + (v - v_b)^2\right]^{1/2} - 3\frac{1}{2}\frac{\partial C_p}{\partial x} \tag{B.12}$$

This can be rewritten to Eq. B.13.

$$\frac{du_b}{d\tau} = \frac{18\nu}{2R'UR}\frac{R_b C_D}{24}(u - u_b) - \frac{3}{2}\frac{\partial C_p}{\partial x} \tag{B.13}$$

By introducing the body Reynolds number as $R_f = \frac{2hU}{\nu}$ finally Eq. B.14 is found.

$$\boxed{\frac{du_b}{d\tau} = \frac{18}{R^2 R_f} \frac{R_b C_D}{24}(u - u_b) - \frac{3}{2}\frac{\partial C_p}{\partial x}} \tag{B.14}$$

The same steps could be taken in the y-direction leading to Eq. B.15.

$$\boxed{\frac{dv_b}{d\tau} = \frac{18}{R^2 R_f} \frac{R_b C_D}{24}(v - v_b) - \frac{3}{2}\frac{\partial C_p}{\partial y}} \tag{B.15}$$

Both Eq. B.14 and Eq. B.15 form the seventh equation of the paper.

C. Application to a two-dimensional half body in an infinite fluid

To get a flow field in which the bubbles move it is chosen to take a potential flow. The flow potential is given in Eq. C.1.

$$\Phi = \frac{1}{2\pi} \ln\left(x^2 + y^2\right) + x \tag{C.1}$$

This flow potential is an uniform flow field ($+x$-part) combined with a source in the point $(0,0)$. The source will account for the body in the flow. The integration constant is set to zero since in practice only the derivatives matter. The body shape found by this potential is given in Eq. C.2.

$$\boxed{x = -y \cot \pi y} \tag{C.2}$$

Eq. C.2 is the eight equation in the paper. And can be derived via the stream function. The analysis of the stream function just as the analysis of the potential have been left out of this derivation, but can be found in this Appendix on the bottom.
The flow potential can be differentiated to x and to y leading to the velocity components, see Eq. C.3.

$$\boxed{\begin{aligned} \frac{\partial \Phi}{\partial x} &= u = 1 + \frac{1}{\pi} \frac{x}{x^2 + y^2} \\ \frac{\partial \Phi}{\partial y} &= v = \frac{1}{\pi} \frac{y}{x^2 + y^2} \end{aligned}} \tag{C.3}$$

The dimensionless pressure gradients can be found by using Bernoulli's formula, in this there will be no time dependency and no gravity so: $p_0 - p = \frac{1}{2}\rho(u'^2 + v'^2)$. This formula in dimendionless form gives: $C_p = 1 - (u^2 + v^2)$. This gives the dimensionless pressure gradient given in Eq. C.4.

$$\boxed{\begin{aligned} -\frac{\partial C_p}{\partial x} &= -\frac{2}{\pi} \frac{x^2 - y^2 + \frac{x}{\pi}}{(x^2 + y^2)^2} \\ -\frac{\partial C_p}{\partial y} &= -\frac{2}{\pi} \frac{y\left(2x + \frac{1}{\pi}\right)}{(x^2 + y^2)^2} \end{aligned}} \tag{C.4}$$

Eq. C.3 and Eq. C.4 are the ninth equation of the paper, where it should be noted that the $\frac{3}{2}$ was already incorporated in 9c and 9d. Filling in Eq. C.3 and Eq. C.4 into Eq. B.14 and Eq. B.15 gives Eqs. C.5-C.6.

$$\frac{du_b}{d\tau} = \frac{18}{R^2 R_f} \frac{R_b C_D}{24} \left[\left(1 + \frac{1}{\pi} \frac{x}{x^2 + y^2} \right) - u_b \right] - \frac{3}{\pi} \left[\frac{x^2 - y^2 + \frac{x}{\pi}}{(x^2 + y^2)^2} \right] \tag{C.5}$$

$$\frac{dv_b}{d\tau} = \frac{18}{R^2 R_f} \frac{R_b C_D}{24} \left[\left(\frac{1}{\pi} \frac{y}{x^2 + y^2} \right) - v_b \right] - \frac{3}{\pi} \left[\frac{y \left(2x + \frac{1}{\pi} \right)}{(x^2 + y^2)^2} \right] \tag{C.6}$$

Since $u_b = \frac{dx}{d\tau} = \dot{x}$ and $v_b = \frac{dy}{d\tau} = \dot{y}$ the two ordinary differential equations (ODE's in Eqs. C.5-C.6) are of second-order. And can be written as Eqs. C.7-C.8.

$$\boxed{\frac{d\dot{x}}{d\tau} = \frac{18}{R^2 R_f} \frac{R_B C_D}{24} \left[\left(1 + \frac{1}{\pi} \frac{x}{x^2 + y^2} \right) - \dot{x} \right] - \frac{3}{\pi} \left[\frac{x^2 - y^2 + \frac{x}{\pi}}{(x^2 + y^2)^2} \right]} \tag{C.7}$$

$$\boxed{\frac{d\dot{y}}{d\tau} = \frac{18}{R^2 R_f} \frac{R_b C_D}{24} \left[\left(\frac{1}{\pi} \frac{y}{x^2 + y^2} \right) - \dot{y} \right] - \frac{3}{\pi} \left[\frac{y \left(2x + \frac{1}{\pi} \right)}{(x^2 + y^2)^2} \right]} \tag{C.8}$$

The bubble Reynolds number can be found by using the relative velocity components from Eq. C.3. This gives Eq. C.9.

$$\boxed{R_b = R R_f \left\{ \left[\left(1 + \frac{1}{\pi} \frac{x}{x^2 + y^2} \right) - \dot{x} \right]^2 + \left[\left(\frac{1}{\pi} \frac{y}{x^2 + y^2} \right) - \dot{y} \right]^2 \right\}^{1/2}} \tag{C.9}$$

Eq. C.9 is the fourteenth equation of the paper.

D. Actual solving of the ODE's

For efficient computation first-order differential equations are preferred, and therefore the second-order nonlinear ODE's given by Eqs. C.7-C.8-C.9 will be written as a system of first-order ODE's. This is done by introducing the vector $\boldsymbol{z}$. The definition of the vector is given in Eq. D.1.

$$\boldsymbol{z} = \begin{bmatrix} \dot{x} \\ x \\ \dot{y} \\ y \end{bmatrix} \tag{D.1}$$

This means that $\dot{\boldsymbol{z}}$ is given by Eq. D.2.

$$\dot{\boldsymbol{z}} = \begin{bmatrix} \frac{18}{R^2 R_f} \frac{R_B C_D}{24} \left[\left(1 + \frac{1}{\pi} \frac{x}{x^2+y^2} \right) - \dot{x} \right] - \frac{3}{\pi} \left[\frac{x^2-y^2+\frac{x}{\pi}}{(x^2+y^2)^2} \right] \\ \dot{x} \\ \frac{18}{R^2 R_f} \frac{R_b C_D}{24} \left[\left(\frac{1}{\pi} \frac{y}{x^2+y^2} \right) - \dot{y} \right] - \frac{3}{\pi} \left[\frac{y\left(2x+\frac{1}{\pi}\right)}{(x^2+y^2)^2} \right] \\ \dot{y} \end{bmatrix} \tag{D.2}$$

Now it can be seen that the following holds: $\dot{\boldsymbol{z}} = f(\boldsymbol{z})$. So the first derivative of a vector $\boldsymbol{z}$ is a function of that same vector, leading to an in general non-linear system of first-order ODE's.

E. Deriving the bubble dynamics equation

E.1 Derivation of Rayleigh-Plesset equation

In this derivation [2] has been used to provide the directions.
The Rayleigh-Plesset equation can be derived from the Navier-Stokes equations (Eq. E.1) together with the mass conservation equation (Eq. E.2).

$$\rho_f \left(\frac{\partial \boldsymbol{w'}}{\partial t} + \boldsymbol{w'} \cdot \boldsymbol{\nabla} \boldsymbol{w'} \right) = -\boldsymbol{\nabla} p + \mu_f \nabla^2 \boldsymbol{w'} + \zeta_f \boldsymbol{\nabla}\boldsymbol{\nabla} \cdot \boldsymbol{w'} \tag{E.1}$$

$$\frac{\partial \rho_f}{\partial t} + \boldsymbol{\nabla} \cdot (\rho_f \boldsymbol{w'}) = 0 \tag{E.2}$$

In these equations the same notation has been used, the new factor ζ_f is the bulk viscosity of the fluid. This viscosity comes into play when the fluid is being contracted or expanded. It is assumed that the fluid is isothermal, and for that reason the energy equation is not used.

If the identity $\boldsymbol{w'}\boldsymbol{\nabla}\boldsymbol{w'} = \frac{1}{2}\boldsymbol{\nabla}\boldsymbol{w'^2}$ and the velocity is represented by a potential then $\boldsymbol{w'} = \boldsymbol{\nabla}\phi$. Eqs. E.1-E.2 then become Eqs. E.3-E.4.

$$\rho_f \left(\frac{\partial \boldsymbol{\nabla}\phi}{\partial t} + \frac{1}{2}\boldsymbol{\nabla}(\boldsymbol{\nabla}\phi\boldsymbol{\nabla}\phi) \right) = -\boldsymbol{\nabla} p + \mu_f \nabla^2 \boldsymbol{\nabla}\phi + \zeta_f \boldsymbol{\nabla}\boldsymbol{\nabla} \cdot \boldsymbol{\nabla}\phi \tag{E.3}$$

$$\frac{\partial \rho_f}{\partial t} + \boldsymbol{\nabla} \cdot (\rho_f \boldsymbol{\nabla}\phi) = 0 \tag{E.4}$$

Assuming a spherical bubble all the time will mean that the velocity field near the bubble will be fully spherical (if the bubble is followed along its track). This means that the local streamlines will never interfere and therefore the viscosity does not play a role, this leads to Eq. E.5.

$$\rho_f \left(\frac{\partial \boldsymbol{\nabla}\phi}{\partial t} + \frac{1}{2}\boldsymbol{\nabla}(\boldsymbol{\nabla}\phi\boldsymbol{\nabla}\phi) \right) = -\boldsymbol{\nabla} p \tag{E.5}$$

Since the spatial differential operator just as the temporal operator is a linear operator, the order of operations may be switched. This leads to Eq. E.6.

$$\rho_f \boldsymbol{\nabla} \left(\frac{\partial \phi}{\partial t} + \frac{1}{2} \boldsymbol{\nabla}\phi \cdot \boldsymbol{\nabla}\phi \right) = -\boldsymbol{\nabla} p \tag{E.6}$$

Eq. E.6 as a weak formulation one finds Eq. E.7.

$$\rho_f \left(\frac{\partial \phi}{\partial t} + \frac{1}{2} \left(\boldsymbol{\nabla}\phi\right)^2 \right) = -p \tag{E.7}$$

If the assumption of only radial velocity components is re-used finally one finds Eq. E.8.

$$\rho_f \left(\frac{\partial \phi}{\partial t} + \frac{1}{2} \left(\frac{\partial \phi}{\partial r}\right)^2 \right) = -p \tag{E.8}$$

For the mass conservation equation (Eq. E.4) more or less the same steps can be taken leading to Eq. E.9.

$$\frac{\partial \rho_f}{\partial t} + \boldsymbol{\nabla}\rho_f \cdot \boldsymbol{\nabla}\phi + \rho_f \nabla^2 \phi = 0 \tag{E.9}$$

If again the sphericity of the bubble is used one finds Eq. E.10.

$$\frac{\partial \rho_f}{\partial t} + \frac{\partial \rho_f}{\partial r}\frac{\partial \phi}{\partial r} + \rho_f \nabla^2 \phi = 0 \tag{E.10}$$

The objective now is to find one equation for the potential, ϕ, this can be accomplished by taking the temporal derivative of the pressure. First it should be noted that the $dp = \frac{dp}{d\rho_f} d\rho_f = c^2 d\rho_f$. Using both Eqs E.8-E.10 Eq. E.11 can be found.

$$\begin{aligned} -\frac{\partial p}{\partial t} &= -c^2 \frac{\partial \rho_f}{\partial t} = c^2 \left[\frac{\partial \rho_f}{\partial r}\frac{\partial \phi}{\partial r} + \rho_f \nabla^2 \phi \right] \quad \text{and:} \\ -\frac{\partial p}{\partial t} &= \frac{\partial}{\partial t} \left(\rho_f \left[\frac{\partial \phi}{\partial t} + \frac{1}{2} \left(\frac{\partial \phi}{\partial r} \right)^2 \right] \right) \end{aligned} \tag{E.11}$$

Clearly both terms of Eq. E.11 can be equated. Equating both parts, using the product rule of differentiation and rearranging one finds Eq. E.12.

$$\nabla^2 \phi = \frac{1}{c^2 \rho_f}\frac{\partial \rho_f}{\partial t} \left[\frac{\partial \phi}{\partial t} + \frac{1}{2} \left(\frac{\partial \phi}{\partial r} \right)^2 \right] + \frac{1}{c^2} \left[\frac{\partial^2 \phi}{\partial t^2} + \frac{1}{2} \frac{\partial \left(\frac{\partial \phi}{\partial r} \right)^2}{\partial t} \right] - \frac{1}{\rho_f}\frac{\partial \phi}{\partial r}\frac{\partial \rho_f}{\partial r} \tag{E.12}$$

If $dH = \frac{dp}{\rho_f}$, $\frac{\partial \rho_f}{\partial t} = \frac{\rho_f}{c^2}\frac{\partial H}{\partial t}$, $\frac{\partial}{\partial t} = \frac{1}{u}\frac{\partial}{\partial r}$, $\frac{\partial r}{\partial t} = u = \frac{\partial \phi}{\partial r}$ and lastly $\frac{1}{2}\frac{\partial y^2}{\partial x} = \frac{\partial \frac{1}{2} y^2}{\partial y}\frac{\partial y}{\partial x} = y\frac{\partial y}{\partial x}$ one finds Eq. E.13.

$$\nabla^2 \phi = \frac{1}{uc^4}\frac{\partial H}{\partial r}\left[\frac{\partial \phi}{\partial t} + \frac{1}{2}\left(\frac{\partial \phi}{\partial r}\right)^2\right] + \frac{1}{c^2}\left[\frac{\partial^2 \phi}{\partial t^2} + u\frac{\partial u}{\partial t}\right] - \frac{u}{c^2}\frac{\partial H}{\partial r} \tag{E.13}$$

Now reuse the momentum equation, to find Eq. E.14.

$$\nabla^2 \phi = -\frac{1}{uc^4}\frac{\partial H}{\partial r}\frac{p}{\rho_f} + \frac{1}{c^2}\left[\frac{\partial^2 \phi}{\partial t^2} + u\frac{\partial u}{\partial t}\right] - \frac{u}{c^2}\frac{\partial H}{\partial r} \tag{E.14}$$

Rearranging gives Eq. E.15.

$$\nabla^2 \phi = \frac{u}{c^2}\left(\frac{\partial u}{\partial t} - \frac{\partial H}{\partial r}\left[1 + \frac{p}{\rho_f c^2 u^2}\right]\right) + \frac{1}{c^2}\frac{\partial^2 \phi}{\partial t^2} \tag{E.15}$$

Knowing that the pressure is of the same order as the density times about the free stream velocity squared, and assuming that this free stream velocity is much smaller than the speed of sound, the term in between square brackets can be reduced to just 1, this finally gives Eq. E.16.

$$\nabla^2 \phi = \frac{u}{c^2}\left(\frac{\partial u}{\partial t} - \frac{\partial H}{\partial r}\right) + \frac{1}{c^2}\frac{\partial^2 \phi}{\partial t^2} \tag{E.16}$$

Eq. E.16 needs to be solved as a function off the wall velocity of the bubble ($\frac{dR}{dt}$). From Eq. E.16 it can be seen that with a velocity field with significant lower velocities the first term cancels ($\frac{u}{c^2} \approx 0$). The linear term involving $\frac{\partial^2 \phi}{\partial t^2}$ can be neglected near the bubble, under the assumption that $c^2 \gg \frac{\partial^2 \phi}{\partial t^2}$. This leads to the conclusion that near the bubble the Laplace equation holds for the potential ($\nabla^2\phi$=0). At the bubble wall the radial velocity is known, namely the velocity of the bubble wall itself. This leads to a solution shown in Eq. E.17.

$$\phi = -\frac{\dot{R}' R'^2}{r} + A(t) \tag{E.17}$$

Where $\dot{R}' = \frac{dR'}{dt}$ and $A(t)$ is a free constant possibly depending on time. The constant $A(t)$ will represent the sound field initiated by the bubbles growth and collapse. Since the bubble is much smaller than the sound wave length (note that this is a crucial assumption, but realistic since the wavelenght of sound of $1\,kHz$ in water is about $1.5\,m$), the sound field will be independent of r at large distances from the bubble. This means that the first term will be omitted far from the bubble so that Eq. E.18 remains.

$$\phi = A(t) \tag{E.18}$$

It is also known that far away from the bubble the potential is equal to the potential at infinity giving $A(t) = \phi_\infty(t)$. So the full potential is given by Eq. E.19.

$$\phi = -\frac{\dot{R}' R'^2}{r} + \phi_\infty(t) \tag{E.19}$$

It can be seen that the velocity $u = \frac{\partial \phi}{\partial r} = \frac{\dot{R}' R'^2}{r^2}$, and that at $r = R'$ the boundary condition indeed holds. Having the velocity, the force balance on the surface of the bubble can be made. This is done in terms of the pressure, see Eq. E.20. The shear viscosity has however now been included via the shear term $\frac{\partial u}{\partial r}(r = R')$.

$$p_g(t) + p_v - p[R'(t)] + 2\mu_f \frac{\partial u}{\partial r}(r = R') = 2\frac{\gamma}{R'} \tag{E.20}$$

Differentiating the velocity field to r leads to Eq. E.21.

$$p_g(t) + p_v - p[R'(t)] - 4\mu_f \frac{\dot{R}'}{R'} = 2\frac{\gamma}{R'} \tag{E.21}$$

The pressure in the bubble of the gas, p_g, is assumed to be spatially uniform, meaning that body forces are not allowed. If Eq. E.8 is used again, and the pressure term of Eq. E.21 is used one finds Eq. E.22.

$$\rho_f \left(\frac{\partial \phi}{\partial t} + \frac{1}{2} \left(\frac{\partial \phi}{\partial r} \right)^2 \right) = -p_g(t) - p_v + 4\mu_f \frac{\dot{R}'}{R'} + 2\frac{\gamma}{R'} \tag{E.22}$$

Knowing that $\frac{\partial \phi}{\partial r} = u$ and filling it in at $r = R'$ gives $\frac{\partial \phi}{\partial r} = \dot{R}'$. $\frac{\partial \phi}{\partial t}$ is derived in Eq. E.23.

$$\frac{\partial \phi}{\partial t} = \frac{\partial}{\partial t} \left(-\frac{\dot{R}' R'^2}{r} \right) + \frac{\partial}{\partial t} \left(\phi_\infty(t) \right) = -\ddot{R}' R' - 2\dot{R}'^2 + \frac{\partial}{\partial t} \left(\phi_\infty(t) \right) \tag{E.23}$$

Using Eq. E.23 in Eq. E.22 gives Eq. E.24.

$$\rho_f \left[R' \frac{d^2 R'}{dt^2} + \frac{3}{2} \left(\frac{dR'}{dt} \right)^2 \right] = p_g(t) + p_v - 4\mu_f \frac{\dot{R}'}{R'} - 2\frac{\gamma}{R'} + \rho_f \frac{\partial \phi_\infty}{\partial t} \tag{E.24}$$

The term $\rho_f \frac{\partial \phi_\infty}{\partial t}$ is the source term in the equation. This can be included in the following way: $\rho_f \frac{\partial \phi_\infty}{\partial t} = -P_0 - P(t)$.

$$\rho_f \left[R' \frac{d^2 R'}{dt^2} + \frac{3}{2} \left(\frac{dR'}{dt} \right)^2 \right] = p_g(t) + p_v - P_0 - P(t) - 4\mu_f \frac{\dot{R}'}{R'} - 2\frac{\gamma}{R'} \tag{E.25}$$

The source term depends in this case on the bubble path, therefore the pressure which the bubble feels, taken as p can be taken as this source. Including this term gives Eq. E.26 is found.

$$\rho_f \left[R' \frac{d^2 R'}{dt^2} + \frac{3}{2} \left(\frac{dR'}{dt} \right)^2 \right] = p_v - p + p_g(t) - 2\frac{\gamma}{R'} - \frac{4\mu_f}{R'} \frac{dR'}{dt} \tag{E.26}$$

To improve the found equation the gas pressure derivative can be included. Furthermore the influence of the radiated sound wave can be included to implement the effect of damping. Lastly it is important to have a realistic equation of state. This will all be examined later.

E.2 Non dimensionalization of Rayleigh-Plesset equation

For the usability of the Rayleigh-Plesset equation it is beneficial to have it in its dimensionless form.
The Rayleigh-Plesset equation is given in Eq. E.26, if $pV^{\frac{c_p}{c_v}} = C$, with C a constant, is used as the equation of state for the gas pressure, and some convenient rewriting is done one finds Eq. E.27.

$$\begin{aligned} \rho_f U^2 \left[R \frac{d^2 R}{d\tau^2} + \frac{3}{2} \left(\frac{dR}{d\tau} \right)^2 \right] =& \frac{1}{2} \rho_f U^2 \left(-\frac{p_0 - p_v}{\frac{1}{2}\rho_f U^2} - \frac{p - p_0}{\frac{1}{2}\rho_f U^2} \right) + p_{g_0} \left(\frac{R_0}{R} \right)^{3\frac{c_p}{c_v}} \\ & - 2\frac{\gamma}{Rh} - \frac{4\mu_f U}{Rh} \frac{dR}{d\tau} \end{aligned} \tag{E.27}$$

Using the definition of the pressure coefficient C_p, the cavitation number σ_v, the Weber number W and the Reynolds number of the flow R_f one finds Eq. E.28.

$$\left[R \frac{d^2 R}{d\tau^2} + \frac{3}{2} \left(\frac{dR}{d\tau} \right)^2 \right] = \frac{1}{2} (-C_p - \sigma_v) + \frac{p_{g_0}}{\rho_f U^2} \left(\frac{R_0}{R} \right)^{3\frac{c_p}{c_v}} - \frac{4R_0'}{WhR} - \frac{8}{R_f R} \frac{dR}{d\tau} \tag{E.28}$$

Noting that $p_{g_0} = p_o - p_v + \frac{2\gamma}{R_0'}$ gives that $\frac{p_{g_0}}{\rho_f U^2} = \frac{1}{2}\sigma_v + \frac{4}{W}$. Using this relation one finds Eq. E.29.

$$\frac{d^2 R}{d\tau^2} = \frac{1}{R} \left[-\frac{3}{2} \left(\frac{dR}{d\tau} \right)^2 + \frac{1}{2} (-C_p - \sigma_v) + \left(\frac{1}{2}\sigma_v + \frac{4}{W} \right) \left(\frac{R_0}{R} \right)^{3\frac{c_p}{c_v}} - \frac{4h}{WR_0'R} - \frac{8}{R_f R} \frac{dR}{d\tau} \right] \tag{E.29}$$

Eq. E.29 is the dimensionless Rayleigh-Plesset equation with the conventions used in the paper.

E.3 Derivation of the Keller equation

In this derivation both [3] and [2] have been used extensively.
The derivation of this equation is comparable to the derivation of the Rayleigh-Plesset equation, with the only difference being that the radiated sound wave is taken in consideration. Waves in general can be solved by a function which is constant in time when the observer of the solution is moving with the wave speed. This holds in both directions, and therefore a general wave solution can be seen in Eq. E.30.

$$Q_{\text{Wave}} = F(t - \frac{r}{c}) + G(t + \frac{r}{c}) \tag{E.30}$$

Since the wave is created by a changing volume in time the units of the solution are $[m^3 s^{-1}]$. It is obvious that if one travels at the speed of sound, c, the argument of the function F is constant, and therefore the value of F. Since the wave is defined in polar coordinates, the wave the other way is not there, so $G = 0$. This leads to $Q_{\text{Wave}} = F(t - \frac{r}{c})$. If the wave is implemented in the potential of Eq. E.17 one finds Eq. E.31.

$$\phi = -\frac{\dot{R}' R'^2}{r} + A(t) = \phi_\infty(t) - \frac{1}{r} F(t - \frac{r}{c}) \tag{E.31}$$

So it can be seen that the potential far away from the bubble is still $\phi_{infty}(t)$, but now with the wave potential of the wave added.
The wave function $F(t - \frac{r}{c})$ can be approximated as $F(t - \frac{r}{c}) = F(t) - \frac{r}{c}\frac{dF(t)}{dt}$ via a first-order Taylor expansion around the point t. Using this relation one finds Eq. E.32.

$$\phi = \phi_\infty(t) - \frac{1}{r} F(t - \frac{r}{c}) \approx \phi_\infty(t) - \frac{1}{r} F(t) + \frac{1}{c}\frac{dF(t)}{dt} \tag{E.32}$$

By comparing Eq. E.31 and Eq. E.32 one finds that $F(t) = \dot{R}' R'^2$ and $A(t) = \phi_\infty(t) + \frac{1}{c}\frac{dF(t)}{ddt}$.
Following the derivation of the Rayleigh-Plesset equation, the found potential should now be included in the reduced momentum equation (Eq. E.8). This involves calculating $\frac{\partial \phi}{\partial t}$ and $\frac{\partial \phi}{\partial r}$ at $r = R'$. These calculations will be done term wise starting with $\frac{\partial \phi}{\partial r}$, see Eq. E.33.

$$\frac{\partial \phi}{\partial r}(r = R') = \frac{\dot{R}' R'^2}{r^2}|_{r=R'} = \dot{R}' \tag{E.33}$$

Calculating $\frac{\partial \phi}{\partial t}$ will be more involved, but will be started in Eq. E.34.

$$
\begin{aligned}
\frac{\partial \phi}{\partial t}|_{r=R'} &= \frac{d\phi_\infty(t)}{dt} - \frac{1}{r}\frac{d(\dot{R}'R'^2)}{dt} + \frac{1}{c}\frac{d^2(\dot{R}'R'^2)}{dt^2} \\
&= \frac{d\phi_\infty(t)}{dt} - \frac{1}{R'}\left(\ddot{R}'R'^2 + 2R'\dot{R}'^2\right) + \frac{1}{c}\frac{d^2(\dot{R}'R'^2)}{dt^2} \\
&= \frac{d\phi_\infty(t)}{dt} - \left(\ddot{R}'R'^2 + 2\dot{R}'^2\right) + \frac{1}{c}\frac{d^2(\dot{R}'R'^2)}{dt^2}
\end{aligned}
\tag{E.34}
$$

The latter part of Eq. E.34 ($\frac{d^2(\dot{R}'R'^2)}{dt^2}$) will be treated separately, which can be seen in Eq. E.35.

$$
\frac{d^2(\dot{R}'R'^2)}{dt^2} = \frac{d}{dt}\left(\ddot{R}'R'^2 + 2\dot{R}'^2R'\right)
\tag{E.35}
$$

The first part ($\frac{d}{dt}\left(\ddot{R}'R'^2\right)$) of Eq. E.35 will lead to a third derivative of the radius of the bubble with respect to time. This is an unwanted derivative, since it requires an extra initial condition on the acceleration of the boundary of the bubble. By that it turns out that this will not work numerically according to [3]. To prevent this problem the third derivative can be expressed in terms of the normal Rayleigh-Plesset equation (Eq. E.26). It can be seen that the term $\ddot{R}R'$ can be extracted from the Rayleigh-Plesset equation. This is a simplification of course, since the objective is to look for a more advanced equation for the bubble dynamics, but it is the best option available. So after some tedious derivation Eq. E.36 is found.

$$
\begin{aligned}
\frac{d}{dt}\left(\ddot{R}'R'^2\right) &= \frac{d}{dt}\left\{R'\left[\frac{1}{\rho_f}\left(p_v - p + p_g(t) - 2\frac{\gamma}{R'} - \frac{4\mu_f}{R'}\dot{R}'\right) - \frac{3}{2}\dot{R}'^2\right]\right\} \\
&= -\frac{3}{2}\dot{R}'^3 - 3R'\dot{R}'\ddot{R}' + \frac{\dot{R}'}{\rho_f}\left(p_v - p + p_g(t)\right) + \frac{1}{\rho_f}\dot{p_g}R'
\end{aligned}
\tag{E.36}
$$

Adding the result of Eq. E.36 with $\frac{d}{dt}\left(2\dot{R}'^2R'\right) = 2\dot{R}'^3 + 4R'\dot{R}'\ddot{R}'$ gives Eq. E.37.

$$
\frac{d^2(\dot{R}'R'^2)}{dt^2} = \frac{1}{2}\dot{R}'^3 + R'\dot{R}'\ddot{R}' + \frac{\dot{R}'}{\rho_f}\left(p_v - p + p_g(t)\right) + \frac{1}{\rho_f}\dot{p_g}R'
\tag{E.37}
$$

Filling in Eq. E.37 into Eq. E.34 and knowing that the source term is the negative pressure of the flow over the density of the liquid so, $\frac{\partial \phi_\infty}{\partial t} = -\frac{p}{\rho_f}$ gives Eq. E.38.

$$
\begin{aligned}
&\frac{\partial \phi}{\partial t}|_{r=R'} = \\
&-\frac{p}{\rho_f} - \left(\ddot{R}'R' + 2\dot{R}'^2\right) + \frac{\dot{R}'}{c}\left[\frac{1}{2}\dot{R}'^2 + \ddot{R}'R' + \frac{1}{\rho_f}\left(p_v - p + p_g(t)\right) + \frac{1}{\rho_f}\dot{p_g}R'\right]
\end{aligned}
\tag{E.38}
$$

Using Eq. E.22 and Eq. E.33 and Eq. E.38 one finds Eq. E.39.

$$
\begin{aligned}
&-p-\rho_f\left(\ddot{R}'R'+\frac{3}{2}\dot{R}'^2\right)+\rho_f\frac{\dot{R}'}{c}\left[\frac{1}{2}\dot{R}'^2+\ddot{R}'R'+\frac{1}{\rho_f}\left(p_v-p+p_g(t)\right)+\frac{1}{\rho_f}\dot{p_g}R'\right]=\\
&-p_g(t)-p_v+4\mu_f\frac{\dot{R}'}{R'}+2\frac{\gamma}{R'}
\end{aligned}
\tag{E.39}
$$

Rewriting Eq. E.39 gives Eq. E.40.

$$
\begin{aligned}
&\left(1-\frac{\dot{R}'}{c}\right)\rho_f R'\ddot{R}'+\frac{3}{2}\dot{R}'^2\rho_f\left(1-\frac{\dot{R}'}{3c}\right)=\\
&\left(1+\frac{\dot{R}'}{c}\right)\left[p_v-p+p_g(t)\right]+\frac{R'}{c}\dot{p_g}(t)-4\mu_f\frac{\dot{R}'}{R'}-2\frac{\gamma}{R'}
\end{aligned}
\tag{E.40}
$$

As can be seen in Eq. E.40 the found equation will reduce to the Rayliegh-Plesset equation if $c \gg \dot{R}'$ plus an extra term with the temporal derivative of the gas pressure. Eq. E.40 is called the Keller equation in [3] and [2].
Eq. E.40 can be derived in a more general way, namely by adding the Rayleigh-Plesset equation the equation resulting in a third order temporal derivative. This leads to the general Keller-Herring equation, which is given in Eq. E.41.

$$
\begin{aligned}
&\left(1-(\lambda+1)\frac{\frac{dR'}{dt}}{c}\right)\rho_f R'\frac{d^2R'}{dt^2}+\frac{3}{2}\frac{dR'}{dt}^2\rho_f\left(1-(\lambda+\frac{1}{3})\frac{\frac{dR'}{dt}}{c}\right)=\\
&\left(1+(1-\lambda)\frac{\frac{dR'}{dt}}{c}\right)\left[p_v-p+p_g(t)\right]+\frac{R'}{c}\frac{dp_g(t)}{dt}-4\mu\frac{\frac{dR'}{dt}}{R'}-\frac{2\gamma}{R'}
\end{aligned}
\tag{E.41}
$$

If the factor λ in Eq. E.41 is set to 0 the Keller Miksis equation is found, and if λ is set to 1 the equation used by Herring and Trilling is found.

E.4 Non dimensionalization of the general Keller-Herring equation

The non-dimensionalization of the general Keller-Herring equation will be similar to the non dimensionalization of the Rayleigh-Plesset equation. Since it is convenient to have an equation of state when one starts to non-dimensionalize the van der Waals equation of state is used. This is done so that the application of this equation of state to the normal Rayleigh-Plesset equation will be clear as well. It is also meant to work the other way around, the ideal gas equation of state will be assumed to be easy to implement by the reader. The van der Waals equation of state is given in Eq. E.42.

$$p_g \left(R'^3 - R'^3_{hc}\right)^\kappa = C \tag{E.42}$$

In Eq. E.42 C is a constant and R'_{hc} is the van der Waals hard core radius which is $R'_{hc} = \frac{R'_0}{8.54}$ ([4]) for air. κ is the specific heat ratio. By implementing the standard non dimensionalization and the equation on state one finds Eq. E.43.

$$\begin{aligned}&\rho_f U^2 \left(1 - (\lambda+1)\dot{R}\frac{U}{c}\right) R\ddot{R} + \frac{3}{2}\rho_f U^2 \dot{R}^2 \left(1 - \left(\lambda + \frac{1}{3}\right)\dot{R}\frac{U}{c}\right) = \\ &\left(1 + (1-\lambda)\dot{R}\frac{U}{c}\right)\left[p_v - p + p_{g0}\left(\frac{R_0^3 - R_{hc}^3}{R^3 - R_{hc}^3}\right)^\kappa\right] + R\frac{U}{c}\frac{d}{d\tau}\left\{p_{g0}\left(\frac{R_0^3 - R_{hc}^3}{R^3 - R_{hc}^3}\right)^\kappa\right\} \\ &- 4\mu_f \frac{U}{h}\frac{\dot{R}}{R} - 2\frac{\gamma}{Rh}\end{aligned} \tag{E.43}$$

Dividing out (2 times) the dynamic pressure, realizing $\frac{p_{g0}}{\rho_f U^2} = \frac{1}{2}\sigma_v + \frac{4}{W}$. And working out the differentiation gives Eq. E.44.

$$\begin{aligned}&\left(1 - (\lambda+1)\dot{R}\frac{U}{c}\right) R\ddot{R} + \frac{3}{2}\dot{R}^2 \left(1 - \left(\lambda + \frac{1}{3}\right)\dot{R}\frac{U}{c}\right) = \\ &\frac{1}{2}\left(1 + (1-\lambda)\dot{R}\frac{U}{c}\right)\left[-\frac{p_0 - p_v}{\frac{1}{2}\rho_f U^2} - \frac{p - p_0}{\frac{1}{2}\rho_f U^2} + \left(\sigma_v + \frac{8}{W}\right)\left(\frac{R_0^3 - R_{hc}^3}{R^3 - R_{hc}^3}\right)^\kappa\right] \\ &+ R\frac{U}{c}\left(\frac{1}{2}\sigma_v + \frac{4}{W}\right)\left[\frac{3\kappa R^2 \left(\frac{R_0^3 - R_{hc}^3}{R^3 - R_{hc}^3}\right)^\kappa}{R_{hc}^3 - R^3}\right] - 4\frac{\mu_f}{\rho_f U h}\frac{\dot{R}}{R} - 2\frac{\gamma}{\rho_f U^2 R h}\end{aligned} \tag{E.44}$$

Now using the pressure coefficient, the cavitation number, the Weber number and the Reynolds number one finds Eq. E.45.

$$\begin{aligned}&\left(1 - (\lambda+1)\dot{R}\frac{U}{c}\right) R\ddot{R} + \frac{3}{2}\dot{R}^2 \left(1 - \left(\lambda + \frac{1}{3}\right)\dot{R}\frac{U}{c}\right) = \\ &\frac{1}{2}\left(1 + (1-\lambda)\dot{R}\frac{U}{c}\right)\left[-\sigma_v - C_p + \left(\sigma_v + \frac{8}{W}\right)\left(\frac{R_0^3 - R_{hc}^3}{R^3 - R_{hc}^3}\right)^\kappa\right] \\ &+ R\frac{U}{c}\left(\frac{1}{2}\sigma_v + \frac{4}{W}\right)\left[\frac{3\kappa R^2 \left(\frac{R_0^3 - R_{hc}^3}{R^3 - R_{hc}^3}\right)^\kappa}{R_{hc}^3 - R^3}\right] - \frac{8}{R_f}\frac{\dot{R}}{R} - \frac{4}{W}\frac{R_0}{R}\end{aligned} \tag{E.45}$$

Finally Eq. E.45 can be written in terms of the second derivative of the dimensionless radius to the dimensionless time, $\ddot{R}$. This is obvious and will not be done.

F. Equation of motion

F.1 Derivation

The equation of motion given in Maxey and Riley (their equation 48) is given in Eq. F.1. The same symbols will be used in this derivation, after which they will be transformed back to the used notation convention. It is important to know that $W_i = V_i(t) - u_i[\boldsymbol{Y}(t), t]$ is the slip velocity but inversely defined and a is the radius of the sphere.

$$\begin{aligned} &\left(m_p + \frac{1}{2}m_f\right)\frac{dW_i}{dt} + 6\pi a^2\mu\int_0^t \frac{dW_i}{d\tau}\left[\pi\nu(t-\tau)\right]^{-1/2}d\tau + 6\pi a\mu W_i = \\ &- m_p\frac{du_i}{dt} + m_f\frac{Du_i}{Dt} + (m_p - m_f)\,g_i + a^3\pi\mu\nabla^2 u_i + \frac{1}{20}a^2 m_f\frac{d}{dt}\left(\nabla^2 u_i|_{\boldsymbol{Y}(t)}\right) \\ &+ \pi\mu a^4\int_0^t \frac{d}{d\tau}\left(\nabla^2 u_i|_{\boldsymbol{Y}(t)}\right)\left[\pi\nu(t-\tau)\right]^{-1/2}d\tau \end{aligned} \tag{F.1}$$

First, this equation of motion will be simplified assuming steady potential flwo. Note that all terms with the Laplacian of the fluid velocity are zero under the assumption of potential flow. This can easily be seen: $\nabla^2 u_i = \nabla^2\frac{\partial\Phi}{\partial x_i} = \frac{\partial}{\partial x_i}(\nabla^2\Phi)$. In potential flow the Laplace of the potential is zero everywhere, so the gradient of this Laplacian must also be zero everywhere. The terms with the Laplacian of the velocity will thus be left out of discussion. Furthermore the time derivative of the fluid velocity is zero since it is steady flow. The equation of motion which will be discussed can be seen in Eq. F.2.

$$\begin{aligned} &\underbrace{\left(m_p + \frac{1}{2}m_f\right)\frac{dW_i}{dt}}_{\text{Accelaration force}} + \underbrace{6\pi a^2\mu\int_0^t \frac{dW_i}{d\tau}\left[\pi\nu(t-\tau)\right]^{-1/2}d\tau}_{\text{History force}} + \underbrace{6\pi a\mu W_i}_{\text{Drag force}} = \\ &\underbrace{m_f\frac{Du_i}{Dt}}_{\text{Pressure force}} + \underbrace{(m_p - m_f)\,g_i}_{\text{Buoyancy force}} \end{aligned} \tag{F.2}$$

Via the Navier-Stokes equation for potential flow it can be seen that $m_f\frac{Du_i}{Dt} = -V_f\boldsymbol{\nabla}p$, the mass of the fluid is however not only the mass of the fluid which would have been in the volume of the bubble, it is also the added mass, leading to $m_f \frac{Du_i}{Dt} = -(1+\frac{1}{2})\frac{4\pi}{3}a^3\rho_f \boldsymbol{\nabla}\frac{p}{\rho_f}$. This leads to Eq. F.3.

$$\begin{aligned}&\underbrace{\left(m_p + \frac{1}{2}m_f\right)\frac{dW_i}{dt}}_{\text{Accelaration force}} + \underbrace{6\pi a^2\mu\int_0^t \frac{dW_i}{d\tau}\left[\pi\nu(t-\tau)\right]^{-1/2}d\tau}_{\text{History force}} + \underbrace{6\pi a\mu W_i}_{\text{Drag force}} = \\ &\underbrace{-\frac{3}{2}\frac{4\pi}{3}a^3\boldsymbol{\nabla}p}_{\text{Pressure force}} + \underbrace{\left(m_p - m_f\right)g_i}_{\text{Buoyancy force}}\end{aligned} \tag{F.3}$$

This equation of motion is derived for the limit of creeping flow. Since this will not be considered, the analytical result for the creeping flow drag relation is replaced by the drag coefficient C_D. Furthermore the equation is derived for solid particles. The solid particles can be changed to volume-changing bubbles by differentiating the whole impulse term with respect to time instead of just the velocity. This can be seen in Eq. F.4.

$$\begin{aligned}&\underbrace{\frac{d}{dt}\left\{\left(m_p + \frac{1}{2}m_f(t)\right)W_i\right\}}_{\text{Accelaration force}} + \underbrace{6\pi a^2\mu\int_0^t \frac{dW_i}{d\tau}\left[\pi\nu(t-\tau)\right]^{-1/2}d\tau}_{\text{History force}} + \underbrace{\frac{1}{2}\rho_f C_D \pi a^2 W_i^2}_{\text{Drag force}} = \\ &\underbrace{-\frac{3}{2}\frac{4\pi}{3}a^3\boldsymbol{\nabla}p}_{\text{Pressure force}} + \underbrace{\left(m_p - m_f\right)g_i}_{\text{Buoyancy force}}\end{aligned} \tag{F.4}$$

It is assumed that the bubble has a constant mass (note that this assumption means no mass transport, even at (very) low pressures inside the bubble). The added mass, however, can change since the radius of the bubble can change. Using the volume of a sphere and the chain rule of differentiation leads to Eq. F.5.

$$\begin{aligned}&\underbrace{\left(m_p + \frac{1}{2}m_f\right)\frac{dW_i}{dt}}_{\text{Accelaration force}} + \underbrace{\frac{1}{2}4\pi\rho_f a^2\frac{da}{dt}W_i}_{\text{Changing volume force}} + \underbrace{6\pi a^2\mu\int_0^t \frac{dW_i}{d\tau}\left[\pi\nu(t-\tau)\right]^{-1/2}d\tau}_{\text{History force}} = \\ &-\underbrace{\frac{1}{2}\rho_f C_D \pi a^2 W_i^2}_{\text{Drag force}} - \underbrace{\frac{3}{2}\frac{4\pi}{3}a^3\boldsymbol{\nabla}p}_{\text{Pressure force}} + \underbrace{\left(m_p - m_f\right)g_i}_{\text{Buoyancy force}}\end{aligned} \tag{F.5}$$

A better understanding of the changing volume force is necessary for understanding the particle trajectory. In four cases the working of this force will be explained. It is important to know that the force can be written as an added mass change in time times the slip velocity of the bubble.

- The bubble grows and the bubble is slower than the surrounding flow.
In this case the bubble will accelerate, this is due to the fact that the added mass of the bubble is growing. The growing added mass needs mass from the flow, this mass is faster than the bubble, and therefore it can be seen as if the mass gets trapped into the added mass of the bubble making the bubble accelerate.

- The bubble grows and the bubble is faster than the surrounding flow.
In that case the bubble will decelerate, this is due to the fact that the added mass is growing. The growing added mass needs mass from the flow, this mass is slower than the bubble, and therefore it can be seen as if the bubble bumps into its future added mass, making the bubble decelerate.

- The bubble shrinks and the bubble is slower than the surrounding flow.
In that case the bubble will decelerate, this is due to the fact that the added mass is shrinking. The shrinking added mass loses mass to the faster flow. The mass in the (former) added mass “wants” to be at the higher speed of the surrounding fluid, letting go of this mass means that the bubble will decelerate.

- The bubble shrinks and the bubble is faster than the surrounding flow.
In that case the bubble will accelerate, this is due to the fact that the added mass is shrinking. The shrinking added mass loses mass to the slower flow. The mass in the (former) added mass “wants” to be at the lower speed of the surrounding fluid, letting go of this mass means that the bubble will accelerate.

The volume-changing force has some self-enlarging effect, for a shrinking bubble. If it is slower than the flow, the bubble will decelerate and enlarge the slip velocity because of this effect. This will lead to strong behavior regarding this force. As it turns out a bubble can, in the model presented, go in the opposite direction of the flow. In reality this effect will probably be significantly less influential, the equations regarding the bubble growth allow for violent collapses (and fast growth) of the bubble. Especially in the collapsing phase the wake, in which the added mass is trapped, will not be able to fully develop. This unsteady phenomena will reduce this effect significantly. A simple approach would be to make the added mass dependent upon the bubble growth.

The history force will not be taken into account for now.

$$\underbrace{\left(m_p + \frac{1}{2}m_f\right)\frac{dW_i}{dt}}_{\text{Accelaration force}} + \underbrace{2\pi\rho_f a^2 \frac{da}{dt} W_i}_{\text{Changing volume force}} = \underbrace{-\frac{1}{2}\rho_f C_D \pi a^2 W_i^2}_{\text{Drag force}} - \underbrace{\frac{3}{2}\frac{4\pi}{3}a^3 \boldsymbol{\nabla} p}_{\text{Pressure force}} + \underbrace{(m_p - m_f)\, g_i}_{\text{Buoyancy force}} \tag{F.6}$$

So having used the assumption of one-way coupled steady potential flow and neglecting the acceleration of the flow an equation of motion is derived (see Eq. F.6). To write this equation of motion in the usual convention it is important to note that the slip velocity W_i was inversely defined, and the equation is now written in vector form. This leads to Eq. F.7.

$$\underbrace{\frac{4}{3}\pi R'^3(\frac{1}{2}\rho_f+\rho_b)\frac{d\boldsymbol{w}_b}{dt}}_{\text{Acceleration force}}=\underbrace{\frac{1}{2}\rho(\boldsymbol{w}-\boldsymbol{w}_b)|\boldsymbol{w}-\boldsymbol{w}_b|C_D\pi R'^2}_{\text{Drag force}}-\underbrace{\frac{3}{2}\frac{4}{3}\pi R'^3\boldsymbol{\nabla}p}_{\text{Pressure force}}+\underbrace{\frac{4}{3}\pi R'^3\boldsymbol{g'}(\rho_b-\rho_f)}_{\text{Buoyancy force}}$$
$$+\underbrace{2\pi\rho_f R'^2(\boldsymbol{w}-\boldsymbol{w}_b)\frac{dR'}{dt}}_{\text{Changing volume force}} \tag{F.7}$$

F.2 Non dimensionalization

The equation of motion can be rewritten to Eq. F.8.

$$(\frac{1}{2}\rho_f+\rho_b)\frac{d\boldsymbol{w'}_b}{dt}=\frac{3}{8}\rho_f\frac{C_D}{R'}(\boldsymbol{w'}-\boldsymbol{w'}_b)|\boldsymbol{w'}-\boldsymbol{w'}_b|-\frac{3}{2}\boldsymbol{\nabla}p+\boldsymbol{g'}(\rho_b-\rho_f)+\frac{3}{2}\frac{\rho_f}{R'}(\boldsymbol{w'}-\boldsymbol{w'}_b)\frac{dR'}{dt} \tag{F.8}$$

Note that in Eq. F.8 the $\boldsymbol{w'}$ means that it is a dimensionfull vector of the velocity components. Now introducing:

$$\tau=\frac{Ut}{h}\ u=\frac{u'}{U}\ v=\frac{v'}{U}\ U_b=\frac{u'_b}{U}\ V_b=\frac{v'_b}{U}\ x=\frac{x'}{h}\ y=\frac{y'}{h}\ R=\frac{R'}{h}\ \boldsymbol{g}=\frac{\boldsymbol{g'}h}{U^2}$$

gives Eq. F.9.

$$(\frac{1}{2}\rho_f+\rho_b)\frac{d\boldsymbol{w}_b}{d\tau}=\frac{3}{8}\rho_f\frac{C_D}{R}(\boldsymbol{w}-\boldsymbol{w}_b)|\boldsymbol{w}-\boldsymbol{w}_b|-\frac{3}{2}\frac{h}{U^2}\boldsymbol{\nabla}_{\boldsymbol{x'}}p+\boldsymbol{g}(\rho_b-\rho_f)+\frac{3}{2}\frac{\rho_f}{R}(\boldsymbol{w}-\boldsymbol{w}_b)\frac{dR}{d\tau} \tag{F.9}$$

The pressure gradient can be non dimensionalized like how it is done before giving Eq. F.10.

$$(\frac{1}{2}\rho_f+\rho_b)\frac{d\boldsymbol{w}_b}{d\tau}=\frac{3}{8}\rho_f\frac{C_D}{R}(\boldsymbol{w}-\boldsymbol{w}_b)|\boldsymbol{w}-\boldsymbol{w}_b|-\frac{3}{4}\rho_f\boldsymbol{\nabla}C_p+\boldsymbol{g}(\rho_b-\rho_f)+\frac{3}{2}\frac{\rho_f}{R}(\boldsymbol{w}-\boldsymbol{w}_b)\frac{dR}{d\tau} \tag{F.10}$$

Lastly introducing $\alpha=\frac{\rho_f}{\rho_b+\frac{1}{2}\rho_f}$ and $\beta=\frac{\rho_b-\rho_f}{\rho_b+\frac{1}{2}\rho_f}$ Eq. F.11 is found.

$$\frac{d\boldsymbol{w}_b}{d\tau}=\frac{3}{8}\frac{C_D\alpha}{R}(\boldsymbol{w}-\boldsymbol{w}_b)|\boldsymbol{w}-\boldsymbol{w}_b|-\frac{3}{4}\alpha\boldsymbol{\nabla}C_p+\boldsymbol{g}\beta+\frac{3}{2}\frac{\alpha}{R}(\boldsymbol{w}-\boldsymbol{w}_b)\frac{dR}{d\tau} \tag{F.11}$$

Since the drag relation is most convenient in the form $\frac{C_D R_b}{24}$ where $R_b=RR_f|\boldsymbol{w}-\boldsymbol{w}_b|$ one finds Eq. F.12.

$$\frac{d\boldsymbol{w}_b}{d\tau} = \frac{9\alpha}{R^2 R_f} \frac{C_D R_b}{24}(\boldsymbol{w} - \boldsymbol{w}_b) - \frac{3}{4}\alpha \boldsymbol{\nabla} C_p + \boldsymbol{g}\beta + \frac{3}{2}\frac{\alpha}{R}(\boldsymbol{w} - \boldsymbol{w}_b)\frac{dR}{d\tau} \tag{F.12}$$

The relation for $\frac{C_D R_b}{24}$ has already been given and will be kept the same, and $R_f = \frac{2hU}{\nu_f}$.

G. Actual solving of the ODE's

The described equations are all meant to solve a system of equations which describe the particle path together with the bubble growth. Since only derivatives in time play a role the system is a system of coupled non-linear second-order ODE's. To solve such a system the ode functions in Matlab are the easiest to implement. But to use these functions it is necessary to reduce the order. The ode functions in Matlab can handle systems in the form of $\dot{\boldsymbol{z}} = f(\boldsymbol{z}, t)$. In this case this comes down to Eq. G.1.

$$\dot{\boldsymbol{z}} = \begin{bmatrix} \dot{U}_b = \frac{9\alpha}{R^2 R_f}\frac{C_D R_b}{24}(u - U_b) - \frac{3}{4}\alpha\frac{\partial C_p}{\partial x} + g_1\beta + \frac{3}{2}\frac{\alpha}{R}(u - U_b)\frac{dR}{d\tau} \\ U_b \\ \dot{V}_b = \frac{9\alpha}{R^2 R_f}\frac{C_D R_b}{24}(v - V_b) - \frac{3}{4}\alpha\frac{\partial C_p}{\partial y} + g_2\beta + \frac{3}{2}\frac{\alpha}{R}(v - V_b)\frac{dR}{d\tau} \\ V_b \\ \dot{R} \\ \ddot{R} = \frac{1}{R}\left[-\frac{3}{2}\left(\dot{R}\right)^2 + \frac{1}{2}\left(-C_p - \sigma_v\right) + \left(\frac{1}{2}\sigma_v + \frac{4}{W}\right)\left(\frac{R_0}{R}\right)^{3\frac{c_p}{c_v}} - \frac{4h}{WR_0'R} - \frac{8}{R_f R}\dot{R}\right] \end{bmatrix} \tag{G.1}$$

Where as an example the Rayleigh-Plesset equation has been taken. The general Keller-Herring equation could be included in the same way. The gravity has been taken into account in both equations of motion since a rotation of the coordinate system should be possible. Furthermore it is important to recognize the easy way of "shutting forces off". For example the gravity can be set to zero. The mass of the bubble can still be neglected, and the force due to a volume change can also be left out of the consideration. This might be useful in determining the influence of the forces. If a solid sphere would be under consideration the $\dot{R}$ could be set to zero just as the $\ddot{R}$. This just goes to show that this system is usable in multiple ways.

In Eq. G.1 it can be seen that indeed $\dot{\boldsymbol{z}} = f(\boldsymbol{z}, t)$. So the system is set, and this is a solvable system. The last part is to set the initial conditions, see Eq. G.2.

$$\boldsymbol{z}_0 = \begin{bmatrix} U_b(0) = U_{b_0} \\ x(0) = x_0 \\ V_v(0) = v_{b_0} \\ y(0) = y_0 \\ R(0) = R_0 \\ \dot{R}(0) = \dot{R}_0 \end{bmatrix} \tag{G.2}$$

Usually the point x_0 is at a place well before the body. The initial bubble velocity is $\mathbf{0}$ or the bubble moves with the flow, and the initial radius is $R_0 = \frac{R_0'}{h}$, the initial bubble growth ($\dot{R}_0$) will be zero. Of course the vertical initial position will be altered again.